

Development of polymeric formulations for potential application in blast mitigation

THESIS

Submitted to the Delhi Technological University for the award of the

degree of

DOCTOR OF PHILOSOPHY

By

**NAHID IQBAL
(2K13/PhD/AC/10)**



**DEPARTMENT OF APPLIED CHEMISTRY
DELHI TECHNOLOGICAL UNIVERSITY
BAWANA ROAD, DELHI-110042**

JUNE 2018

**Copyright ©Delhi Technological University-2018
All rights reserved.**

Development of polymeric formulations for potential application in blast mitigation

THESIS

Submitted to the Delhi Technological University for the award of the

degree of

DOCTOR OF PHILOSOPHY

By

**NAHID IQBAL
(2K13/PhD/AC/10)**



**DEPARTMENT OF APPLIED CHEMISTRY
DELHI TECHNOLOGICAL UNIVERSITY
BAWANA ROAD, DELHI-110042**

JUNE 2018

Dedicated
To
My Family

DECLARATION

I hereby declare that this PhD thesis entitled “**Development of polymeric formulations for potential application in blast mitigation**” was carried out by me for the degree of Doctor of Philosophy under the joint guidance and supervision of Prof. D. Kumar, Department of Applied Chemistry, Delhi Technological University and Dr. P. K. Roy, Centre for Fire, Explosive and Environment Safety, Delhi.

This thesis is a presentation of my original research work. Wherever contributions of others are involved, every effort has been made to indicate this clearly.

For the present thesis, which I am submitting to the University, no degree or diploma has been conferred on me before, either in this or in any other University.

Nahid Iqbal

Delhi Technological University

CERTIFICATE

This is to certify that the thesis entitled “**Development of polymeric formulations for potential application in blast mitigation**” submitted by **Nahid Iqbal** to **Delhi Technological University**, for the award of the degree of “Doctor of Philosophy” is a record of bonafide work carried out by him. Nahid Iqbal has worked under the joint guidance and supervision of **Prof. D. Kumar** and **Dr. P. K. Roy**, and has fulfilled the requirements for the submission of this thesis, which to our knowledge has reached requisite standards.

The results contained in this thesis are original and have not been submitted to any other university or institute for the award of any degree or diploma.

Dr. P. K. Roy

Scientist ‘F’
Centre for Fire, Explosive and
Environment Safety (CFEES, DRDO)
Delhi-110054

Prof. D. Kumar

Professor
Department of Applied Chemistry
Delhi Technological University
Bawana Road, Delhi-110042

Head of Department

Department of Applied Chemistry
Delhi Technological University
Bawana Road, Delhi-110042

ACKNOWLEDGEMENT



The path towards this thesis spans several years of work and many people have been involved and contributed directly and indirectly, to only few of them it is possible to give mention here. The author acknowledges his debt to those who have helped along the way and influenced the formation of understanding and the approach for the research presented in thesis.

This endeavour was accomplished only by the kind help, unparalleled support and extreme patience of my thesis supervisors, Prof. (Dr.) Devendra Kumar, Department of Applied Chemistry, Delhi Technological University, Delhi, and Dr. Prasun Kumar Roy, Scientist 'F', CFEEES. Their good advice, unsurpassed knowledge, continued encouragement and invaluable suggestions were the guiding realms for carrying out this work. The discussions held with them were very enlightening and always motivated me to work with greater zeal and enthusiasm.

I wish to convey my sincere thanks to Dr. Chitra Rajagopal, Outstanding Scientist, CC R&D (SAM) and Director, for their constant guidance and inspiration

Thanks are also due to Sh. Rajiv Narang, Scientist 'G', Director, CFEEES and DRDO for allowing me to carry out this research work and providing the necessary facilities.

I would like to express my profound gratitude to Prof. (Dr.) Archana Rani, Head of Department, Department of Applied Chemistry, Delhi Technological University, for helping me in all the related problems during the entire duration of PhD. Thanks are due to the accounts, academic and technical staff of DTU for their help. The financial assistance of DTU is deeply acknowledged.

I am extremely grateful to Dr. Manorama Tripathi and Ms. Surekha Parthasarathy for extending their help and support throughout the work. I also convey my sincere

thanks to Dr. P.K. Rai, Dr. Arti Bhatt, Dr. Pankaj Sharma, Mr. Pankaj Sharma, Mr. Rajesh Chopra, and Mr. Naveen Saxena for their active support.

I was fortunate to have an excellent work environment in the laboratory which facilitated my work to a great zeal. I must thank Saurabh Chaudhary, Pratibha Sharma, Allam Pallam Vijayraghvan Ullas, for their constant help in every possible way to carry forward my research work.

When one owes to so many, it is almost impossible and invidious to single out names. However I acknowledge my friends Sanaullah Khan, Adil Hussain, Saurabh jha, Neerajha, Ashish Gupta, and Owais Jalil for their support. I also thank them for keeping me cheerful throughout entire period of work.

I would also like to thank my critics; especially reviewers who have unknowingly helped me turn out as a better researcher.

For pursuing this dream, I had the blessing of my kith and kin. The immense love and understanding shown by my parents Mr. Saghir Alam and Mrs Hasbun Nisha for helping me in every possible way in realizing my goals. Their cooperation, concern and encouragement actually pulled me through the tougher and trying times. At this juncture, I fail not to mention, my wife Mrs. Uzma Noor Iqbal for her invaluable understanding in difficult times, all the emotional support and care she provided, and for her unequivocal support throughout, as always, my mere expression of thanks likewise does not suffice. I wish to thank my entire extended family for their wishes and support.

Nahid Iqbal

ABSTRACT

Elastomeric coatings are being advocated as excellent candidates for retrofitting applications, particularly for blast mitigation and ballistic protection. Polyurea, an elastomer formed by the reaction of isocyanate and amine, possesses hard domains dispersed randomly within the soft domains, forming a heterogeneous landscape with a nano-segregated microstructure, with each domain exhibiting its own characteristic glass transition temperature. Commercialised in the late eighties, this relatively new entrant in the field of elastomers has received enormous attention in view of its excellent blast mitigation properties and ballistic protection. Since the blast mitigation and ballistic protection ability is decided by the hard and soft domains of polyurea, respectively, the properties need to be tuned for a particular application through judicious choice of the raw materials as well as the processing technique.

In this work, the effect of the various components of the amine resin blend, i.e. soft segment length, chain extender and crosslinker on the material properties of polyurea have been studied. To quantify the effect of soft segment length, a series of polyurea formulations was prepared by reaction of commercially available isocyanate prepolymer with polypropylene oxide based amines of varying molecular weights (230-2000g/mol) by solution casting technique. The effect of increasing the chain length of the soft segment on the mechanical properties of polyurea under both quasi-static as well as dynamic conditions was determined. The ductility expressed as “elongation at break” was found to increase proportionally with increasing soft segment length, with a concomitant decrease in the tensile strength. All the compositions exhibited sub-ambient glass transition temperatures (T_g), however the same was found to reduce with increasing soft-segment length. Time-temperature superposition principle was used to derive the master curves for the compositions. It was of particular interest to establish the effect of increasing soft-segment length on the frequency necessary to initiate the process of dynamic “rubber to glass” transition in polyurea. The frequency essential to initiate the dynamic glass transition process increased was directly proportional to the soft segment length.

In view of the fast reaction kinetics, the most important concern associated with the processing of polyurea is the requirement of rapid mixing of reactants; which held back its commercialization till the late 1980s. For all practical applications, polyurea coatings are processed by using reactive spraying where, the isocyanate and amine are stored separately and are forced to react in the mixing-module, just prior to being pushed out of the orifice under pressure. However, the viscosity of isocyanate prepolymer (Side A) is significantly higher than that of the amine resin blend (Side B) even at high temperatures used during processing ($\sim 70^{\circ}\text{C}$). This results in stoichiometric imbalance which hinders formation of high molecular weight polymer.

An experimental study into the consequences of diluting isocyanate with a zero VOC diluent (propylene carbonate) towards processing of polyurea was performed. Viscosity-Blending Index based equations were found to be more reliable towards prediction of isocyanate precursor-propylene carbonate blend viscosity. Spraying of undiluted isocyanate precursor with amine formulations led to formation of “noodle-like” fibrous product, irrespective of the type of chain extender being used. Diluting isocyanate with propylene carbonate (10% v/v), led to reduction in the viscosity of the precursor from 85 to 50 mPa.s (at 70°C). This the formulations could be effectively sprayed to form polyurea films with excellent mechanical properties. Dilution with propylene carbonate also increased the “tack free” time appreciably from ~ 1 to ~ 4 s, which directly reflects on the improved processability. Rheological studies were performed to quantify the activation energy associated with the isocyanate-amine reaction for polyurea preparation.

The properties of polyurea can further be tuned by the prudent choice of chain extenders. An experimental study into the consequences of chain extension of polyurea formulation with different type of chain extenders (both aromatic as well as aliphatic) was undertaken, with an aim to gain an insight into their role in improving properties. Rheological studies were performed to understand the effect of their inclusion on the processing conditions and quantification of the gelation time. Aromatic chain extenders were found to be far more reactive than their aliphatic

counterparts, which lead to significantly short ‘gel-time’ as quantified by rheometry. The degree of H-bonding was qualitatively established by the red-shift associated with N-H and >C=O bands in the FTIR spectra of the polymer. Introduction of either type of chain extender lead to remarked processability of polyurea formulations through spray coating technique. An optimal aromatic: aliphatic chain extender ratio was found to result in optimal H-bonding, which in turn reflected in terms of mechanical properties. Dynamic studies were performed and all formulations were found to exhibit sub-ambient T_g and is appreciably affected by the type of chain extender used. Higher aromatic: aliphatic chain extender ratio was found to result in higher storage modulus and lower dissipation potential.

It was further considered of interest to study the evolution of material properties of polyurea with respect to time. In view of the fast kinetics associated with the isocyanate and amine reaction, the polymerization process occurs in a matter of seconds, which leads to extremely short ‘tack free’ times. Polyurea is therefore promoted for all applications where fast curing is beneficial e.g. pipes, vehicle liners and masonry retrofits. Interestingly, although polyurea is considered as an “instantaneous setting” system, the properties of polyurea evolve with time: an issue hadnot been studied systematically. During the processing of polyurea by spray coating process, internal stresses develop within the matrix, which in turn reflected in terms of their inferior mechanical properties. Polyurea was observed to achieve its optimal properties after a finite period time, necessary for relaxation period required to expend the in-built stresses, of the order of ~15 days.

In addition to the chain extender and long chain amine, the amine resin blend also contains a crosslinker, which can affects the properties of the coating substantially. To study this, a long chain trifunctional amine was introduced as a co-reactant in the resin blend, the amount of crosslinker being varied from 0-5 mole % (crosslinking density 100-500 mol/m³). The mechanical properties of spray coated polyurea films, both in quasi-static as well as dynamic conditions were determined. Physically crosslinked polyurea coatings (in the absence of chemical cross-linking)

exhibited tensile strength $\sim 7.4 \pm 0.7$ MPa and elongation of 121 ± 3.7 %. Introduction of long chain amine led to an improvement in these characteristic properties till a maxima, subsequent to which both strength and elongation decreased. Chemical cross-linking led to restraining of the segmental motions reflecting in terms of increased glass transition temperature, as evidenced by dynamic mechanical analysis and differential scanning calorimetry. The chemical resistance of polyurea also improved substantially due to crosslinking, which reflected in terms of decreased swelling ratio in different organic media.

Subsequently, the efficacy of polyurea towards improving the performance of a concrete substrate towards shock and ballistic loading was demonstrated. Concrete tiles (25 cm x 25 cm x 2cm) were coated with polyurea (coating thickness 1-6 mm) and subjected to controlled blast loadings. Unreinforced concrete tiles underwent extensive fragmentation at peak pressures < 50 psi, while polyurea coated tiles could withstand much higher peak pressures. The extent of mitigation increased with the coating thickness and composites with 6 mm polyurea could withstand 87 psi. At higher loadings ($P_r = 90$ psi), polyurea-concrete debonding was evidenced, however the membrane arrested the fragments formed. Dynamic mechanical studies revealed that polyurea exhibited a dynamic glass transition at $\sim 10^{15}$ Hz at room temperatures, which essentially means that polyurea remains as an elastomer under the frequency range associated with the shock tube testing ($\sim 10^2$ Hz). Polyurea acts as a catcher system for the fragments formed due to blast loading.

CONTENTS

DECLARATION.....	I
CERTIFICATE.....	II
ACKNOWLEDGEMENT.....	III
ABSTRACT.....	V
CONTENTS.....	IX
LIST OF FIGURES.....	XIII
LIST OF TABLES.....	XVIII
LIST OF SCHEMES.....	XIX
ABBREVIATIONS.....	XX

Chapter 1 Introduction

1.1 Introduction.....	1
1.2 Existing solutions to improve blast-mitigating performance.....	2
1.2.1Retrofitting with Fibre Reinforced Plastics.....	3
1.2.2 Spray-on coatings	4
1.3 Polyurea coating	4
1.3.1Quasi-static and Dynamic mechanical properties of polyurea..	10
1.3.2 Retrofitting with polyurea: Effect on underlying substrate.....	15
1.3.2.1 Retrofitting Unreinforced Masonry Structures.....	15
1.3.2.2 Application on Steel Structures and Plates.....	17
1.3.2.3 Application on Composite Sandwich Systems and Structures.....	20
1.3.3 Mechanisms underlying polyurea-induced Ballistic/ Blast- mitigation.....	21
1.3.3.1 Shock wave mitigation.....	21
1.3.3.2 Ballistic protection.....	25
1.4 Research objective.....	26
1.5 Implementation of work plan.....	28

Chapter 2 Polyurea coatings: Dependence of material properties on soft segment length

2.1 Introduction.....	29
2.2 Experimental.....	31
2.2.1 Materials.....	31
2.2.2 Polyurea synthesis.....	32
2.2.3 Film preparation	33

2.2.4 Characterization method.....	33
2.3 Results and discussions.....	35
2.3.1 Chemo-rheological response	37
2.3.2 Structural characterization.....	38
2.3.3 Calorimetric studies.....	41
2.3.4 Mechanical properties: Effect of soft-segment length.....	42
2.3.5. Dynamic mechanical analysis.....	43
2.3.6 Thermal characterization.....	46
Chapter 3 Spray-processing of polyurea: Importance of viscosity matching	
3.1 Introduction.....	49
3.2 Experimental.....	51
3.2.1 Materials.....	51
3.2.2 Spraying of polyurea	52
3.2.3 Characterization.....	53
3.3 Results and Discussion.....	54
3.3.1 Temperature dependence of viscosity of isocyanate and amines.....	54
3.3.2 Theoretical calculations on reactant ratio.....	55
3.3.2.1 Stoichiometric imbalance in PU1.....	55
3.3.1.2 Stoichiometric imbalance in PU2.....	56
3.3.3 Predicting the effect of isocyanate: amine on degree of polymerization.....	56
3.3.4 Predicting blend viscosity.....	59
3.3.5 Chemo-rheological behaviour during polyurea formation....	62
3.3.6 Reaction monitoring	66
3.3.7 Mechanical properties	67
3.3.8 Thermal properties	68
Chapter 4 Effect of chain-extender on the material properties of polyurea	
4.1 Introduction.....	71
4.2 Experimental	73
4.2.1 Materials.....	73
4.2.2 Spraying of polyurea.....	73
4.2.2.1 Contribution of Amines to total urealinkages.....	74
4.2.3. Characterization.....	76
4.3 Results and Discussion.....	76
4.3.1. Rheological behavior of isocyanate and amines.....	76
4.3.2 Chemo-rheological response	77
4.3.3 Mechanical properties.....	79

4.3.3.1 Evolution of mechanical properties.....	79
4.3.3.2 Mechanical properties of cured polyurea films (post 15 days).....	82
4.3.4 FTIR spectroscopy	88
4.3.4.1 Structural evolution in polyurea	90
4.3.4.2 Structural features of polyurea (post 15 days)	91
4.3.5. Dynamic mechanical analysis.....	92
4.3.5.1 Evolution of Dynamic mechanical properties.....	93
4.3.5.2 Dynamic mechanical properties of polyurea (post 15 days).....	94
4.3.6 Thermal properties	96
4.3.6.1. Thermogravimetry.....	96
4.3.6.2. Calorimetric studies.....	99
Chapter 5 Effect of chemical crosslinker on the material properties of polyurea	
5.1 Introduction.....	101
5.2 Experimental.....	102
5.2.1 Materials.....	102
5.2.2 Spraying of polyurea	102
5.2.3 Characterization.....	104
5.3 Results and discussion.....	105
5.3.1 Effect of Crosslinking on mechanical properties.....	105
5.3.2 FTIR spectroscopy	108
5.3.3. Dynamic mechanical analysis	110
5.3.4 Swelling studies.....	113
5.3.5 Thermal properties.....	115
5.3.5.1Calorimetric studies	115
5.3.5.2. Thermogravimetry	115
Chapter 6 Improving the blast survivability of concrete by coating with polyurea	
6.1 Introduction.....	117
6.2 Experimental.....	118
6.2.1 Materials.....	118
6.2.2 Coating on concrete tiles.....	119
6.2.3 Characterization.....	120
6.2.4 Shock loading system	120
6.2.4.1 Concrete tile geometry and boundary conditions.....	121
6.3 Results and discussion.....	122
6.3.1 Mechanical properties of polyurea.....	122
6.3.2 Blast performance of polyurea coated concrete tiles.....	123
6.3.3Mechanism behind improved blast resistance.....	126

Chapter 7	Summary and Conclusions.....	133
	Appendix : A.....	139
	Appendix : B.....	143
	References.....	145

LIST OF FIGURES

- Figure 1.1** Effect of hydrogen bonding on the melting point of different classes of polymers
- Figure 1.2** Micro-structural changes in polyurea upon tensile loading
- Figure 1.3** Uniaxial compression stress-strain behaviour of polyurea ranging from 10^{-3} s^{-1} to 9000 s^{-1} (each SHPB curve is labelled by its true strain rate of 0.6). Reproduced with permission from Elsevier
- Figure 1.4** Hydrogen bonding within the urea linkages in polyurea
- Figure 1.5** Cyclic compression and tension data, comparing model results with experimental data (a) stress-strain curves under cyclic compression at a strain rate of 0.1 s^{-1} (b) stress-strain curves under cyclic tension at a strain rate of 0.015 s^{-1} . Reproduced with permission from Royal Society of Chemistry
- Figure 1.6** Shockwave capture and neutralization in phase separated materials
- Figure 1.7** Representative dielectric loss spectra for dry PU96 at $P = 0.1 \text{ MPa}$, for temperatures from $T = 223$ to 328 K in steps of 15 K . Reproduced with permission from Elsevier
-
- Figure 2.1** Transparent tensile coupons of polyurea (PU 230)
- Figure 2.2** Representative stress-strain curves for PU 230 prepared with varying isocyanate index (i_{NCO}) a) 0.9, b) 0.95, c) 1, d) 1.05, e) 1.1, f) 1.15
- Figure 2.3** Variation of characteristic mechanical properties as a function of isocyanate index for PU 230
- Figure 2.4** Evolution of storage and loss modulus in polyurea formulations (a) PU 230, (b) PU 400 and c) PU 2000
- Figure 2.5** Changes in the FTIR spectra due to the reaction of isocyanate with amine (PU 230)
- Figure 2.6** DSC traces a) PU 2000, b) PU 400 and c) PU 230
- Figure 2.7** Variation in glass-transition temperatures of polyurea networks PU-2000 (HS-23), PU-400 (HS-57) and PU-230 (HS-73) with hard segment

- Figure 2.8** Effect of increasing hard segment on characteristic mechanical properties
- Figure 2.9** Variation of storage and loss modulus with temperature at different frequencies a) PU-230, b) PU-400 c) PU-2000
- Figure 2.10** Master curves depicting the systematic variation in loss modulus in polyurea a) PU-230, b) PU-400 c) PU-2000
- Figure 2.11** TG-DTG trace of polyurea samples
- Figure 3.1** Variation of reactant viscosity with temperature. Inset shows an enlarged view of the viscosity-temperature profile for the low viscosity region
- Figure 3.2** Effect of increasing stoichiometric imbalance on the degree of polymerization
- Figure 3.3** Digital photograph of PU 1 and PU 2
- Figure 3.4** Predictions related to the effect of blending propylene carbonate on the viscosity of isocyanate prepolymer ($T = 70^{\circ}\text{C}$)
- Figure 3.5** Evolution of storage and loss modulus in formulations containing DETA in (a-c) presence and (d-f) absence of diluent (a,d = 50°C , b,e = 60°C and c,f = 70°C)
- Figure 3.6** Evolution of storage and loss modulus in formulations containing DETDA in (a-c) presence and (d-f) absence of diluent (a,d = 50°C , b,e = 60°C and c,f = 70°C)
- Figure 3.7** Arrhenius plot of $\ln t_{\text{gel}}$ vs $1000/T$ for polyurea formulations containing a) DETA and b) DETDA
- Figure 3.8** Changes in the FTIR spectra due to formation of polyurea
- Figure 3.9** Stress-strain curve of polyurea specimens prepared after diluting
- Figure 3.10** TG/DTG traces of polyurea containing aromatic and aliphatic chain extender
- Figure 4.1** Percentage contribution of long chain amine, aliphatic and aromatic chain extender towards the total urea linkage present in the polymer
- Figure 4.2** Variation of reactant viscosity with temperature

- Figure 4.3** Evolution of storage and loss moduli in polyurea formulations (70°C)
- Figure 4.4** Evolution of tensile strength and % elongation of representative polyurea formulations as a function of time
- Figure 4.5** Evolution of tear strength of representative polyurea formulations as a function of time
- Figure 4.6** Variation in tensile strength and elongation of polyurea (post 15 days) due to chain extension. The relative contribution of aromatic and aliphatic hard segment is also included in the figure
- Figure 4.7** Variation in tear strength (post 15 days) due to chain extension. The relative contribution of aromatic and aliphatic hard segment is also included in the figure
- Figure 4.8** Increase in the vicinity of urea linkages through chain extension process
- Figure 4.9** Theoretical N-N distance in DETDA and D 230
- Figure 4.10** Representative Hydrogen bonding sites in polyurea chains formed by aromatic and aliphatic chain extenders
- Figure 4.11** Representative hard-segment models, based on the hydrogen bonding between proton acceptor ($>C=O$) and proton donor (N-H). a) Between D230 and D230 b) DETDA and DETDA and c) DETDA and D230
- Figure 4.12** FTIR Spectra of individual components of formulations
- Figure 4.13** a) Change in the FTIR spectra due to reaction of isocyanate with amine b) Decrease in isocyanate absorbance
- Figure 4.14** FTIR spectra of polyurea formulations
- Figure 4.15** Variation of storage and loss modulus of polyurea formulations with temperature
- Figure 4.16** Variation of storage and loss modulus with temperature at different frequencies
- Figure 4.17** Variation of glass transition temperature with increasing hard segment
- Figure 4.18** Variation of loss factor with hard segment

- Figure 4.19** TG-DTG traces of polyurea formulations containing aromatic and aliphatic chain extender
- Figure 4.20** Changes in the FTIR spectra of sample as a result of thermal degradation of PUAr63 a) 50°C, b) 150°C, c) 250°C, d) 350°C and e) 450°C)
- Figure 4.21** DSC traces of polyurea at different periods of curing
- Figure 4.22** DSC traces for polyurea formulations
-
- Figure 5.1** Percentage contribution of individual amine towards the total urea linkage present in the polymer
- Figure 5.2** Variation of reactant viscosity with temperature
- Figure 5.3** Variation in tensile strength and elongation of polyurea due to crosslinking
- Figure 5.4** Change in the FTIR spectra of PUX22 as a function of time (in minutes)
- Figure 5.5** FTIR spectra of polyurea formulations
- Figure 5.6** Variation of storage and loss modulus with temperature
- Figure 5.7** Comparison of experimentally determined (affine and phantom) and theoretically predicted (Scanlan) crosslink density as a function of crosslinker concentration
- Figure 5.8** Representative formulation (PUX22) showing samples before and after swelling
- Figure 5.9** DSC traces for polyurea formulations a) PUX0 b) PUX2 c) PUX12 d) PUX22 e) PUX35
- Figure 5.10** TG-DTG traces of the crosslinked polyurea formulations
-
- Figure 6.1** Shock tube layout
- Figure 6.2** Shock tube facility
- Figure 6.3** a) Sketch of the specimen depicting the loading and boundary areas. (b) Actual specimen placement c) Front view
- Figure 6.4** Representative pressure time profile during shock tube

experimentations. The time duration (“rise time”) considered for estimation of blast loading frequency is also labeled for reference

- Figure 6.5** Variation of (a) Storage and loss modulus (b) Tan delta with temperature at different frequencies
- Figure 6.6** Master curves representing the variation in loss modulus in PU-Ar 63
- Figure 6.7** Failure mechanisms in retrofitted plain cement concrete
- Figure 6.8** Progressive failure in polyurea coated concrete
- Figure 6.9** Visual examination a) View of the blast facing side (fragment removed to reveal the adhering layer of concrete) b) enlarged view c) debonded polyurea
- Figure 6.10** FTIR spectra of polyurea, concrete and debonded polyurea

LIST OF TABLES

Table 1.1	Relative reaction rate of reactants with isocyanate
Table 2.1	Characteristic properties of reagents
Table 2.2	Characteristic absorption frequencies in segmented polyurea
Table 2.3	Mass loss associated with step-wise thermal degradation of polyurea
Table 3.1	Structure and physical properties of reactants
Table 3.2	Details of formulation used for preparation of polyurea
Table 3.3	Degree of polymerization X_n , for different values of r
Table 3.4	Pure mixing rules for blends
Table 3.5	Viscosity blend index equations
Table 3.6	Variation of gelation time (t_{gel}) with temperature (T) and activation energy for polyurea formulations
Table 3.7	Mechanical properties of polyurea samples
Table 4.1	Details of polyurea formulations prepared
Table 4.2	Individual contribution of long chain amine (D2000), aromatic (DETDA) and aliphatic chain extender (D230) to the total hard segment
Table 4.3	‘Gel-time’ and ‘tack free’ time of formulations during spraying
Table 4.4	Characteristic mechanical properties of polyurea samples (post 15 days)
Table 4.5	Details of composition and properties of non chain extended polyurea
Table 4.6	Characteristic thermal properties as derived from thermogravimetric analysis
Table 5.1	Individual contribution of isocyanate and chain extenders to the total hard segment
Table 5.2	Formulation details of crosslinked polyurea
Table 5.3	Characteristic mechanical properties of polyurea coatings
Table 5.4	Variation in swelling ratio with extent of crosslinking
Table 6.1	Response of polyurea coated concrete tiles
Table 6.2	Pressure time profile and operating conditions associated with blast loading (shock tube test)
Table 6.3	Assignment of bands in the spectra (before and after debonding)

LIST OF SCHEMES

- Scheme 1.1** Relative reaction rate of reactants with isocyanate
- Scheme 2.1** Schematic, illustrating the reaction of diisocyanate with diamines of varying molecular weight
- Scheme 3.1** Schematic of the reactive spray process
- Scheme 3.2** Reaction of propylene carbonate with amines
- Scheme 4.1** Representative diisocyanate-diamine reaction leading to formation of polyurea
- Scheme 5.1** Schematic of formation of crosslinked polyurea

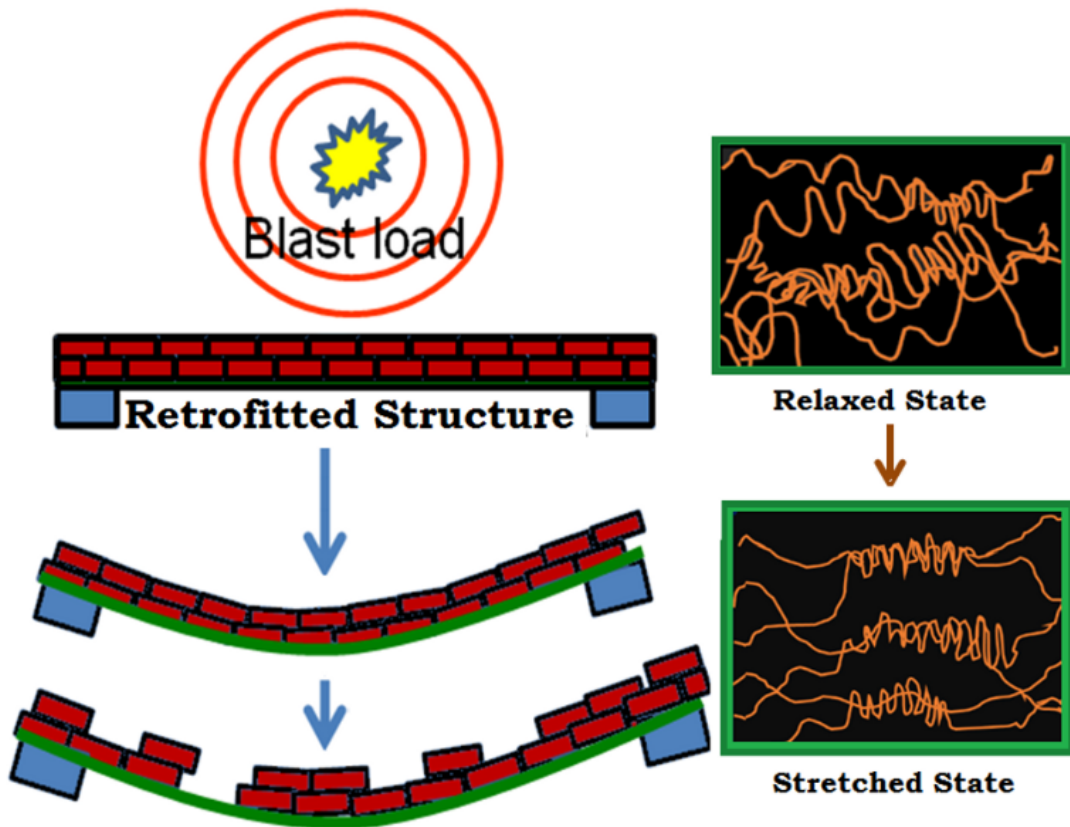
ABBREVIATIONS

FRP	Fiber reinforced polymer
HUMVEE	High Mobility Multi-purpose Vehicle
VOC	Volatile Organic Compound
CED	Cohesive Energy Density
DSC	Differential scanning calorimetry
ΔE_{vap}	Energy of Vaporization
V_m	Molar Volume
TBI	Traumatic Brain Injury
TTS	Time-Temperature Super-positioning
PMMA	Polymethylmethacrylate
SHPB	Split Hopkinson Pressure Bar
FTIR	Fourier Transform Infrared Spectroscopy
URM	Unreinforced Masonry
MDI	4,4'-Methylenebis(phenyl isocyanate)
SDOF	Single Degree-of-Freedom
CMU	Concrete Masonry Unit
EVE	E-glass reinforced vinyl-ester
kPa	Kilo pascal
MPa	Mega pascal
msec	Milli second
ms	Milli second
T_g	Glass transition temperature
H-bond	Hydrogen bond
DETDA	Diethyltoluenediamine
PPO	Polypropylene oxide
TGA	Thermogravimetric analysis
PTMO	Poly(tetramethyleneoxide)

DMA	Dynamic Mechanical Analysis
NCO	Isocyanate
mPa.s.	Milli pascal second
D	Difunctional
T	Trifunctional
RPM	Rotation per minute
PU	Polyurea
Ar	Aromatic
X	Crosslinked
G'	Storage Modulus
G''	Loss Modulus
HS	Hard Segment
SS	Soft Segment
ν	Frequency
K	Kelvin
t_{rise}	Rise time
Hz	Hertz
DTG	Derivative Thermogravimetric
wt	Weight
DETA	Diethylene triamine
d	Diluted
Å	Armstrong
E'	Storage modulus
E''	Loss modulus
EPA	Environmental Protection Agency

Chapter 1

Introduction



1.1 Introduction

In the wake of terrorist threats, enormous attention is nowadays being directed towards designing of strategic buildings, where such a possibility is even remotely envisioned. Unfortunately, a majority of the structures existing today were not originally designed to endure dynamic loads, which are characterized by their impulsive nature, transmitting extremely high-pressures ca. $10 - 10^3$ kPa. On the other hand, static loads are time independent, presumably acting on the structure for infinitely extended time durations (e.g. gravity loads). By and large, time dependent dynamic loads are classified on the basis of their relative intensity and frequency. Natural dynamic loads like those induced by earthquakes exhibit strong time dependencies and continue for much longer duration as compared to blast loads. Detonation, on the other hand, being an extremely short duration phenomena (~ms) falls under the category of high intensity as well as high frequency load and in view of the associated inertial effects, the resulting damage is often unpredictable.

Terrorist attacks usually take the form of small bombings, which lead to structural damage, generating high velocity fragments; the extent of damage being dependent on the amount of explosive employed. It is also generally accepted that the structural disintegration and propulsion of the debris result in more casualties as compared to the pressure, heat or other events associated with explosion [1, 2].

In order to reduce the extent of damage, one of the solutions envisaged involves enhancing the strength of existing structures, which in turn can be achieved through retrofitting. The solution has to be economically viable both in terms of material cost as well as maintenance expenses. In addition, miscellaneous factors cannot be negated,

particularly maintenance of floor space, non-interruption of existing services and non-requirement of skilled technicians for installation. This chapter reviews the materials and methods, commonly employed for improving blast resistance of buildings, with an emphasis on elastomeric spray-on polyurea coatings.

1.2 Existing solutions to improve blast-mitigating performance

Maintaining a sufficient stand-off distance is undoubtedly the most effective way of protecting any structure from damage resulting from blast loadings, the underlying reason being the rapid decrease in overpressure with increasing stand-off distance [3]. This can be achieved with bollards, fences and walls, but is impractical in urban environments where space is often unavailable. Other arrangements include fixing catcher systems on the inner face of walls, which prevent fragments from entering the occupied space [4]. This can be achieved by covering the entire wall with a fabric securely anchored both at the floor as well as ceiling. However, since no structural strength is provided by this technique, special arrangements have to be made for load bearing walls. In addition, this technique is not befitting for structures where openings are essential, particularly doors and windows, as the fabric needs to span continuously without interruption for optimal protection.

The ability of a structure to withstand blast loads can also be enhanced by increasing its mass and ductility, which can be achieved by additional reinforced concrete for concrete structures and larger sections for steel structures. However, this requires ensuring the ability of existing structure to withstand the additional weight requirements prior to installation [5]. Alternately, external-strengthening techniques using composite laminate / steel jacketing have also been attempted. Lengthy installation times and

vulnerability to corrosion, which lead to increased maintenance costs are additional disadvantages associated with this technique.

Another alternate solution involves retrofitting the structure with additional light-weight layers, e.g. fibre reinforced polymer (FRP) and elastomeric coatings [6]. The primary requirement of the retrofitting material is to possess enough resilience to deflect and hold back the structural debris in place, thereby providing sufficient response time for the inhabitants to take suitable protective measures in the event of explosion.

1.2.1 Retrofitting with Fibre Reinforced Plastics

With rapid advances in the field of Fibre Reinforced Plastics (FRP), affordable high strength composites are now available and are being explored for blast mitigating applications [7-9]. The corrosion free characteristics and ease of applicability bestow these materials excellent candidature for retrofitting applications [6]. FRPs possess obvious advantages in terms of mechanical properties and being lightweight, the additional strength requirement of the existing structure is rather lenient. The reason most commonly cited against the use of FRPs includes its high apparent material and installation cost as compared to other materials. However, a direct comparison on a unit price basis may not be appropriate if transportation costs are included during comparison. FRPs can often compete with conventional materials if the comparisons include through-life costs. Carbon[10],glass[11], aramids [9] and their hybrids are the most commonly used fibres, with epoxy being the most widely used matrix [12-18]. Studies reveal that in general, FRPs exhibit bending failure, but nonetheless contribute positively towards structural blast strengthening [4, 19, 20]. FRPs, however, have their own set of limitations. For example, in some situations, the excessively thin sheets of the material require an impractical number of layers or wraps on the structure to function effectively.

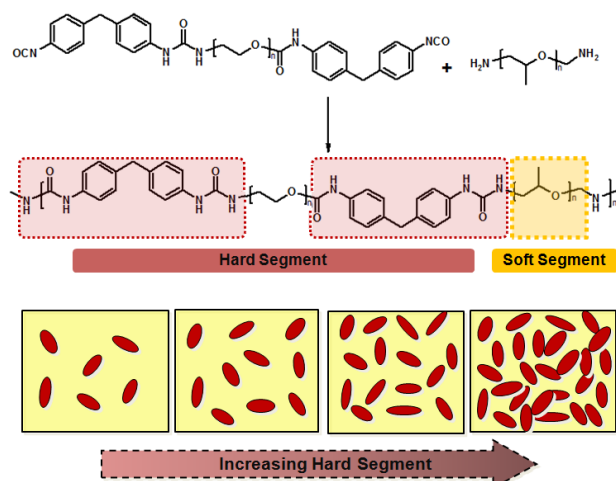
Besides, in cases of close-in detonations, the strain demand of the strengthening material is beyond the capacity of FRPs [7]. Another drawback of FRP strengthening is that it may lead to a premature brittle failure, such as through FRP de-bonding and FRP-concrete delamination when subjected to high intensity blasts [21].

1.2.2 Spray-on coatings

Another approach, which has emerged as an economically viable solution in the context of blast mitigation is the application of elastomeric coatings as a retrofit [22, 23]. Among the many desirable properties of any retrofitting polymer, the most important include ease of application, rapid cure time, adhesive properties and excellent mechanical properties, particularly strength and elongation. Elastomers, when subjected to blast and impact loads tend to exhibit high strain to failure, thereby absorbing or dissipating the energy arising from dynamic loads [24-26]. US Air Force was the first to demonstrate the potential of this approach by coating polyurea on building walls. US Navy subsequently extended the use of these coatings to enhance the penetration resistance of structure and vehicles under the impact by blast-fragments and projectiles [25], a much cited success story being the up armoring of High Mobility Multi-purpose Vehicle (HUMVEE).

1.3. Polyurea coatings

Polyurea is an elastomeric polymer formed by reacting an isocyanate ($\text{N}=\text{C}=\text{O}$) with amine (NH_2) by a step growth polymerization process. Commercialized in the late eighties, this sub-category of elastomers can be designed to exhibit a wide range of mechanical properties, from soft rubber to hard plastic by judicious choice of the raw materials. A representative reaction between the amine and isocyanate and the resulting microstructure is presented in the Scheme 1.1.



Scheme 1.1: A schematic illustrating the reaction of diisocyanate with diamine.

Polyurea spray coatings exhibit rapid cure even at sub-zero temperatures (in view of the high reactivity of isocyanates with amines), exceptional physical properties such as high hardness, flexibility, tear strength, tensile strength, chemical and water resistance.

The isocyanate group can react with any compound containing a reactive hydrogen. Reaction of an isocyanate with an alcohol yields a urethane, reaction of an isocyanate with an amine yields a urea and reaction of an isocyanate with water will result in a carbamic acid, which is unstable and decomposes to yield carbon dioxide and amine. Other potential isocyanate co-reactants include carboxylic acids urethanes, and ureas. The relative reaction rate of reactants with isocyanate is presented in Table 1.1. From this table it can be inferred that, the rate of reaction of isocyanate with primary amines is many-fold higher, which means that the possibility of formation of urea linkages is far higher than that of others.

Table 1.1: Relative reaction rate of reactants with isocyanate

Reactants	Relative reaction rate at room temperature
Primary aliphatic amine	100,000
Secondary aliphatic amine	20,000-50,000
Primary aromatic amine	200-300
Primary Hydroxyl	100
Water	100
Secondary aromatic amine	100
Carboxylic acid	40
Secondary hydroxyl	30
Ureas	15
Tertiary hydroxyl	0.5
Urethanes	0.3
Amide	0.1

Theoretically, for the formation of a linear polyurea chain, a single molecule of diisocyanate reacts with another molecule of diamine, the underlying calculation being:

$$m_{iso} \cdot n_{eq,iso} = [m_{amine} \cdot n_{eq,amine}] i_{NCO} \dots\dots\dots (1.1)$$

where m_{iso} and m_{amine} refer to the mass of isocyanate and diamine respectively and $n_{eq,iso}$ and $n_{eq,amine}$ are the equivalent number of isocyanate and amine. Here, the isocyanate index (i_{NCO}) refers to the ratio of the equivalent amount of isocyanate used relative to the theoretical equivalent amount. Theoretical equivalent amount is equal to one equivalent

isocyanate per one equivalent B-side compounds; which automatically refers to an index of 1.

$$\text{Isocyanate index}(i_{NCO}) = \frac{\text{Actual amount of isocyanate}}{\text{Theoretical amount of isocyanate}} \dots\dots\dots (1.2)$$

An isocyanate index of 1 refers to perfect stoichiometry: every reactive site in the isocyanate/ A- side is expected reacted with every amine site in the polyamine / B side. However, it is to be noted that very few systems are prepared while maintaining an index of 1.00. An isocyanate index of above 1 refers to an excess of isocyanate; less than 1 indicates a shortage of isocyanate, or an excess of polyamine.

In the scenario of polyurethanes, most rigid systems are over-indexed, and run at $i_{NCO} > 1.05$. Analogously, most flexible polyurethane systems – foams in particular, are prepared by maintaining a $i_{NCO} < 1$. Equivalent weight calculations are used to determine the stoichiometric ratio; the index is user-defined, and based on the material, required properties, etc.

It has already been mentioned that the rigid urea groups form the hard segments, which are dispersed within the soft segment comprising primarily of the long chains of polyether. The hard segment content is generally estimated as the ratio of mass of isocyanate and chain extender to the total mass of the system, as per established procedure (Eq. 1.3) [27].

$$HS = \frac{m_{iso} + m_{chain\ extender}}{m_{iso} + m_{chain\ extender} + m_{amine}} \dots\dots\dots (1.3)$$

Where, m_{iso} and m_{amine} refer to the amount (g) of isocyanate and amine respectively.

The reaction is rapid with gel times measured in seconds, which means the reaction proceeds largely independently of ambient temperature and humidity, facilitating application of polyurea under diverse conditions. Polyurea are reportedly 100 % solids, a feature which renders them compliant with the strictest Volatile Organic Compound (VOC) regulations [28]. It is however, to be noted that the term, “Zero VOC”, does not necessarily mean complete absence of solvents, as many commercial formulations do contain reactive diluents, which do not fall under the category of volatile organics e.g. alkylene carbonate included in A part (isocyanate). The rest of the additives, especially colouring agents and adhesion promoters are included in the B-part consisting primarily of amines. It is to be noted that polyurea formulations do not require catalysts, which are indispensable ingredients in polyurethanes (formed by reaction of isocyanate with polyols).

An important concern associated with polyurea coatings is the requirement of rapid mixing of the reactants, an issue which has been overcome using a suitable mixing module by impingement at high pressures. The viscosity of both the components (isocyanate and resin) needs to be almost equal, which mandates a heating arrangement, with higher viscosity reactants requiring higher pressures for spraying. It is to be noted that the spraying pressure and reaction temperature of the reactants greatly affect the properties of the product formed.

The micro-structure of polyurea comprise of two distinct domains [29]; hard domains, formed by hydrogen bonded polar urea linkages ($-\text{NH}-\text{CO}-\text{NH}-$) and possibly π - stacking of aromatic moieties, if the polyurea is prepared using aromatic diisocyanates. The soft domains consist of well-mixed hard and soft long chain aliphatic chains [30-32].

It is to be noted however, that discrete hard domains are formed only when the molecular weight of the soft segment cross a particular threshold. In the case of lower amines, the nano-segregation process results in the formation of a fully percolated hard domain phase. Hydrogen bonding between the urea linkages leads to the formation of nanometre-sized ribbon-shaped hard segments [33] which exhibit a super-ambient glass-transition temperature and are relatively ordered or crystallized. The soft domains on the other hand possess sub-ambient glass transition temperature, usually lower than $-30\text{ }^{\circ}\text{C}$ [33]. The soft-segment molecular weight can also have a profound effect on the nano-segregation process, affecting both the extent of segregation and the degree of ordering/crystallization within the hard domains [34].

It is the strong hydrogen bonding within the hard segments which is responsible for the high melting point exhibited by polyureas. A study on the thermo-mechanical measurements from a series of homologous polyurethane and polyurea materials, was performed, which quantitatively elucidated the role of the urea linkage with respect to the property distinctions between urethanes and ureas. The high melting point of polyurea is a result of the high Cohesive Energy Density (CED), which is defined as the ratio of the energy of vaporization (ΔE_{vap}) and molar volume (V_m) [35]. The effect of increasing chain length on the melting point of a homologous series of polymers is presented in Figure 1.1. Among the polymers shown, polyurea, polyamide and polyurethanes possess high CEDs as a result of their higher degrees of hydrogen bonding. The urea linkages, being resistant to hydrolysis, bestow polyureas with excellent resistance to alkali and acids [36].

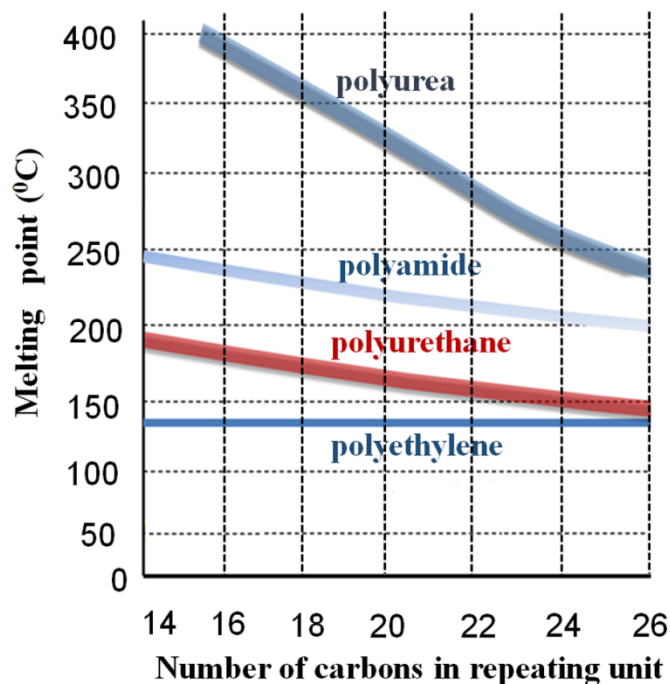


Figure 1.1: Effect of hydrogen bonding on the melting point of different classes of polymers [37]

Non-chain extended polyureas, do not have any covalent inter-chain cross-linking, and hence are often referred as thermoplastic cross-linked elastomers [38, 39]. However, depending upon the amount of higher-functionality isocyanate and amine, the polyurea structure may be designed to possess varying degree of covalent inter-chain cross-linking. It is this segregated microstructure which led researchers to explore the potential of polyurea in specialized fields, including linings in personnel-protective gear and as suspension pad material for minimizing traumatic brain injury (TBI) [40-43].

1.3.1 Quasi-static and Dynamic mechanical properties of polyurea.

In view of the enormous potential of polyurea in specialised applications, studies with reference to understanding their mechanical response under static and dynamic loads

have been performed [38, 40-42, 44, 45]. Defining a loading regime is essential to quantify the strain rate to which a material is subjected to. Extremely low strain rates ($<10^0\text{s}^{-1}$) as achievable by using universal testing machine, where the inertial effects can be largely neglected, is referred to as quasi static regime. Characterising elastomers at high strain rates is a difficult proposition, even at small amplitudes and conventional dynamic mechanical spectrometers are limited to low frequencies. Although time-temperature super-positioning (TTS) is often invoked to extend the effective frequency range of data, the results are considered rather inaccurate for measurements in the glass transition zone [46-48].

High strain rate studies are performed using the Split Hopkinson Pressure bar [49, 50]. It is to be noted, however, that in view of the low impedance of polyurea, classical methods of performing Split Hopkinson testing lead to erroneous results, and several modifications have been suggested. These include: use of sensitive piezoelectric sensors, hollow transmission bars and lower impedance polymeric pressure bars in addition to pulse shaping techniques. A comparative study of all these modifications has also been performed, which led the researchers to conclude that polymeric pressure bars of poly(methylmethacrylate) (PMMA) and hollow aluminium transmission bar are most suitable for high-strain rate characterization of polyurea [50, 51].

It has been realised that there exists a large gap between the low strain rate tests and the SHPB data. To address this issue, a drop weight tester was developed, which was capable of achieving large tensile strains at intermediate strain rates [52]. The developed facility was found to be capable of generating material properties free of artefacts due to inertia, inhomogeneous strains, and irregular strain rates.

It is to be noted that the highest strain rate possibly generated by SHPB system is limited to 10^4 s^{-1} . To extend the time-frequency scale, compressive relaxation experiments on polyurea using quasi-static tests have been performed under varied temperatures (-49°C to 22°C) which was subsequently used to construct a relaxation master curve over a reduced time range of 10^{-10} to 10^{-7} s, using the time temperature superposition (TTS) principle [53]. The validity of the same was demonstrated using simulation and SHPB measurements [54]. Subsequently, the applicability of this principle was contested [55], and dielectric spectroscopy measurements were conducted [56], [57] which allowed characterisation over much higher frequency range (10^{-2} to 10^6 Hz) and elevated pressures. To achieve even higher strain rates, laser spallation techniques have been developed, which use laser-generated high amplitude acoustic stress pulses of sharp temporal rise and fall times ($\sim 10^{-9}$ s) to dynamically load thin samples to excessively high strain rates [58] ($\sim 10^7 \text{ s}^{-1}$). This technique has recently been used to subject polyurea to ultra-high strain rates, and the studies have clearly highlighted the potential of polyurea films in high energy absorption (50–65 %) under high strain rates [59].

It is to be noted that generally the mechanical behaviour of all viscoelastic materials is strain rate sensitive [54]. Upon application of stress to any such material, certain sections of the elastic soft domain tend to rearrange, which in turn leads to generation of "back stress" in the material. During unloading, it is these accumulated stresses, which results in the return of the polymer to its original form, as shown in Figure 1.2.

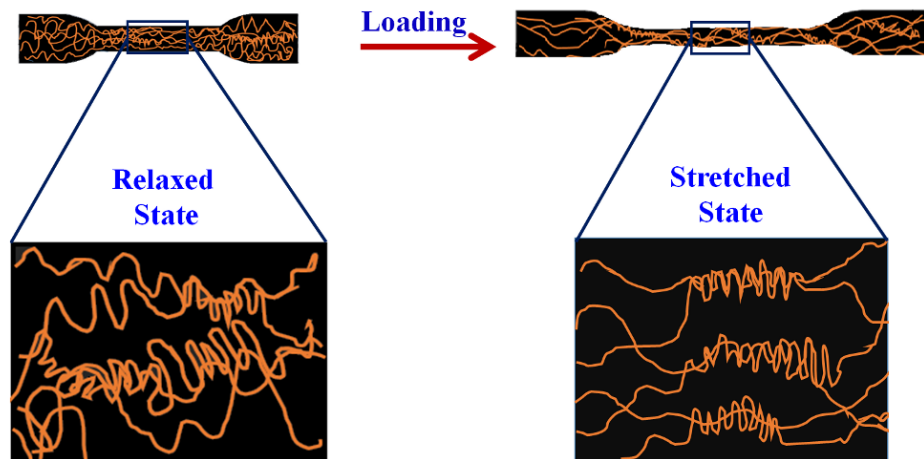


Figure 1.2: Micro-structural changes in polyurea upon tensile loading

The effect of increasing strain rate on the mechanical response of polyurea is presented in Figure 1.3. As can be seen, an apparently appearing ductile polyurea (under quasi-static regime) tends to exhibit higher modulus as the strain rate increases. At low strain rates, the polymer has enough time to respond to the applied load and with increase in the loading rate, these segmental motions are practically frozen. In general, this change in the material response (from ductile to brittle) is not associated with much energy absorption. However, in the case of polyurea, this very region encompasses a dynamic transition [57, 60] and therefore a lot of blast energy is absorbed and in certain cases, dissipated. It can also be assumed that this transition should be relatively easier for polymers which possess T_g closer to the test temperature. However, in certain cases where T_g is not especially high, a rubber-glass transition is still induced, a feature which has been attributed to the existence of a broad transition zone. This large breadth implies that even above the T_g , a large number of segmental modes are still active at frequencies associated with the rate of impact. This implies that the glass transition mechanism remains operative at temperatures well above T_g .

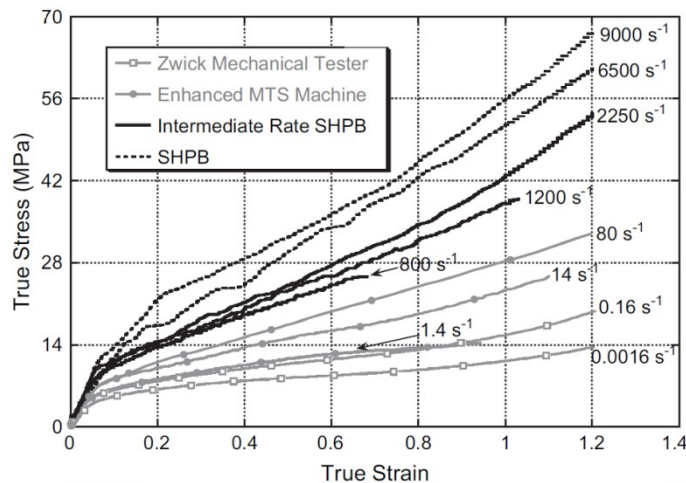


Figure 1.3: Uniaxial compression stress-strain behaviour of polyurea ranging from 10^{-3} s^{-1} to 9000 s^{-1} (each SHPB curve is labelled by its true strain rate of 0.6). Reproduced with permission from Elsevier [44].

The mechanical response of polyurea displays material constitutive non-linearity which shows in terms of high strain hardening at large strains, strain-rates as well as pressures [34]. The large strain stress-strain behaviour of polyurea shows strong hysteresis [61, 62], cyclic softening in addition to strong rate-dependence [63]. This unique combination of properties of polyurea is clearly a result of its complex nano-scale microstructure [62, 64-72] which in turn rationalizes its superior performance in blast-/shock-wave-mitigation applications.

The micro structural changes occurring during the deformation of polyurea have been studied with techniques like Wide angle XRD, Small angle X Ray scattering and time resolved FTIR [73, 74]. With increasing deformation, rotation and orientation of hard segment lamellar domains towards axis of elongation has been observed. This is also associated with stretching and shearing of soft segment chains. At very large strains ($> 300\%$) the hard segment domains were observed to reassemble to form fibrils [74].

The data obtained from quasi-static and high strain rate studies have been used to develop several constitutive models for polyurea [75-77]. In a recent review, many of these models were used to construct shock-Hugoniot relations which in turn, were validated with appropriate experimentations. It was reported that while different material models yield vastly different relations, predictions of most of the models are in reasonably good agreement with their experimental counterparts [78].

1.3.2 Retrofitting with polyurea: Effect on underlying substrate

The following section summarizes the findings related to retrofitting of structural element with polyurea coatings.

1.3.2.1 Retrofitting Unreinforced Masonry Structures

Preliminary investigations undertaken by the Air Force Research Laboratory (AFRL) dealt with the application of polyurea coating towards strengthening of masonry structures and light weight steel structures [1]. It was the positive outcome of this investigation, which paved the way for this technique to be evaluated on other types of structural materials [79, 80], like steel, FRPs etc. When polyurea reinforced masonry structures were subjected to explosive blast loadings, the elastomeric coating was found to undergo large deflections [2]. Although severely fractured, the coating reportedly improved the blast resistance of the masonry wall by containing the debris.

The success of this preliminary testing incited researchers towards exploring the potential of other polymers as retrofits [2]. Extruded thermoplastics, although possessing higher strength and modulus, were not taken up for further studies, in view of the inconvenience associated with their installation. Brush-on polymers were rejected in view of their brittle nature and lengthy curing time. Of the spray-on polymers, pure polyurea

was selected based on its strength, flammability resistance and economic viability [2]. Subsequent blast studies indicated that coating polyurea on the interior face of Unreinforced Masonry (URM) walls improved blast mitigation ability of the structure and were particularly beneficial towards containment of fragments. While the application of polyurea on both sides of the wall improved the capacity of the wall against blast loads, it was not considered worthwhile to merit additional cost [81]. These studies indicated that polyurea coated walls (~6 mm thick) withstood peak pressures greater than 400 kPa (60 psi) for one-way action walls as compared to a capacity of less than 35 kPa (5 psi) for URMs. It is however to be noted, that the search for the most appropriate polymer for the purpose of blast mitigation is still not over. If suitable techniques can be developed, whereby tough thermoplastic polymers can be made to adhere to the substrate, higher levels of blast mitigation may be expected. This is definitely an area, which will attract the attention of researchers in the near future.

Explosive tests have been conducted on URM walls with window or door openings, where polyurea has been coated only on a single face of the wall not confronting the blast [81]. The primary aim was to understand the failure and behaviour and establish the underlying failure mechanisms. It was proposed that the propagation of stress waves through walls led to fracture of weak sections. Localized large stress in the mortar-block interface led to the tearing of the polymer coatings at sites nearest to the supports. Flexural compression led to the fracture of front face of the shell of a few blocks. This was followed by tensile mode polymer tearing when the wall flexed and mortar joints cracking followed by debonding of the polymer coating at the boundary to the host structure.

Subsequently, an equivalent Single Degree-of-Freedom (SDOF) model was expounded to simulate the dynamic response of polyurea-retrofitted walls subjected to blast loads. The model was based on coupling of the bending and membrane resistance of the Concrete Masonry Unit (CMU)[82]. For the purpose of validation, a blast trial was conducted (Peak pressure: 5.8 kPa and pulse duration 20 msec) on a wall (3.05 × 3.05 m × 19.4 cm thick) which was spray coated with polyurea (2.1 mm). The wall recorded a deflection of ~ 178 mm during the trials. Interestingly, the apparent disparity between the prediction of deflection from the analytical model and the finite element code decreased as the maximum deflection of the wall increased between 1 to 2 times of the wall thickness [82].

Later, Hrynyk et al evaluated the efficacy of two schemes, i.e. a spray-on polyurea retrofit and a Glass Fibre reinforced polymer (GFRP)-polyurea composite (GFRP grid embedded in polyurea matrix), towards strengthening framed URM infill walls. Static load (one way arching action) was applied in order to simplify the testing program. A total of 8 URM walls were evaluated, of which 2 were constructed of clay brick (CL) units, 3 were constructed of CMU and the remaining 3 were constructed from masonry units produced from Wood-Fiber Fly Ash (WFFA). While all the retrofitting schemes exhibited improvements in energy dissipation capabilities, the polyurea retrofit was found to be the most effective in the context of energy dissipation and containment of fragments of the collapsed walls [84].

1.3.2.2 Application on Steel Structures and Plates

Ever since Defence Science and Technology Organisation (DSTO), Australia reported the efficacy of polyurea coating towards improving the blast resistance of steel plates [85, 86] studies on ballistic protection of steel using polyurea has been extensively

reported[40-43]. In a representative study,D36 steel plates (36 mm thick) were coated with different thicknesses of polyurea coatings and subjected to dynamic loads resulting from explosive charge (0.5 kg pentolite, 61 mm stand-off). Steel plates reportedly undergo ductile fracture through void nucleation, growth and coalescence, ultimately leading to the formation of dimpled fracture surfaces [87]. Polyurea coating was found to substantially improve the blast resistance of steel plates, where retrofitted plates recorded much reduced deformation as compared to the bare plate [88]. As expected, the degree of deformation was found to decrease with increasing polyurea thickness [86]. Studies on the application of polyurea onto armour grade steel plates and an examination of resulting failure modes have also been performed [26]. The effect of increasing thickness and locations of the polyurea on the blast mitigating ability was of particular interest. The studies clearly suggest that in comparison to increasing the steel thickness alone, increasing the thickness of polyurea is more efficient towards absorbing energy and preventing fragmentation [26]. A detailed numerical and experimental program of rigid projectile penetration through polyurea coated DH-36 steel plates was subsequently performed by Xue et al [89]. A positive contribution from the polyurea coating in terms of improving resistance against ballistic impact when applied at the back face of the plates was observed.

Several computational and experimental assessments of ballistic effects on high strength structural steel plates retrofitted with polyurea have been performed [90, 91]. Further, a set of reverse ballistic test was devised to assess the effect of polyurea coating on the dynamic response of steel plates [92-94]. All the studies revealed that retrofitting with polyurea led to positive outcomes, in terms of failure mitigation and energy absorption, when it was applied on the back face or the unloaded face of the plate. It was

interesting to note that the same coating, when applied on the blast-receiving face increased the destructive effects of the blast, which was attributed to the strain rate sensitivity of polyurea. It was proposed that the stiffness of polyurea increased manifolds (10-20 folds) when subjected to increasing pressure. This led to an impedance match of the polyurea with the steel plate thereby causing more energy to be transmitted to the underlying plate, leading to more damage. On the other hand, when polyurea coating was applied on the back face, the steel plate absorbed substantial amount of energy with a relatively smaller fraction being transmitted to the polyurea coating. The authors concluded that in the event of polyurea coating application on the blast-facing side of the sample, its presence may actually enhance the destructive effects of the blast, the actual scenario depending on the bond properties between the two materials at the interface [92-94].

In a separate study, however the experimental results indicated that the variation in coating location, either on front (blast-facing) or back face, did not cause any major effect to the maximum displacements recorded in the panels. Contrary to observation of Amini et al the plates which were coated on the blast-facing side, indicated lower kinetic energy as compared to the panels which were coated on the back or on both faces. The researchers considered it to be more worthwhile to apply polyurea coating on the blast-facing side. It was also suggested that the optimal ratio of the polyurea and steel for effective blast protection required further investigation, since there exists an upper limit in terms of polyurea thickness versus their effectiveness in terms of the deflection and kinetic energy [95].

1.3.2.3 Application on Composite Sandwich Systems and Structures

Fracture mitigation of polyurea coatings on composite substrates has also been studied extensively. Experimental investigations have been carried out to characterize the effect of polyurea coatings on E-glass reinforced vinyl-ester (EVE) composites subjected to blast loadings [25]. Permanent deformation, fiber breakage and delamination are primary amongst the numerous mechanisms responsible for blast-induced failure of fiber reinforced composite materials with the extent of damage increasing with increasing blast pressure amplitude [96-98].

The studies clearly suggest that composite materials prepared by sandwiching polyurea coatings between two composite skins are more effective as compared to neat composites and the polyurea plates. However, mechanisms responsible for the advantageous behaviour are not yet clear, and mandate more studies.

The dynamic behaviour of sandwich composites of EVE facesheets and Corecell™ A-series foam with a polyurea interlayer was subsequently studied under blast loadings using a shock tube [99]. The materials used were identical, with the only difference being the location of the polyurea interlayer. The results indicated that the application of polyurea behind the foam core and in front of the back facesheet led to reduction in the back face deflection, particle velocity, and in-plane strain, thereby improving the overall blast performance without compromising the structural integrity.

Bahei-El-Din & Dvorak [100-102] studied the mechanical response of composite sandwich plates with a polyurea interlayer under blast loads, where a detailed assessment on the influence of underlying material and their properties on through thickness propagation of the blast waves was conducted. Both conventional (designed as a closed cell foam core construction), as well as modified composite sandwich plate designs, were

modelled during the study, assuming a blast pressure of 100 MPa with a positive phase of 0.05 m sec on the outer facesheets of the plates. The studies indicated that the conventional plate underwent extensive thinning in the central foam core and the layer separated from both the outer (nearer to blast) and inner facesheets of the plate. However, both the modified designs exhibited significantly reduced deformations.

The effectiveness of polyurea coatings towards improving the blast mitigating properties of hollow composite cylinders have also been investigated in “under-water” conditions [103]. Studies reveal that thick interior coatings significantly reduce the energy released in the pressure pulse by slowing the collapse and softening the initial wall-to-wall contact. In contrast, thick exterior coatings increase this energy by suppressing damage, thereby reducing the energy absorption capacity of the structure.

1.3.3 Mechanisms underlying Polyurea-Induced Ballistic/ Blast-Mitigation

The fundamental objective behind employing elastomeric polyurea for retrofitting is to minimise the amount of load transferred to the main frame by allowing the wall to fail and dissipate energy, i.e. to use the polymer as a catching system. However the basic phenomena behind the ballistic and blast-/shock-wave mitigation capability of polyurea are apparently different, and are hence discussed separately in the following section.

1.3.3.1 Shock-Wave Mitigation: The shock-wave attenuation ability of polyurea is believed to be controlled primarily by the hard domains [31, 33, 40-43, 76, 104-110]. Presently, there is no general consensus regarding the mechanism underlying polyurea induced shock-wave mitigation. The most accepted mechanisms include the following:

Shock-wave-induced hard domain ordering

Shock-wave-induced hard- domain compaction and ordering has been identified as one, among the many, shock-wave-attenuation and dispersion mechanisms. The extent

of this blast-mitigation effect is expected to be directly proportional to the hard-domain volume fraction [33].

Shock-wave-induced hard domain crystallization/densification

The hard domains of polyurea experience an irreversible compaction and densification with an associated increase in their degree of order upon being subjected to shock-wave loading. These micro structural changes lead to dissipation and absorption of shock-wave kinetic energy and are hence considered to be responsible for the shock-mitigation ability of polyurea [33].

Shock wave induced hydrogen bond cleavage and formation

Bi-dentate H-bond (Figure 1.4) between the urea linkages (bond strength $\sim 21.8\text{kJ/mol}$) results in the formation of a phase separated micro-structure [111]. Exposure to shock loadings lead to the cleavage of these H-bonds, which subsequently rearrange to form more numerous H-bonds within the hard domains, thereby leading to the absorption and dispersion of shock energy [43, 109, 112].

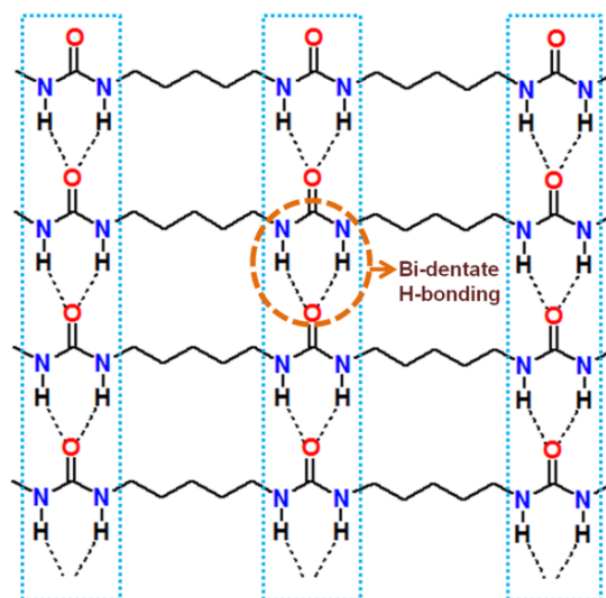


Figure 1.4: Hydrogen bonding within the urea linkages in polyurea

Viscoelastic stress relaxation within the hard-domains/soft matrix interfacial regions

Unlike purely elastic substances, viscoelastic materials like polyurea possess both elastic as well as viscous components. It is this viscous component, which endows strain rate sensitivity to polyurea. Purely elastic materials do not dissipate energy (in the form of heat) during cyclic loadings. Viscoelastic material, on the other hand, lose substantial energy, which is evidenced in the form of a hysteresis in the stress–strain curve, with the area of the hysteretic loop being proportional to the energy lost during the loading cycle [110, 113]. Representative mechanical response of polyurea under cyclic compression and tensile loadings is presented in Figure 1.5, where this hysteresis is clearly visible.

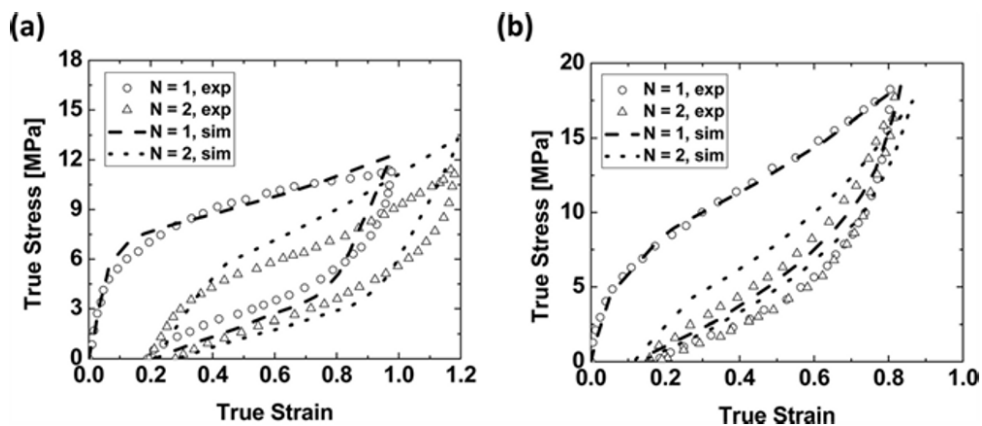


Figure 1.5: Cyclic compression and tension data, comparing model results with experimental data (a) stress–strain curves under cyclic compression at a strain rate of 0.1 s⁻¹ (b) stress–strain curves under cyclic tension at a strain rate of 0.015 s⁻¹. Reproduced with permission from Royal Society of Chemistry [113]

Shockwave-capture-and-neutralization

The ability of a material to mitigate shock waves is related to the shock-wave front profile within the material, more specifically by its width. The shock-wave front is generally broader in materials with higher shock-mitigation capacity. Thus, arrival of a shock-wave to a material boundary/interface is associated with a slow rate of momentum

transfer. In addition, shock-waves tend to propagate at much lower velocity in materials with higher shock- mitigation capacity. A dominant shockwave-mitigation mechanism in polyurea is the “Shockwave-capture-and-neutralization” phenomenon. Shock waves travel as a single wave in homogeneous materials. However, upon loading of a layered heterogeneous material system, e.g. polyurea, a two-wave structure is obtained—a leading shock front followed by a complex pattern that varies with time. This dual shock-wave pattern is attributed to the material architecture through which shock wave propagates, i.e. the impedance (and geometric) mismatch present at various length scales, and nonlinearities arising from material inelasticity and failure. This secondary trailing shock-wave (release wave), reportedly catches up with and attenuates the leading shockwave [34], thereby leading to shock attenuation. A schematic of this process is presented in Figure 1.6. Computational studies [34] reveal that larger is the ratio of release-wave speed to shockwave speed, the more efficient is the capture-and-neutralize shock-mitigation mechanism. It is to be noted that the shockwave speed is strongly dependant on the polyurea microstructure and for each shockwave-strength level, an optimum soft-segment molecular weight is optimal. This study clearly indicates that there is enormous scope in terms of designing polyurea for specific applications.

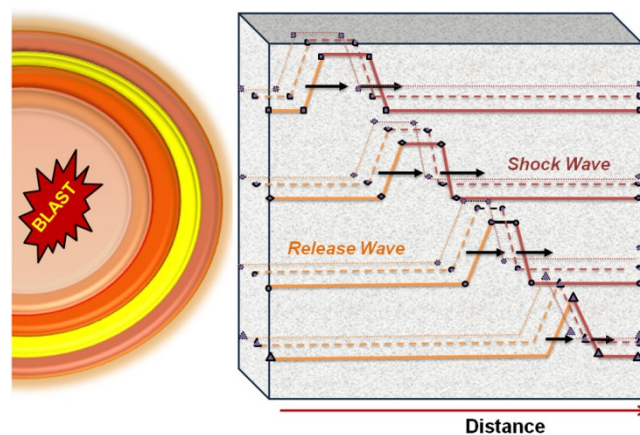


Figure 1.6: Shockwave capture and neutralization in phase separated materials

1.3.3.2 Ballistic Protection

The ballistic-protection efficacy of polyurea, on the other hand, is more due to its soft matrix than to its hard domains [114]. Interestingly, the contribution of H-bonds in this context is rather negligible. The most accepted mechanism behind the ballistic performance is the “rubber to glass second order transition” which occurs in polyurea when it is subjected to high strain rates [57]. Under such conditions, rubbers tend to respond in a glassy fashion, and undergo brittle failure. The reorientation and translational modes of the amorphous segments are unable to respond to the load and “freeze out”, leaving behind only the vibrational and secondary motions. These strain rates are comparable to the frequency range of segmental dispersion of polymers having high T_g (but lower than the test temperature), which induces a transition from the rubbery state to glassy state, dissipating significant amount of energy [60].

Conventionally, brittle fracture does not dissipate such large amount of energy, but in elastomers e.g. polyurea, brittleness is a direct consequence of the deformation which encompasses the glass transition zone. However, if the T_g of the elastomer differs from the test temperature substantially, exposure to high strain rates is incapable of inducing this transition and hence the extent of ballistic/ blast resistance is much lower than expected [60].

Dielectric spectroscopy has been used as an effective technique to illustrate the “rubber to glass transition” phenomenon in polyurea as a function of increasing frequency, which can be considered to be analogous to increasing strain rates. A set of ballistic impact experiments with a complimentary set of dielectric spectroscopic investigations has been performed and representative dielectric loss spectra for polyurea at different temperatures is presented in Figure 1.7 [55, 60]. The transition from rubber to

glass results in an increase followed by a decrease in the dielectric loss which appears as a hump in the spectra [55]. It is however to be noted that the frequency associated with this dynamic rubber- glass transition is ca. 10^6 Hz, which is only possible under ballistic loadings, and appears to be remote under blast loadings.

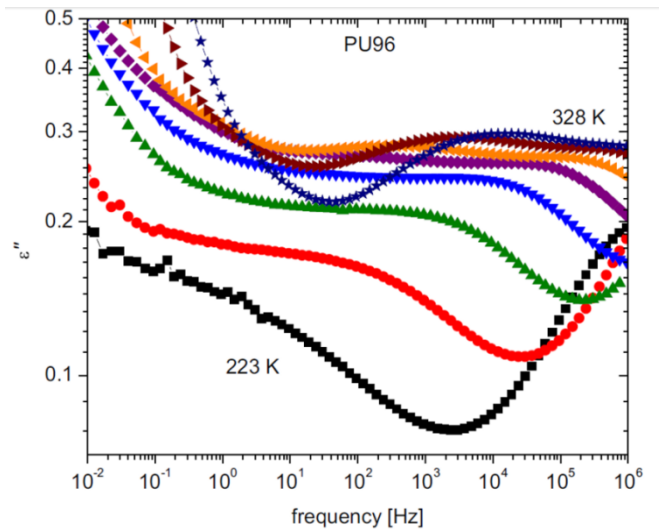


Figure 1.7: Representative dielectric loss spectra for dry PU96 at $P = 0.1$ MPa, for temperatures from $T = 223$ to 328 K in steps of 15 K. Reproduced with permission from Elsevier [55]

1.4 Research objective

Literature survey provided an overview of the strategies adopted for protecting structures susceptible to blast loadings. Polyurea coatings were found to be excellent candidates as retrofitting polymers. However, in view of the proprietary nature of polyurea, the compositional details of the formulations are not known, in terms of the type and amount of crosslinker, long chain amine and chain extender. It is extremely important to understand the effect of these individual components on the material properties in order to arrive at the optimal formulation, depending on the end application. Based on the literature survey, the following research gaps were identified

- The dependence of material properties on the soft segment length need to be established.
- The optimization of the ratio the aliphatic to aromatic chain extenders and the effect of concentration of crosslinker on material properties of polyurea need to be explored.
- The importance of viscosity matching of the co-reactants, i.e. amine and isocyanate for effective polyurea spray processing.
- The factor responsible for the evolution of material properties in the chain extended polyurea with time are to be demonstrated.
- The effect of thickness of the polyurea coating on the blast mitigating performance.

The main goal of this research is to develop sprayable polyurea formulations with optimal properties and to demonstrate the efficacy of the coatings towards retrofitting of structures susceptible to blast loadings. More specifically, the objective of this research includes:

- Development of polyurea formulations, which are processable using spray coating technique.
- Understanding the effect of the individual components of resin blend (namely chain extender, crosslinker and long chain amine) on the material properties of the cured polyurea coating.
- Monitoring the emergence of structural and mechanical properties with time.
- Exploring the efficacy of polyurea coatings towards improving the blast survivability of underlying substrate under blast loading conditions.

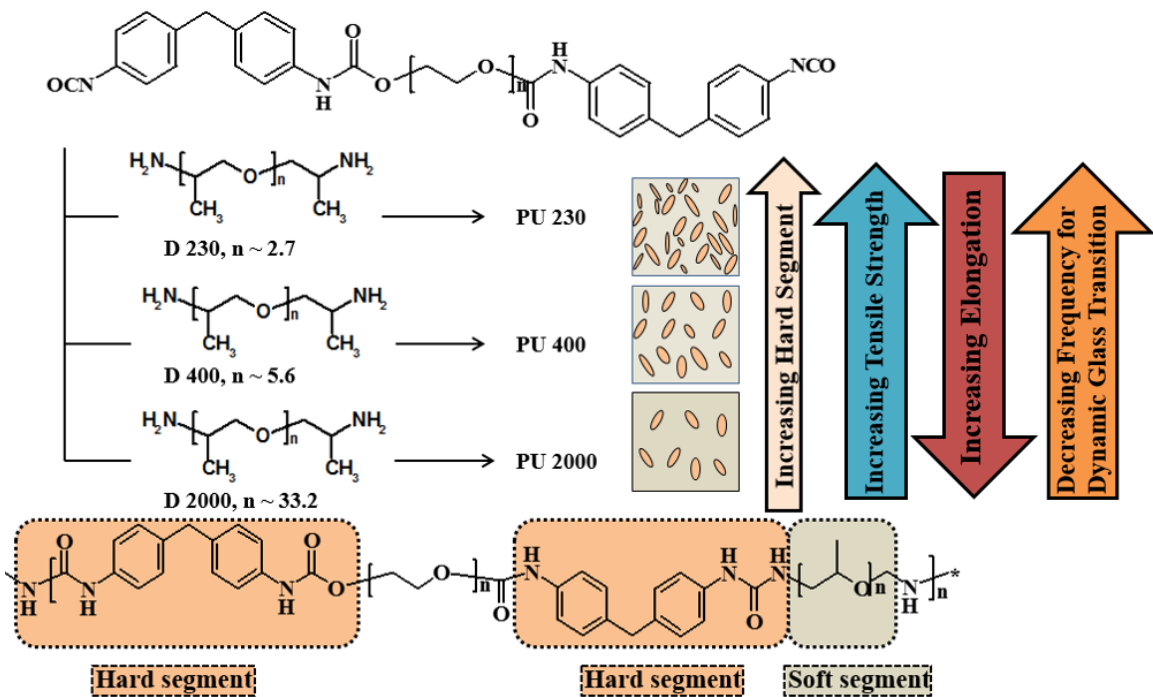
1.5 Implementation of work plan

A systematic methodology was adopted for the proposed work, which involves following steps:

- Identification of suitable reactants (isocyanate and amine) along with diluents for preparation of polyurea formulations.
- Preparation of isocyanate and resin blend formulations to study:
 - The effect of increasing chain length of soft segment
 - The effect of type and amount of chain extenders
 - The effect of crosslinker concentration
- Matching the viscosity of reactants towards smooth processing of polyurea formulations by spray-coating.
- Monitoring the evolution of material properties in polyurea coatings.
- Shock tube testing of the polyurea coated concrete to establish the survivability of retrofitted structures under blast loadings.

Chapter 2

Polyurea coatings: Dependence of material properties on soft segment length



2.1 Introduction

Polyurea is formed by the rapid reaction of diisocyanate ($-N=C=O$) with diamine ($-NH_2$) forming hard domains, which remain heterogeneously dispersed within a matrix of flexible chains, commonly referred to as the soft phase [29, 55, 115]. Thermodynamic incompatibility between the hard and soft segments result in phase segregation, leading to a two-phase morphology [30, 116]. The hard segments are extensively H-bonded and serve both as reversible physical cross-links as well as reinforcing fillers, thereby bestowing excellent mechanical properties to the polymer [29, 117, 118]. What renders this particular class of polymer fascinating is that the formulations can be tuned to offer a range of mechanical properties, from soft rubber to hard plastic, by tuning the causal ‘hard’ and ‘soft’ domain structure. In this chapter, we attempt to understand the effect of increasing soft segment length on the material properties of segmented polyureas.

The soft domains in polyurea are formed of long polyether chains, which exhibit a glass transition temperature (T_g) much below ambient [33, 117, 119]. The material thus exists in the “rubbery” region at room temperatures. It is surprising to note that although PPO based amines are the “workhorse” of the polyurea industry, systematic studies on the mechanical response of such formulations are unavailable in public domain, which inspired us to take up this study. In addition, both the methodology adopted for preparation of polyurea as well as the operating conditions involved also affect the morphology as well as resulting properties of the polymer [118, 120]. Due to the difference in the T_g of the soft and hard segments, polyurea behaves like a cross-linked elastomer reinforced by the nano-size hard domains [32] which serve as focal centers for mechanical constraints. The wide transition zone of polyurea from rubbery

state to glassy state renders the viscoelastic properties of polyurea highly sensitive to several parameters especially temperature, pressure and strain rate [56].

In all commercial polyurea formulations, chain extenders are included in the “amine component” to increase the hard segment content and the extent of microphase separation, which reflect in terms of its mechanical properties. Wilkomm et.al [120] studied the mechanical properties of polyurea in which the hard segment content was increased by introducing diethyltoluenediamine (DETDA) in the formulation. The toughness of polyurea was found to be inversely proportional to the soft segment content, with formulations containing higher hard segment (70%) being relatively more brittle. Subsequently, Wang et.al [115] followed the curing process of DETDA extended polyurea prepared from PPO based amine and methylene diphenyl diisocyanate (MDI) through fluorescence and IR spectroscopic techniques. The studies revealed that although the solidification resulting from the reaction of isocyanate and amine takes place instantaneously, the curing process requires substantially longer periods (~50 minutes) for completion.

Substantial information can be gathered from studies on non-chain extended polyureas, particularly with respect to the effect of increasing chain length on the mechanical properties. Interestingly, studies on segmented non-chain extended polyureas are relatively less reported [38]. The effect of increasing soft segment length on the structure-property relationship of non-chain extended polyureas containing poly(tetramethyleneoxide) (PTMO) based soft segments have been studied, which revealed that increasing the soft segment length adversely affected the “service window” of polyurea [38]. The influence of soft segment length based on PTMO on the phase-separated microstructure of polyurea and the state of hydrogen-bonded associations in the

polymer has also been studied [32]. Surprisingly, studies on non-chain extended polyureas, where the soft segment is based on PPO have not been reported. In view of the increasing use of PPO based amines in commercial formulations, such studies are definitely desirable. The aim of this chapter is to demonstrate thoroughly, the effect of increasing soft segment length on the mechanical properties of polyurea, by varying the molecular weight of the reacting PPO based polyether chains.

The underlying mechanism responsible for the ballistic and blast/shock-wave mitigation capability of polyurea has been extensively discussed in the literature [33, 43, 60, 117, 121]. One of the most accepted mechanisms is a dynamic “Rubber-glass transition” when polyurea is subjected to blast/ ballistic loading, whereas vitrification process reportedly transpires in polyurea [55, 121, 122]. The quantification of the frequency mandated for this process can be determined by systematic dynamic mechanical analysis (DMA) over a range of frequencies and temperatures. These studies can be used to understand the mechanical response of the polymer upon being subjected to dynamic loadings. In this study, a classical time–temperature superposition (TTS) is used to approximate the mechanical properties of polyurea using the dynamic mechanical analysis data, since directly measurement in such a broad frequency range is not readily available. Of particular interest is to identify the frequency associated with the dynamic loading process, which can initiate the dynamic ‘glass transition’ process in polyurea.

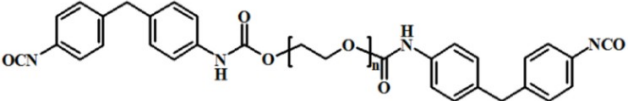
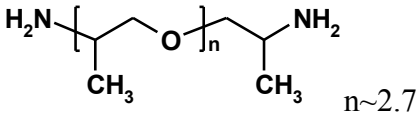
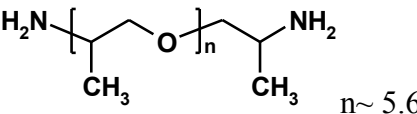
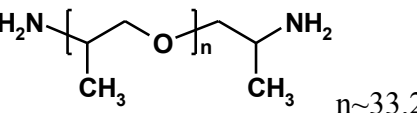
2.2 Experimental

2.2.1 Materials

Commercial MDI prepolymer, especially designed for polyurea spray elastomers applications, Suprasec 2054 with a NCO = 15 %, viscosity of 775 mPa.s at 25 °C, was purchased from Huntsman. Poly(propyleneoxide) (PPO) based amines of different

molecular weights JEFFAMINE[®]D-230, JEFFAMINE[®]D-400 and JEFFAMINE[®]D-2000 were procured from Huntsman. Here ‘D’ refers to ‘difunctionality’ and the subsequent number refers to the approximate molecular weight of each species. Physico-chemical properties of the reactants are presented in Table 1. CH₂Cl₂ (CDH) was used as the diluent without further purification.

Table 2.1: Characteristic properties of reagents

Designation	n _{eq}	ρ(g/cc)	Structure
Suprasec 2054	3.57	1.09	
Jeffamine D 230	8.1- 8.7	0.93	
Jeffamine D 400	4.1- 4.7	0.96	
Jeffamine D 2000	0.96 - 1.05	0.98	

2.2.2 Polyurea synthesis

All the polymerization reactions were conducted in three-necked, round bottom flask equipped with an overhead stirrer and nitrogen inlet. The reactions were effected at room temperature in dichloromethane (15-20% solid content) under dropwise addition of diamine solution to the diisocyanate solution under strong agitation (350 rpm). The exact quantity of the diamines was calculated as per the established formula (Equation 1.1)

in equation 1.1, the m_{iso} and m_{amine} refer to the mass of isocyanate and diamine respectively and $n_{eq,iso}$ and $n_{eq,amine}$ are the equivalent number of isocyanate and amine (Table 2.1) and i_{NCO} is the NCO index maintained for the formulation. A preliminary set of experiments was performed to arrive at the optimal isocyanate index, for which the i_{NCO} was varied from 0.9 to 1.15. The hard segment content is generally calculated as the ratio of mass of isocyanate and chain extender to total mass (Refer Equation 1.3), however in the absence of chain extender, the following formula was used for its estimation.

$$\text{Hard Segment (\%)} = \frac{m_{iso}}{m_{iso} + m_{amine}} \times 100 \dots \dots \dots (2.1)$$

Where, m_{iso} and m_{amine} refer to the amount (g) of isocyanate and amine respectively

2.2.3 Film preparation

Films of requisite thickness (~1 mm) were obtained by pouring the polymer solution thus obtained into Teflon molds. The molds were adequately covered to permit solvent evaporation at a sufficiently slow rate so as to prevent bubble formation. Subsequently, the molds were placed in a vacuum oven at 60 °C to ensure complete removal of solvent, the process being monitored gravimetrically. The resulting films were then removed and stored under vacuum for consequent analysis. The polyurea films were designated as PU followed by a numerical suffix indicating the molecular weight of diamine from which it is derived. For example, PU 230 refers to the polyurea films prepared using isocyanate precursor (Suprasec 2054) and Jeffamine D230.

2.2.4 Characterization methods

Anton Paar Rheometer MCR-CTD 620 was used to investigate the chemorheological behavior of the formulation during the polymerization reaction using 25 mm disposable aluminium parallel plates. The oscillatory shear flow studies were conducted

under isothermal conditions. The test fixture was initially preheated to the desired isothermal cure temperature. The plates were subsequently separated and the polyurea formulation was rapidly inserted. The plates were then brought back to a gap of approximately 1.0 mm and the sample was trimmed flush with the edges of the fixture. The experiment was finally initiated when the desired set temperature was achieved. The viscoelastic properties of the sample during cure, including the complex dynamic viscosity (η^*), shear storage modulus (G'), and shear loss modulus (G'') were monitored.

The thermal properties of the samples were investigated using Differential Scanning Calorimetry (TA instruments, Q 20 module) under nitrogen atmosphere. 5 mg of the sample was placed in a 40 μ L aluminium cap without pin and sealed with a lid. Samples were heated under a nitrogen gas flow of 50 mL min^{-1} from room temperature to 250 $^{\circ}\text{C}$ at a rate of 10 $^{\circ}\text{C min}^{-1}$ to prevent oxidative degradation of the sample during analysis, with two replicates being analysed for each set. The T_g was estimated from the midpoint of the glass transition phenomenon. The thermal degradation behavior of samples was investigated using Perkin Elmer Diamond STG-DTA-DSC under N_2 atmosphere in the temperature range of 50-800 $^{\circ}\text{C}$. A heating rate of 10 $^{\circ}\text{C/min}$ and a sample mass of 5.0 ± 0.5 mg were used for each experiment.

The FTIR spectra of polyurea samples were recorded for the structural characterization in the wavelength range 4000 - 600 cm^{-1} using Fourier Transform Infrared (FTIR) spectroscopy on a Thermo Fisher FTIR (NICOLET 8700) with an attenuated total reflectance (ATR) crystal accessory having characteristic angle of incidence of 45° , with the resolution of 4cm^{-1} and 32 scans

Dynamic mechanical analysis was performed on rectangular specimens (50 mm \times 8 mm \times 3 mm) using DMA (Artemis 242E, Netzsch). A dual-cantilever bending mode

was used, which permitted controlled movement of the sample during testing. The nominal sample size for the DMA test is 50 mm × 8 mm × 3 mm (l × b × h). Experiments were conducted at different frequencies (1, 5, 10 and 20 Hz) over a broad temperature range (-70 to 150°C @2°C/min).

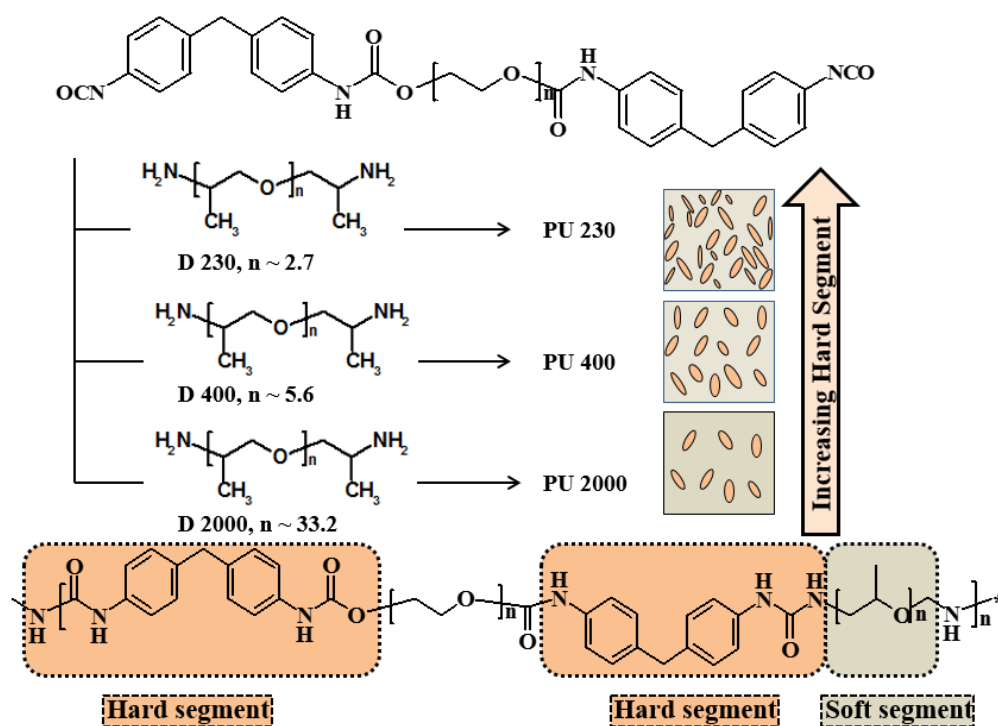
Mechanical properties were measured in tensile mode using Universal Testing Machine (International Equipments) as per ASTM D 412C at 50 mm/min. Transparent tensile coupons of a representative formulation (PU 230) are presented in Figure 2.1. At least five specimens were tested and the average results along with the standard deviation values have been reported.



Figure 2.1: Transparent tensile coupons of polyurea (PU 230)

2.3 Results and discussions

The reaction between the isocyanate precursor ($O=N=C-R-C=N=O$) with diamine (NH_2-R-NH_2) is presented in Scheme 2.1. An expressive representative phase separated microstructure is also included for the sake of visualization. It has been pictorially represented that as the molecular weight of the polyether amine increases, the hard segment content decreases and so does the extent of phase separation.



Scheme 2.1: Schematic, illustrating the reaction of diisocyanate with diamines of varying molecular weight

Theoretically, for the formation of a linear polyurea chain, a single mole of diisocyanate reacts with another mole of diamine. However, the isocyanate index can be varied in order to obtain the most effective isocyanate to amine ratio. A preliminary set of studies was performed to arrive at the optimal isocyanate index, where polyurea films were prepared with varying index ($i_{NCO} = 0.9 - 1.15$). Representative tensile stress-strain curves along with the variation of mechanical properties for a representative formulation (PU 230) are presented in Figure 2.2 and Figure 2.3. When subjected to tensile deformation, polyurea exhibits yielding, followed by a large upturn in the stress [123]. The consequent large energy dissipation, reflecting a large internal friction and irreversible structural changes, leads to superior toughness in the polymer.

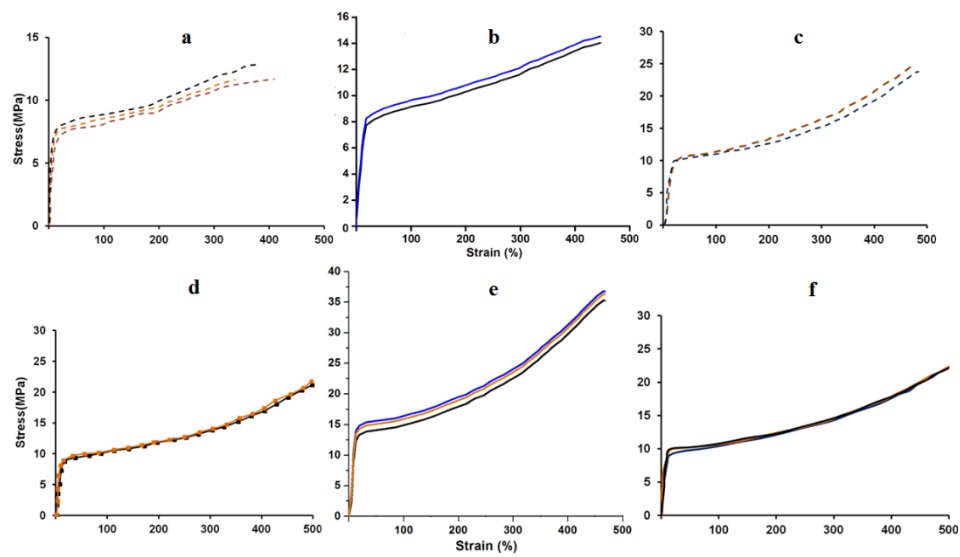


Figure 2.2: Representative stress-strain curves for PU 230 prepared with varying isocyanate index (i_{NCO}) a) 0.9, b) 0.95, c) 1, d) 1.05, e) 1.1, f) 1.15

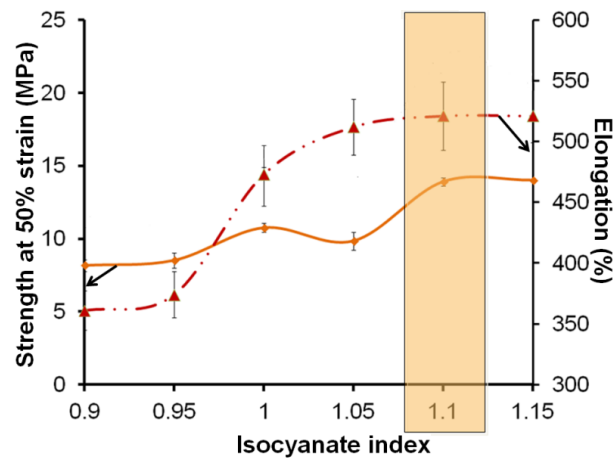


Figure 2.3: Variation of characteristic mechanical properties as a function of isocyanate index for PU 230

Since optimal properties were achieved at an isocyanate index of 1.1, further detailed studies were performed on films prepared from formulations with i_{NCO} of 1.1.

2.3.1 Chemo-rheological response

The effect of increasing molecular weight of the polyetheramines ('soft' segment) on the chemo-rheological response during polyurea formation was studied under

isothermal conditions (50°C) and the variation of storage (G') and loss modulus (G'') is presented in Figure 2.4. In view of the predominance of the viscous nature of the reactants, the loss modulus is relatively higher than the storage modulus in the initial stages of the reaction. Due to the reaction between the diisocyanate and diamine, both G' and G'' increase, and a crossover gelation region is reached, when G' equals G'' . This region marks a sudden transition of the viscous liquid to an elastic solid, where equal amount of energy is stored as well as dissipated by the material.

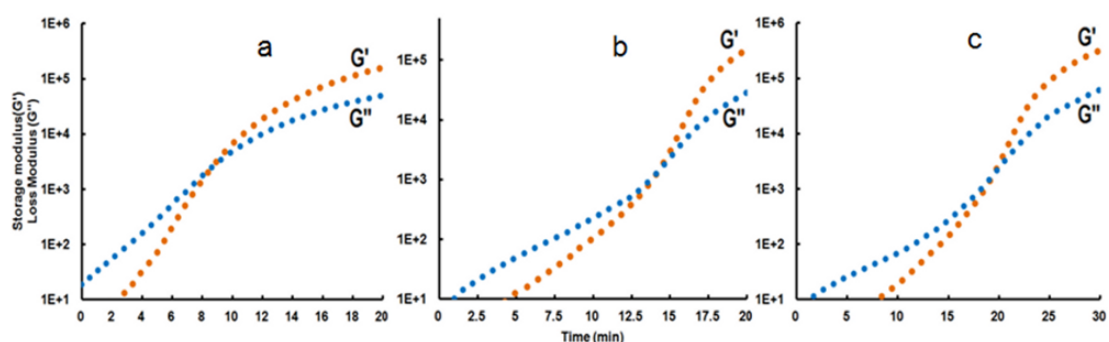


Figure 2.4: Evolution of storage and loss modulus in polyurea formulations (a) PU 230, (b) PU 400 and c) PU 2000

It is interesting to note that the dependency of “gelation time” on the molecular weight of the co-reactant polyetheramines. PU 230 gels within 10 minutes of reaction, while PU 400 and PU 2000 require ~15 and ~20 minutes respectively. This can be attributed to the relatively larger number of reacting moieties per unit volume in the former, which decreases with increasing molecular weight of the polyether amine.

2.3.2 Structural characterization

The reaction between isocyanate and amine leads to the formation of urea linkages, and the reaction was followed through FTIR spectroscopy. The FTIR spectra was found to be similar for all the formulations, and the changes as a result of time for a representative formulation (PU 230) is presented in Figure 2.5. Appreciable shifts in the

positions of the amine (N-H) and carbonyl (>C=O) groups result due to inter-molecular or intra-molecular hydrogen bonding in urea. The relative peak intensities can generate valuable quantitative information on the extent of microphase separation in the sample. The peak positions associated with >C=O and N-H groups, and the changes occurring as a result of the reaction is presented in (Table 2.2).

Table 2.2: Characteristic absorption frequencies in segmented polyurea

Group	Mode	Wavenumber (cm ⁻¹)
N-H	Free	3445-3450
N-H	N-H...N-H	3315-3340
N-H	N-H...O (ether)	3260-3290
N-H (wag)		1500-1600
>C=O (urethane)	Free	1730-1740
>C=O (urethane)	>C=O...H-N	1703-1710
>C=O (urethane)	>C=O...H-N	1680-1695 (ordered)
>C=O (urea)	Free	1690-1700
>C=O (urea)	>C=O...H-N	1660-1670 (disordered)
>C=O (urea)	>C=O...H-N	1630-1645 (ordered)
N=C=O	Free	2270
NH-C=O	Amide II	1540-1560

Presence of free carbonyl (>C=O) in the isocyanate prepolymer leads to appearance of a sharp peak in the 1730–1740 cm⁻¹, however H-bonded and ordered carbonyl peak (>C=O...H-N) formed as a result of the formation of urea functionalities appear in the region 1680–1695 cm⁻¹. It can be seen in Figure 2.5 that the intensity of the initially strong, free >C=O peak at 1730 cm⁻¹ reduces with time. On the other hand, the strongly hydrogen bonded >C=O peak at 1680 cm⁻¹, which is not present initially, increases and strengthens with time.

The N-H stretching of amine appears in the region 3300-3000 cm^{-1} . In the spectra of the primary amine (D230), two bands due to N-H stretching are noticeable: a broad peak due to asymmetrical stretching at $\sim 3300\text{--}3400 \text{ cm}^{-1}$ and another due to symmetrical stretching at $\sim 3330\text{--}3250 \text{ cm}^{-1}$. Due to the reaction of the amine with isocyanate, urea linkages are formed, and a shift in the position of the N-H stretching band is perceptible, which shifts to slightly lower wavenumber as a result of hydrogen bonding within the urea hard segments. Another characteristic change is the decrease in the intensity associated with the isocyanate ($\text{N}=\text{C}=\text{O}$) groups, appearing at 2270 cm^{-1} . It was observed that the complete disappearance of this peak mandates $\sim 8 \text{ h}$, irrespective of the chain length of the polyetheramine involved. Our studies further confirm that although the polyurea formulations gel in a very short time frame, which lead to very short ‘tack free’ time [124], the reaction continues within the matrix for much longer periods.

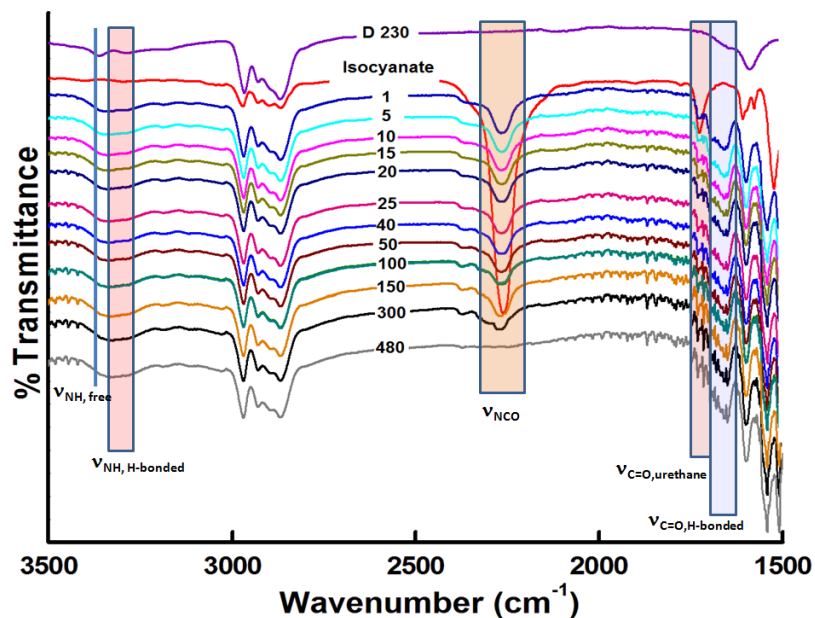


Figure 2.5: Changes in the FTIR spectra due to the reaction of isocyanate with amine (PU 230)

2.3.3 Calorimetric studies

Thermodynamic incompatibility between the ‘soft’ and ‘hard’ segments at low temperatures results in their segregation during the polymerization stage itself. The remarkable properties of segmented polyureas are, in fact, an indirect manifestation of this microphase separation between the incompatible domains, which are linked through covalent bonds. Previous studies have revealed that the domain dimensions associated with the hard segments vary from few to tens of nanometers in size[125]. The DSC traces (second heating scan) of all the formulations prepared are presented Figure 2.6, with the T_g 's being explicitly mentioned in the figure.

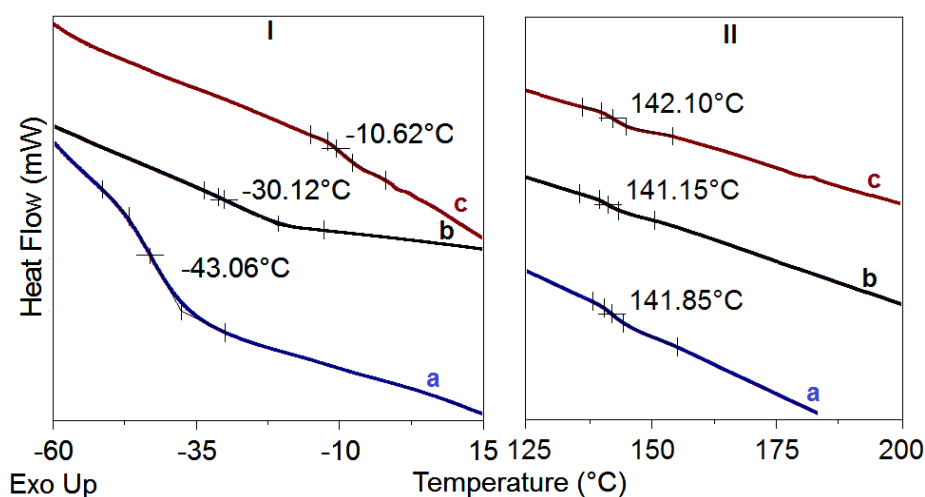


Figure 2.6: DSC traces a) PU 2000, b) PU400 and c) PU 230

Polyurea has been reported to exhibit two glass transition temperatures [30]: the T_g at lower temperature being associated with the soft segmental motion, while the higher temperature T_g is attributed to the motions of hard segment [126]. It is the sub-ambient glass transition temperature associated with the soft segmental motions, which are responsible for the elastomeric nature of the polymer at room temperature. The dependencies of both the glass transition temperatures on the % hard segment are presented in Figure 2.7. It is interesting to observe the dependence of the low temperature

T_g on the ‘soft’ segment length. As expected, PU 2000 with the largest ‘distance between physical crosslinks’ exhibits lowest T_g , which increases with decreasing molecular weight of the polyetheramine reactant.

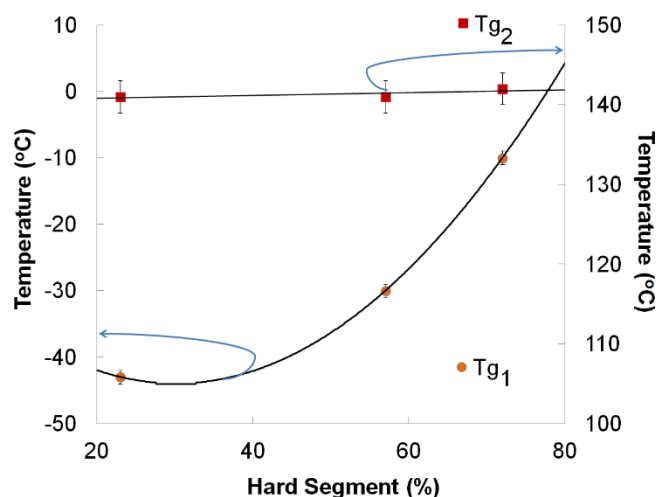


Figure 2.7: Variation in glass-transition temperatures of polyurea networks PU- 2000 (HS-23), PU-400 (HS-57) and PU-230 (HS-73) with hard segment

Interestingly, there is no significant change in the glass transition temperature associated with the segmental motions of the “hard domains”, which remain practically constant at $\sim 140\text{-}144^\circ\text{C}$. It is the presence of these urea-rich hard segments, self-assembled through hydrogen bonds, which mechanically constrain the movement of soft segments during mechanical stress.

2.3.4 Mechanical properties: Effect of soft-segment length

The variation in tensile strength and elongation at break with increasing soft segment molecular weight is presented in Figure 2.8. It is clear from the figure that with increasing hard segment content, tensile strength increases with a proportional decrease in percentage elongation at break.

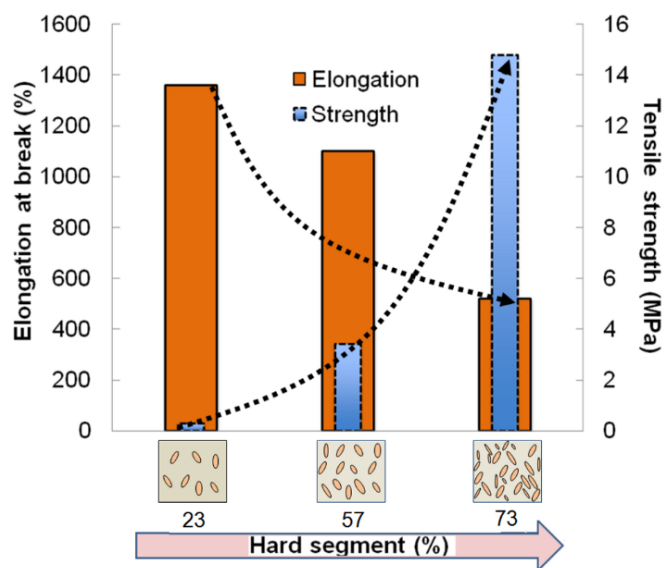


Figure 2.8: Effect of increasing hard segment on characteristic mechanical properties

2.3.5 Dynamic mechanical analysis

Dynamic mechanical analysis was performed on the polyurea formulations in dual cantilever mode. The ratio of dynamic stress to dynamic strain yielded complex modulus (E^*), which was resolved to obtain the in-phase component (Storage modulus, $E' = E^* \sin \Theta$), and the out-of-phase component (Loss modulus, $E'' = E^* \cos \Theta$). The former (E') represents the stiffness of the material, and E'' is indicative of the ability of the material to dissipate mechanical energy. The ratio of loss and storage moduli (referred to as $\tan \delta$) is representative of the ratio of the dissipated and stored mechanical energy in each loading cycle.

The variation of storage and loss modulus of the polyurea formulation with varying soft segment length as a function of temperature (at $\nu = 1, 5, 10$ and 20 Hz) is presented in Figure 2.9. A single relaxation peak is clearly evident in all the formulations, which is attributed to the segmental motions linked with the soft segments in the polymer. Throughout the transition zone of polyurea, its stiffness, as indicated by E' decrease drastically as the material transitions from 'glass' to 'rubber'. It is to be noted

that the soft segments comprising of the polyether chains are chemically linked to the hard segments through the urea linkages. Under such conditions of permanent attachment, the resulting composite is expected to exhibit separate glass transitions [127]: one associated with the soft chains far from the hard domains, while the other is at relatively higher temperatures, due to the movement of chains in the vicinity of the hard segments.

It is noteworthy to observe a systematic shift of the relaxation peak towards higher temperature as the soft segment length decreases. The glass transition temperature is quantified in terms of the loss modulus peak. A sub-zero T_{gl} [128, 129] was evidenced at -42°C (1Hz) for PU 2000, which shifted to -23°C and -16°C for PU 400 and PU 230 respectively. It is interesting to note the large width associated with the glass transition phenomenon ($\Delta T \sim 80^{\circ}\text{C}$), which is a property rather unique to polyurea [118].

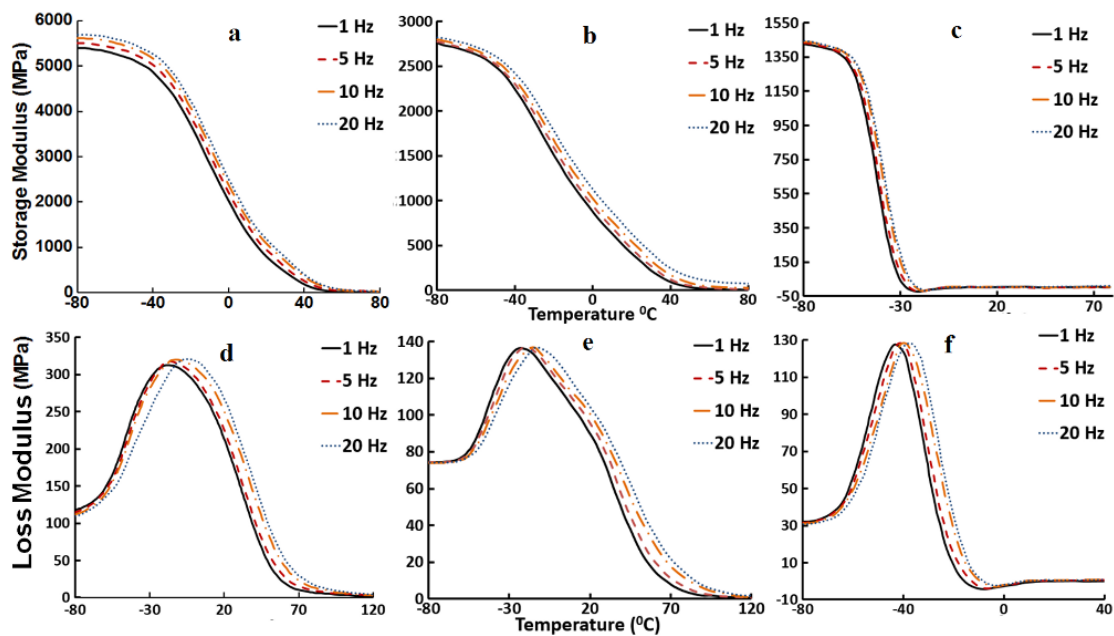


Figure 2.9: Variation of storage and loss modulus with temperature at different frequencies a) PU-230, b) PU-400 c) PU-2000

As the frequency of the dynamic loading is increased, an organized shift in both the loss and storage modulus trace towards higher temperature is clearly evidenced [118, 128-130]. It is to be noted that increasing the testing temperature has the same effect on its mechanical properties as decreasing the speed of testing i.e. the frequency associated with the dynamic tests [128]. This particularly interesting association permits the determination of mechanical properties over a wide frequency range by conducting tests at relatively narrow frequencies. This procedure, commonly referred to as the Time–Temperature Superposition (TTS), was applied to arrive at the frequency domain master curves, spanning over a large frequency range of 10^{-15} to 10^{20} Hz. The master curves hence obtained in terms of loss modulus variation at different temperatures (245 K to 298 K) for the various formulations are presented in Figure 2.10. A significant shift in the loss modulus peak is clearly evident in all formulations with increasing temperatures. This can be credited to the requirement of higher frequencies for ‘freezing’ of segmental motions at higher temperatures [121].

The purpose of performing DMA studies on polyureas with different soft segment length was to establish the frequency required for the material to undergo dynamic glass transition process. Under blast loading conditions, rise-time (t_{rise}) in pressure-time profile has been found to vary from 2 to 6 ms, ($v_{\text{blast}} \sim 150\text{-}500$ Hz) [25, 131]. Our studies indicate that under ambient temperatures, the dynamic glass transition process necessitates relatively high frequencies ($\sim 10^{15}$ Hz) for PU 2000, while the same is of the order of 10^5 Hz for PU 230. However, it can be concluded that the frequency associated with blast loadings ($\sim 10^2$ Hz) is insufficient for the process of vitrification vide the much-cited “dynamic glass transition” phenomenon to occur. Our studies reveal that polyurea essentially remains in the rubbery regime, even under exposure to blast loading conditions

and therefore the coating acts as a “catcher system” for the fragments formed. Parallely, shock-wave-induced hard domain ordering and crystallization, rearrangements in the H-bonds and shock wave capture and neutralization also contribute to the blast mitigating ability of polyurea [33, 43, 109, 132].

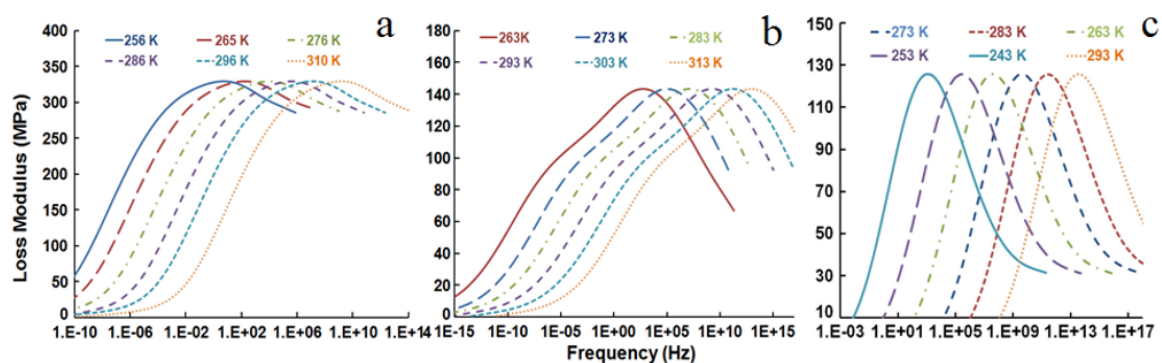


Figure 2.10: Master curves depicting the systematic variation in loss modulus in polyurea a) PU-230, b) PU-400 c) PU-2000

2.3.6 Thermal characterization

The TG traces of the polyurea formulations (under nitrogen atmosphere) are presented in Figure 2.11. The corresponding derivative thermogravimetric (DTG) traces are also included in the figure. As can be seen, all the polyurea samples exhibited two-step degradation, located at ~ 350 and ~ 400 °C (peak of the DTG trace). The first mass loss is attributed to the decomposition of hard segment (primarily urea linkages), in view of their relatively lower thermal stability. Previously, studies using hyphenated techniques have revealed that this initial decomposition step leads to evolution of carbon dioxide primarily. The subsequent mass loss occurs due to the pyrolytic decomposition of the soft segments, polyether linkages in the present case, leading to evolution of hydrocarbons in larger amounts [126]. As expected, the mass loss associated with the first and second stages vary with the percentage hard segment present in the composition. The mass loss associated with the thermal degradation steps along with the char content (at 600°C) is

presented in Table 2.3.

Table 2.3: Mass loss associated with step-wise thermal degradation of polyurea

Sample	Mass loss (%)		Char content at 600°C (%)
	(1 st step, hard segment)	(2 nd step, soft segment)	
PU 230	69.5	25.2	5.3
PU 400	56.4	37.0	6.6
PU 2000	30.0	65.5	4.5

In line with our expectations, the polymer with larger soft content (PU 2000) was found to exhibit larger mass loss with the second degradation step. In all the cases, the decomposition process of polyurea was found to result in the formation of char residue (~6 wt.%).

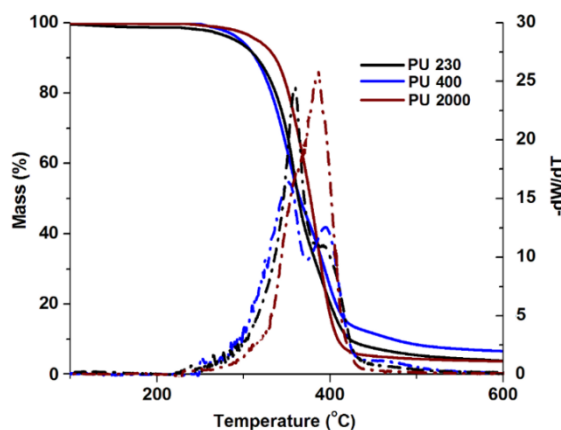


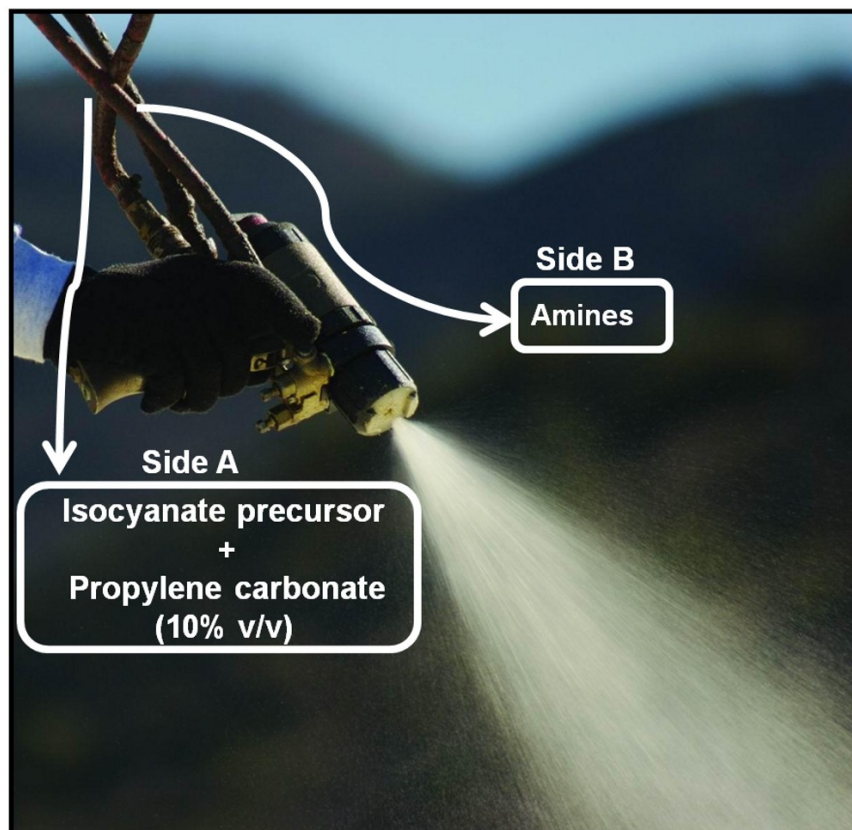
Figure 2.11: TG-DTG trace of polyurea samples

Our studies reveal that the soft segment chain length plays an extremely pronounced role in defining the material properties of polyurea. Characteristic mechanical properties, namely “strength” and “elongation at break” can be tuned by regulating the soft-segment length, which in turn can be achieved by varying the molecular weight of the diamine used for its preparation. The tensile strength was found to vary inversely with the soft segment length, while the elongation was found to be directly proportional. The mechanical properties of polyurea are a direct manifestation of its phase-separated

microstructure, comprising of hard segments dispersed heterogeneously within soft domains. The low temperature T_g associated with the segmental motions associated with the polyether soft segments was found to increase significantly with its chain length (-43°C for PU 2000 to -10°C for PU 230), while the high temperature T_g remained practically constant at 140-144°C. Detailed dynamic mechanical studies indicated that the arresting of segmental motions associated with longer 'soft segments' mandate relatively higher frequencies. As a consequence, the dynamic glass transition process necessitates much high frequency for polyurea with longer soft segment length ($\sim 10^{15}$ Hz for PU 2000), while the same is much lower for polyurea with lower chain length ($\sim 10^5$ Hz for PU 230).

Chapter 3

Spray-processing of polyurea: Importance of viscosity matching



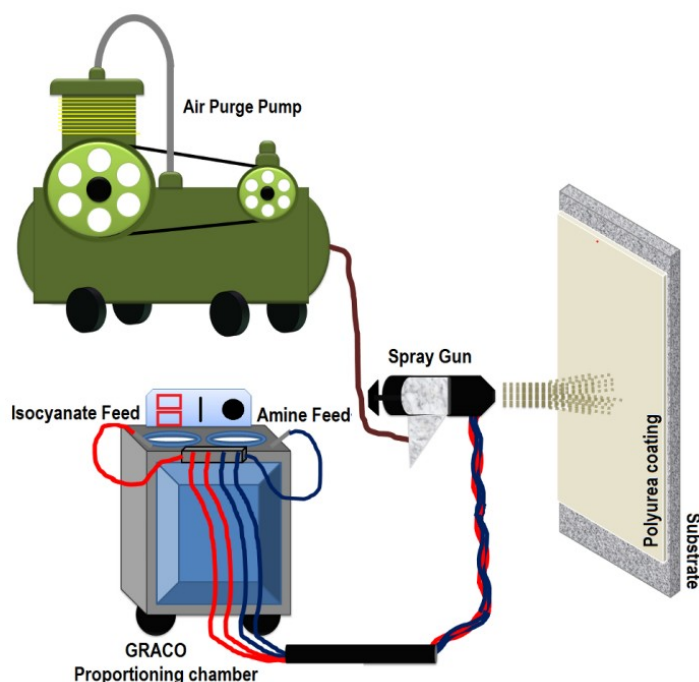
3.1 Introduction

The most important concern associated with the processing of polyurea is the requirement of rapid mixing of reactants, namely isocyanate and amine, in view of the fast reaction kinetics; which held back its commercialization till the late 1980s. Conventional technique of brush coating, which is successful for similar polyurethane systems, cannot be applied to the processing of polyurea. Commercially, polyurea is formed by the reactive spraying of isocyanate precursor (Side A) with a homogenous solution of amines including additives like adhesion promoters and colorants, collectively being referred to as “Side B”. Most standard spray coating formulations use MDI based prepolymers with NCO content of 15-16%, a range, where there exists a reasonable compromise between the viscosity and reactivity. The isocyanate and amine are stored separately and are made to react in the mixing-module, just prior to being pushed out of the orifice under pressure [119]. High NCO prepolymers exhibit reduced viscosity, which helps in their mixing with the amine, but in view of their high reactivity, such compositions tend to build up higher internal stresses.

A general schematic of polyurea-spray coating process are presented in Scheme 3.1. In this process the liquid reactants (isocyanate and amine) are pumped under pressurized conditions into a mixer manifold / static mixer, where they react intimately and flow through a spray hose into a spray gun. The volume ratio of the reactants is maintained at 1:1 v/v. The material upon exiting the spray nozzle is atomized and sprayed on any surface. The reaction is extremely fast, which leads to an almost exponential increase in the viscosity, prior to being sprayed. Post-spraying, the substance turns into a solid in a matter of seconds. It is to be noted that the physical properties of the polyurea

are strongly dependent on processing conditions, and most commercial formulations are sprayed at elevated temperatures ($\geq 70^{\circ}\text{C}$) and pressures $\sim 13000\text{kPa}$ or higher.

Most standard spray coating formulations (Side A) use MDI based prepolymers with NCO content of 15-16%, a range, where there exists a reasonable compromise between the viscosity and reactivity. High NCO prepolymers exhibit reduced viscosity, which helps in their mixing with the amine, but in view of their high reactivity, such compositions tend to build up higher internal stresses.



Scheme 3.1: Schematic of the reactive spray process

Irrespective of the NCO content, all isocyanate precursors exhibit much higher viscosity than the co-reactant amines, and since the reaction takes place under pressurized conditions, it is expected to lead to a stoichiometric imbalance during spraying. This requires dilution of the isocyanate prepolymer with a suitable solvent. Although dilution of isocyanate with suitable diluents like propylene carbonate is regularly practiced, this issue has never been discussed in the literature [133].

In fact, the purpose of this chapter is to address this knowledge gap and to establish the amount of dilution necessary to prepare spray processable polyurea via spray coating. The significance of viscosity matching of both sides (isocyanate and amine) by diluting the former with a suitable solvent to facilitate effective processing is discussed. Since polyureas are advocated as 100% solids, for the present study propylene carbonate has been chosen as a solvent, as the latter does not add to the volatile content and also meet the strictest VOC regulations.

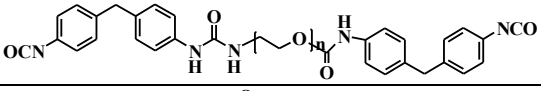
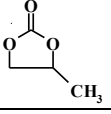
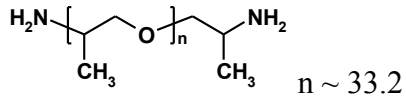
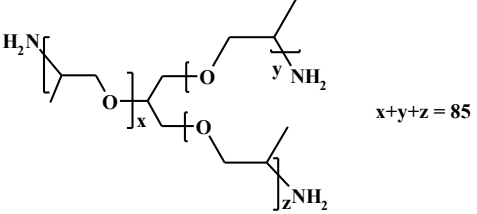
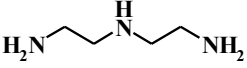
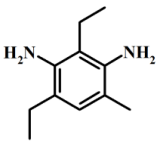
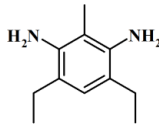
Propylene carbonate, in view of its reaction with amines, is expected to alter the kinetics of the isocyanate-amine reaction. Surprisingly, there are no such studies reported in the literature, although all-commercial formulations contain propylene carbonate to some extent [133]. In view of the increasing usage of polyurea in the last few years, we feel it is extremely important to be mindful of these issues: which instigated us to undertake this study.

3.2 Experimental

3.2.1 Materials

Commercial isocyanate prepolymer, Suprasec 2054 (Huntsman), NCO = 15 % was used without any further purification. Poly(propylene oxide) (PPO) based polyether amines JEFFAMINE[®]D-2000 and JEFFAMINE[®]T-5000, were procured from Huntsman: the designation number referring to the approximate molecular weight of each species, with D and T referring the functionality (D: difunctional and T: trifunctional). Two different chain extenders, diethylenetriamine (DETA, AZKO NOBEL) and diethyltoluenediamine (DETDA 80, Lonzacure[™]) were used without any further purification. The structure and physical properties of all the reactants are presented in Table 3.1.

Table 3.1: Structure and physical properties of reactants

Reactant	Structure	Density (g/cm ³)	n _{eq}	Viscosity (30 °C, mPas.S)
Side A				
Suprasec 2054		1.09	3.57	878.3
Propylene carbonate		1.2	-	2.2
Side B				
Jeffamine D 2000		0.985	1	182.9
Jeffamine T 5000		0.990	0.60	524.2
DETA		0.934	29.13	7.1
DETDA	 3,5-diethyltoluene-2,4-diamine  3,5-diethyltoluene-2,6-diamine	1.022	11.24	106.8

3.2.2 Spraying of polyurea

Suprasec 2054, both before and after dilution, was used as the isocyanate (NCO) source, and a formulated mixture of D-2000, T-5000 and DETA/DETDA was used as the source of amine (NH₂) for polyurea preparation. Formulations were prepared while maintaining an isocyanate index of 1.1. The details of formulation are presented in Table

3.2. PU1 and PU2 refer to the formulations containing aliphatic and aromatic chain extenders, i.e. DETA and DETDA respectively and formulations with ‘d’ as the suffix (PU1d and PU2d), refer to their diluted analogues.

Table 3.2: Details of formulation used for preparation of polyurea

Sample designation	A side (Isocyanate)		B side (Amine)			
	Suprasec 2054	Propylene carbonate	Chain Extender		D2000	T 5000
			DETA	DETD		
PU1	10	-	0.92	-	8.51	0.57
PU1d	9.08	0.92	0.87	-	8.57	0.56
PU2	10	-	-	2.5	6.21	1.29
PU2d	9.08	0.92	-	2.19	7.26	0.55

Polyurea samples were prepared using a spray-coating machine (Graco E 10 HP equipped with a fusion air-purge spray gun (AW2222, Graco). In all the runs, block and hose heaters were maintained at a constant temperature of 70°C and the spraying operation was performed at 1380±690kPa (2000 ± 100 psi). The mixing ratio of A and B components was 1:1(v/v). Polyurea films of uniform thickness (2mm) were obtained by spraying of formulation over a Teflon sheet.

3.2.3 Characterization

Structural and thermal characterization of polyurea was performed using techniques discussed in the previous chapter. The mechanical properties were measured in tensile mode as per ASTM D 412C.

3.3. Results and discussion

3.3.1. Temperature dependence of viscosity of isocyanate and amines

Temperature dependence of reactant viscosities are presented in Figure 3.1. It is clear that the viscosities of isocyanate and amines vary significantly at low temperatures. Even at temperatures close to spraying condition (70°C), the viscosity of isocyanate precursor (85 mPa.s) is much higher than that of the formulated amine (35 mPa.s for formulation containing DETA and 50 mPa.s for formulation containing DETDA). This is expected to lead to a stoichiometric imbalance within the high-pressure impinger, where the isocyanate and amine react after passing through the hose.

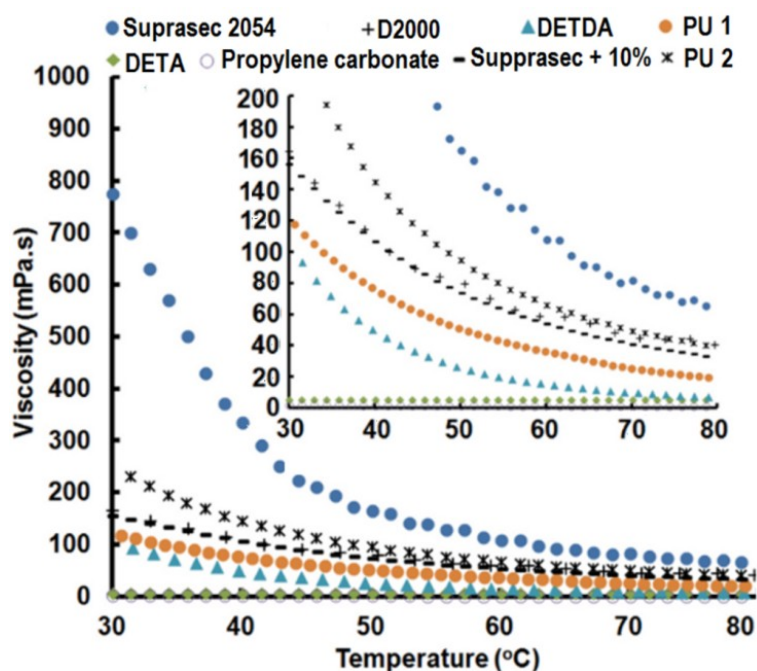


Figure 3.1: Variation of reactant viscosity with temperature. Inset shows an enlarged view of the viscosity-temperature profile for the low viscosity region.

The molar ratio of the isocyanate and amine available for reaction in the impinge was calculated using the Hagen Poiseuille equation, which is basically a relationship between the pressure drop, viscosity and volumetric flow rate for an incompressible

Newtonian fluid exhibiting laminar flow through a long cylindrical pipe of constant cross section.

$$\Delta P = \frac{8\mu LQ}{\pi R^4} \dots\dots\dots (3.1)$$

where:

ΔP : pressure difference between two ends,

L : length of pipe,

μ :dynamic viscosity,

Q :volumetric flow rate,

R : piperadius.

3.3.2 Theoretical calculations on reactant ratio

3.3.2.1 Stoichiometric imbalance in PU1

Assuming η_{NCO} and η_{amine} to be 85 mPa.s and 35 mPa.s respectively, the Length of pipe, L to be 30 feet, radius of hose, R to be $\frac{1}{4}$ inch and pressure difference, ΔP to be 2000 psi, the ratio of amount of iso and amine reacting at the impinger is:

$$\frac{volum e_{iso}}{volum e_{amine}} = \frac{Flowrateofiso}{Flowrateofamine} \propto \frac{\mu_{amine}}{\mu_{iso}} = \frac{35}{85} = \frac{1}{2.4} \dots\dots\dots (3.2)$$

The density of isocyanate precursor and amine was experimentally determined to be 1.09 g/cc and 0.92g/cc respectively. Therefore, the mass ratio of the iso and amine in the impinger is:

$$\frac{mass_{iso}}{mass_{amine}} = \frac{volum e_{iso} \times density_{iso}}{volum e_{amine} \times density_{amine}} = \frac{1 \times 1.09}{2.4 \times 0.92} = \frac{1}{2.04} \dots\dots\dots (3.3).$$

For calculating the moles of amine and isocyanate, the molar mass of Suprasec, Jeffamine D2000, DETA and T 5000, was assumed to be 2501, 2000, 103 and 5000 g/mol respectively.

Therefore, the ratio of moles of reactant is $\frac{moles_{iso}}{mol es_{amine}} = \frac{1}{6.609} \dots\dots\dots (3.4)$

3.3.2.2 Stoichiometric imbalance in PU2

The ratio of amount of iso and amine for PU2 reacting at the impinger is

$$\frac{\text{volume}_{iso}}{\text{volume}_{amine}} = \frac{\text{Flowrateofiso}}{\text{Flowrateofamine}} \propto \frac{\mu_{amine}}{\mu_{iso}} = \frac{50}{85} = \frac{1}{1.7} \dots \dots \dots (3.5)$$

Within the impinger, the mass ratio of the iso and amine is:

$$\frac{\text{mass}_{iso}}{\text{mass}_{amine}} = \frac{\text{volume}_{iso} \times \text{density}_{iso}}{\text{volume}_{amine} \times \text{density}_{amine}} = \frac{1 \times 1.09}{1.7 \times 0.92} = \frac{1}{1.434} \dots \dots \dots (3.6)$$

The molecular mass of DETDA is 178 g/mol, therefore,

$$\frac{\text{moles}_{iso}}{\text{moles}_{amine}} = \frac{1}{6.41} \dots \dots \dots (3.7)$$

3.3.3 Predicting the effect of isocyanate: amine on degree of polymerization

Carother's equation was used to predict the degree of polymerization (X_n) for different stoichiometric ratio of the reactants ($r = \text{iso}/\text{amine}$) [134], assuming fractional conversion, $p = 99\%$).

$$X_n = \frac{1+r}{1+r-2rp} \dots \dots \dots (3.8)$$

The calculations performed for both the formulations PU1 and PU2 [135]. The results are tabulated in Table 3.3 and pictorially depicted in Figure 3.2. It is clear that under the conditions prevalent, where the amine is in large excess [136], the reaction product comprise of amine terminated oligomers with extremely low degree of polymerization [137].

It can be seen that the reactant ratio has a pronounced effect on the degree of polymerization. It can be concluded that the stoichiometric imbalance of isocyanate: amine:: 1:6.60 (PU1) and 1:6.4 (PU2), which differ substantially from the required stoichiometry of 1:1, leads to a pronounced drop in the X_n to 1.35 and 1.37 respectively.

Table3.3: Degree of polymerization X_n , for different values of r

S. No.	Isocyanate: Amine	Stoichiometric ratio(r)	Degree of polymerization, (X_n)
1	1:1	1	100
2	1:1.5	0.67	4.81
3	1:2	0.50	2.94
4	1:2.5	0.40	2.30
5	1:3	0.33	1.98
6	1:3.5	0.29	1.79
7	1:4	0.25	1.66
8	1:4.5	0.22	1.56
9	1:5	0.20	1.49
10	1:5.5	0.18	1.44
11	1:6	0.17	1.39
12	1:6.5	0.15	1.35
13	1:7	0.14	1.33
14	1:7.5	0.13	1.30
15	1:8	0.13	1.28
16	1:8.5	0.12	1.26

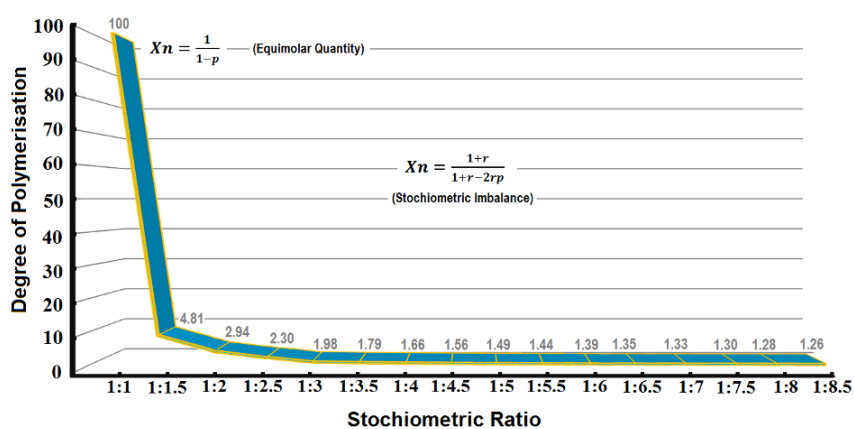


Figure 3.2: Effect of increasing stoichiometric imbalance on the degree of polymerization

In line with our predictions, spray coating of PU1 and PU2 (undiluted isocyanate precursor with formulated amine) led to the formation of fibrous product with “noodle-like” morphology. Digital photographs of the product obtained are presented in Figure 3.3. Interestingly, in view of the extensive H bonding [138], even these low molecular weight oligomers were found to be insoluble in common solvents e.g. DCM, DMF, THF, xylene, chloroform and water.

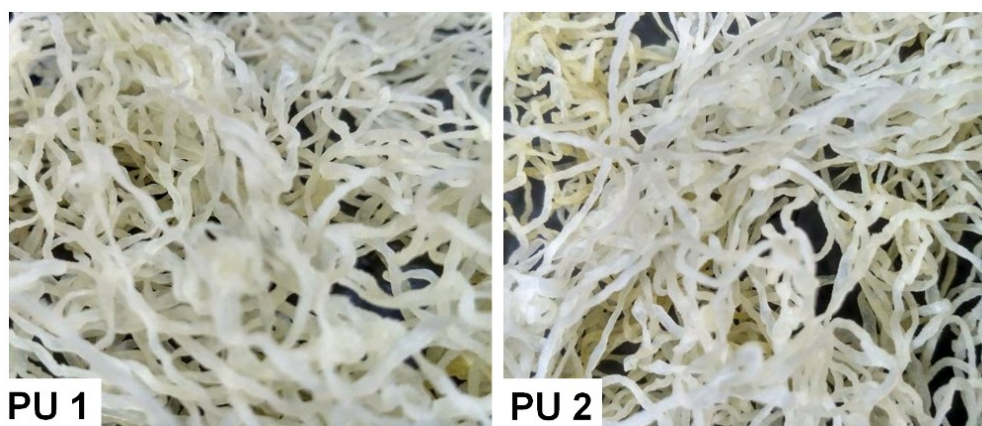
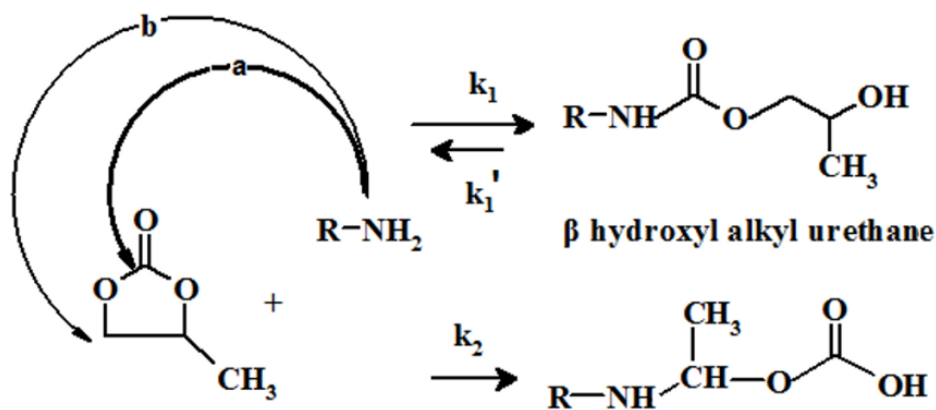


Figure 3.3: Digital photograph of PU 1 and PU 2

Both theoretical and experimental studies clearly highlight the need for dilution of the isocyanate precursor. However, presence of solvent is expected to increase the volatile organic content of polyurea. Therefore, for the present study, “VOC exempt” reactive diluent, namely propylene carbonate was chosen, which has been reported to react with aliphatic amines as per Scheme 3.2. In addition to their ability to act as a reactive diluent, the presence of propylene carbonates in Side A leads to increased shelf-life and improved leveling of the spray coated films [139-141].

The reaction of alkylene carbonate with amine to form β -hydroxymethyl urethane(a, rate constant ' k_1 ') is a reversible process, while the alkoxylation reaction (b, rate constant ' k_2 ') is reportedly irreversible [142]. For this reason, primary amine, albeit

in low concentrations is always present. It is to be noted that the rate of urethane formation (k_1) is approximately twice that of the competing alkoxylation process (k_2) but in view of the irreversible nature of the latter, concentration of alkoxylation products reportedly increase with time.



Scheme 3.2: Reaction of propylene carbonate with amines

It is to be noted that in view of its high boiling point, propylene carbonate (b.pt 242°C) is not used as an evaporative solvent. Its removal would mandate extreme conditions, like high temperatures and/or low pressures. Since, the coating under study has not been subjected to any such treatment, the diluent is expected to remain within the sprayed coating, and the same was confirmed gravimetrically. In view of the possible reaction of the propylene carbonate with the amines (Scheme 3.2), which render them candidature as reactive diluent, they are expected to react and form an integrated part of the polyurea network over a period of time.

3.3.4 Predicting blend viscosity

To estimate the amount of propylene carbonate required for isocyanate dilution, the applicability of several mixing rules was explored [143, 144]. Common mixing rules [145, 146] e.g. Arrhenius, Bingham, Cragoe, and Kendall & Monroe have a simple

mathematical structure (e.g., linear, logarithmic, inverse, power-law) and only require determination of experimental viscosities of the constituents, which were estimated through rheological studies (Table 3.4).

Table 3.4: Pure mixing rules for blends

Arrhenius	$\log v_{blend} = \chi_{v_1} \log v_1 + \chi_{v_2} \log v_2$
Bingham	$1/v_{blend} = x_{v_1}/v_1 + x_{v_2}/v_2$
Cragoe	$\frac{1}{\ln(2000 \cdot v_{blend})} = \frac{x_{v_1}}{\ln(2000 \cdot v_1)} + \frac{x_{v_2}}{\ln(2000 \cdot v_2)}$
Kendall & Monroe	$V_{blend}^{1/3} = x_{v_1} \cdot v_1^{1/3} + x_{v_2} \cdot v_2^{1/3}$

In addition, mixing rules based on Viscosity Blending Index (VBI) [147] were also explored, which assume a linear relationship between the VBI of the constituents and the resulting blend (Table 3.5).

Figure 3.4 depicts the variation in viscosity (at 70°C) of the blend as predicted by various mixing rules. The experimentally determined viscosities are also presented for ready reference.

Table 3.5: Viscosity blend index equations

<p>Refutas Index Method</p>	$VBI_i = 10.975 + 14.534 \cdot \ln \ln(v_i + 0.8) \dots\dots\dots (a)$ $VBI_{blend} = x_{w1} \cdot VBI_1 + x_{w2} \cdot VBI_2 \dots\dots\dots (b)$ $v_{blend} = \exp \left(\exp \left(\frac{VBI_{blend} - 10.975}{14.534} \right) \right) - 0 \dots\dots\dots (c)$
<p>Chevron</p>	$VBI_i = \frac{\log v_1}{3 + \log v_1} \dots\dots\dots (a)$ $VBI_{blend} = x_{v1} \cdot VBI_1 + x_{v2} \cdot VBI_2 \dots\dots\dots (b)$ $v_{blend} = 10^{\frac{3 \cdot VBI_{blend}}{1 - VBI_{blend}}} \dots\dots\dots (c)$

Clearly, the experimental viscosities vary substantially from those predicted using pure mixing rules and lie in the range of values predicted using “Chevron”. Also, diluting the isocyanate precursor with propylene carbonate (10%v/v) results in a blend with viscosity matching that of the formulated amines. It is expected that the diluted isocyanate will not cause any stoichiometric imbalance in the impinger, and hence lead to formation of high molecular weight polyurea during spraying. In line with our expectations, processing of the formulations resulted in the formation of polyurea films with properties strongly dependent on the type of chain extender employed. It was also observed that the tack free time was substantially higher during the spraying operation (3-4 s in comparison to <1 s for undiluted formulations).

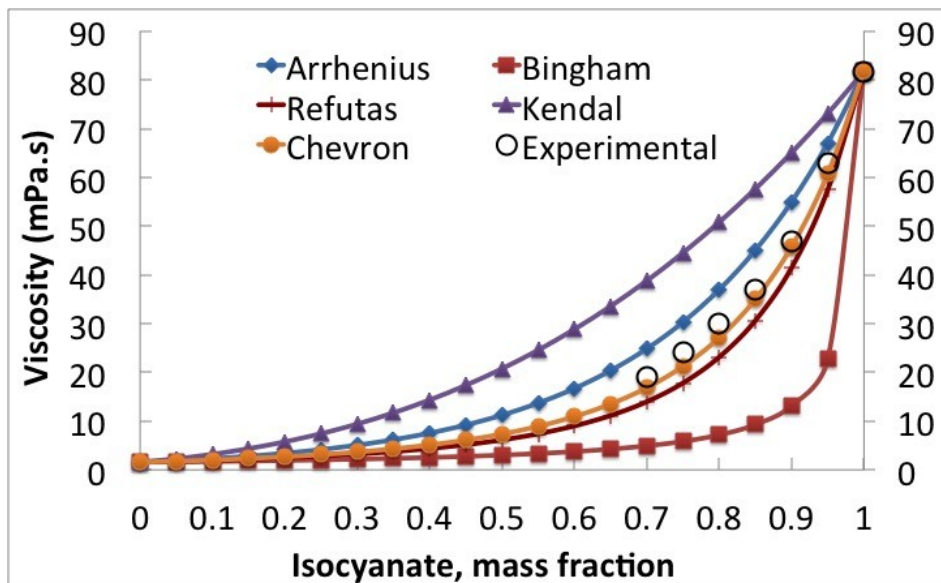


Figure 3.4: Predictions related to the effect of blending propylene carbonate on the viscosity of isocyanate prepolymer ($T = 70^{\circ}\text{C}$)

3.3.5 Chemo-rheological behavior during polyurea formation

Rheological studies under isothermal conditions were performed at varying temperatures ($50\text{-}70^{\circ}\text{C}$) to arrive at the kinetic parameters associated with polyurea formation. The variation of storage (G') and loss modulus (G'') in the presence of both types of chain extenders (DETA and DETDA) is presented in Figure 3.5 and Figure 3.6. Initially, in view of the liquid nature of the reactants, the loss modulus of the formulation is substantially higher than the storage modulus. Due to the reaction between the isocyanate and amine, both G' and G'' increase rather rapidly and a crossover gelation region is observed; where the storage modulus becomes equal to the loss modulus. This region marks a sudden transition of the viscous liquid to an elastic solid, where the amount of energy stored by the material can be equated to the amount of energy dissipated. In general, the gelation time is expected to be inversely proportional to the

temperature of curing, which was observed in all cases, irrespective of the type of chain extender used.

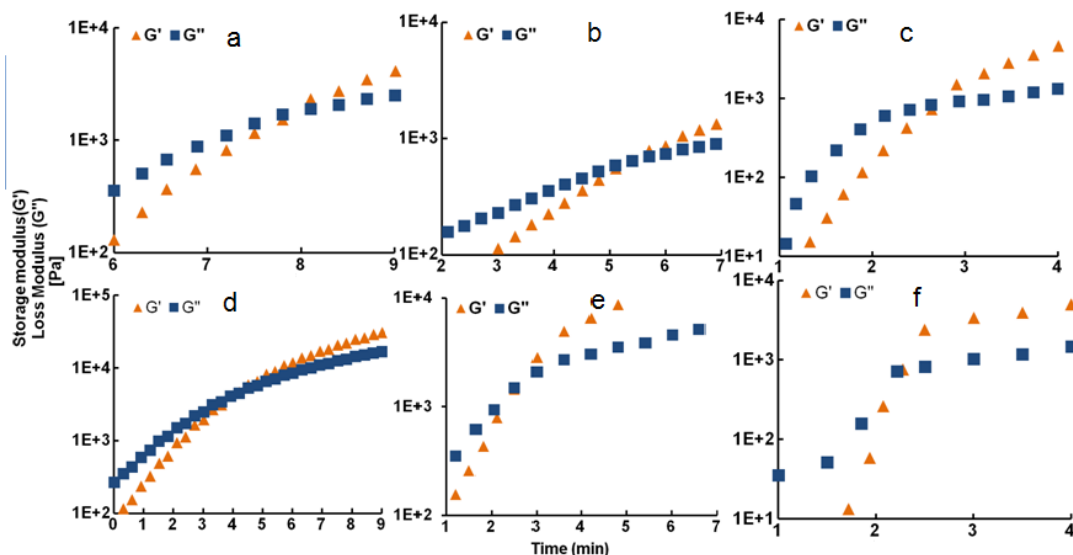


Figure 3.5: Evolution of storage and loss modulus in formulations containing DETA in (a-c) presence and (d-f) absence of diluent (a,d = 50°C, b,e = 60°C and c,f=70°C)

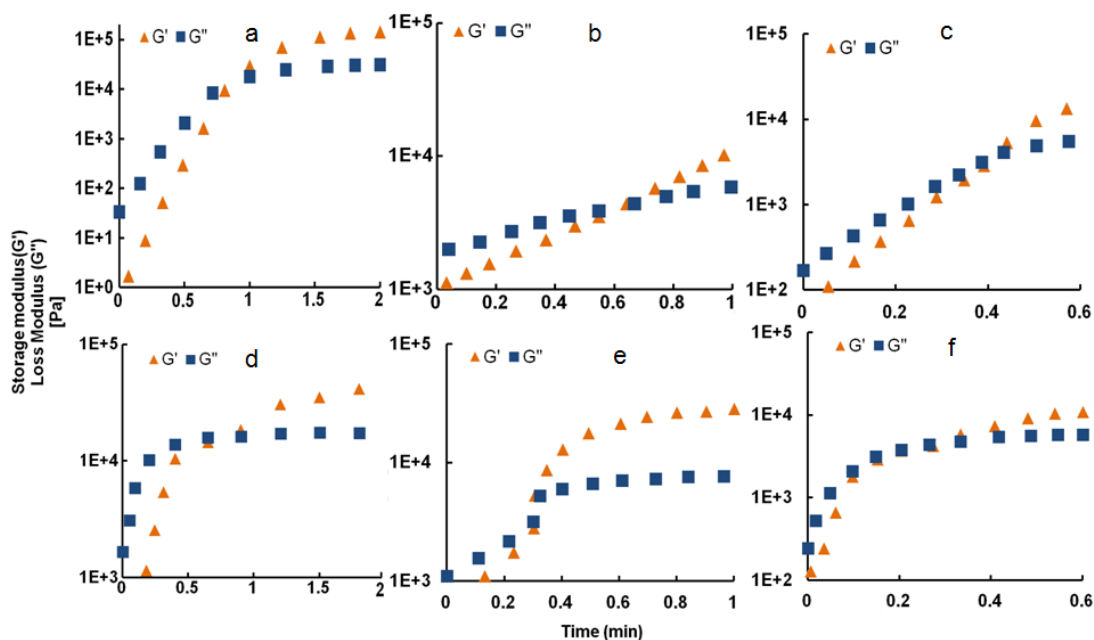


Figure 3.6: Evolution of storage and loss modulus in formulations containing DETDA in (a-c) presence and (d-f) absence of diluent (a,d = 50°C, b,e = 60°C and c,f=70°C)

The relationship between the gelation times (t_{gel}) with temperature was used to arrive at the activation energy for the reaction. It has been assumed that curing reaction can be expressed by differential equations containing unique apparent activation energy, as follows: [148]

$$\frac{dx}{dt} = A e^{\left(\frac{-E_a}{RT}\right)} f(x) \dots \dots \dots (3.9)$$

Where, A is a constant factor, E_a is apparent activation energy for the reaction, R is gas constant, T is the absolute isothermal cure temperature and $f(x)$ is a function of the reaction mechanism and the extent of reaction and is assumed to be independent of the cure temperature.

Integrating eq 1 from $x = 0$ to $x = x_{gel}$ by taking natural logarithm:

$$\ln \int_0^{x_{gel}} \frac{dx}{f(x)} = \ln A + \ln(t_{gel}) - \left(\frac{E_a}{RT}\right) \dots \dots \dots (3.10)$$

The extent of reaction at gelation point is constant, so the above equation can be expressed as:

$$\ln(t_{gel}) = \mathbf{constant} + \frac{E_a}{RT} \dots \dots \dots (3.11)$$

Thus, from the slope of the plot of $\ln(t_{gel})$ and the inverse of temperature, the activation energy can be calculated and presented in Table 3.6.

Formulations containing aromatic chain extenders exhibited slightly higher activation energies. Interestingly, presence of propylene carbonate in the reaction medium led to a slight increase in the activation energy, although dilution of the reactants is not expected to alter the reaction kinetics. This could be due to the reaction of propylene carbonate with the amines as discussed in Scheme 3.2.

Table 3.6: Variation of gelation time (t_{gel}) with temperature (T) and activation energy for polyurea formulations

Sample designation	Temperature (K)	t_{gel} (s)	Activation energy (kJ/mol)
PU1	323	240	32.0
	333	150	
	343	120	
PU1d	323	480	43.8
	333	300	
	343	180	
PU2	323	30	42.2
	333	18	
	343	12	
PU2d	323	54	50.5
	333	30	
	343	18	

The variation of t_{gel} as a function of absolute temperature and the derived activation energy is presented in Figure 3.7.

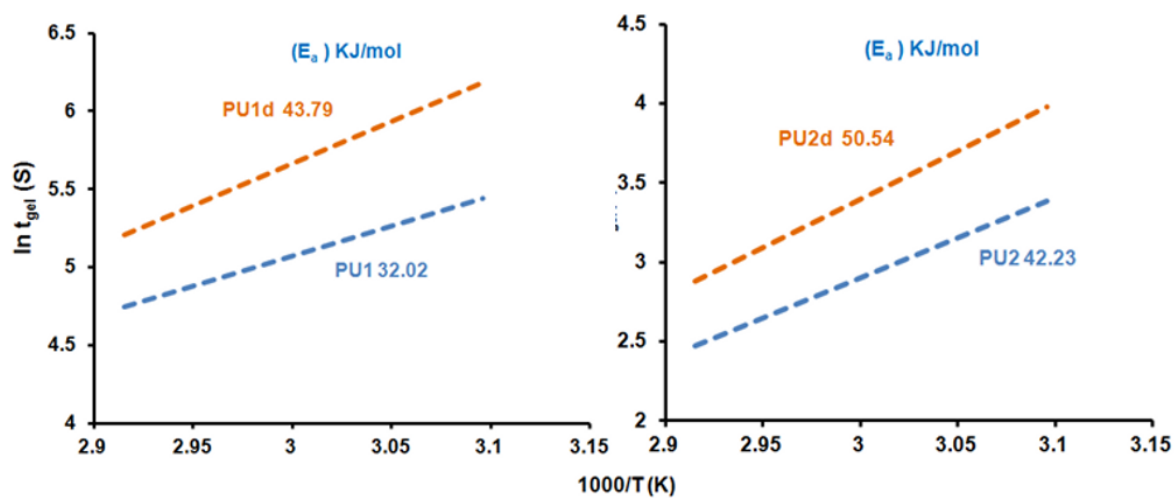


Figure 3.7: Arrhenius plot of $\ln t_{gel}$ vs $1000/T$ for polyurea formulations containing a)

DETA and b) DETDA

3.3.6 Reaction monitoring

The isocyanate-amine reaction, was also studied through FTIR spectroscopy and the changes in the spectra for a representative formulation (PU1) is presented in Figure 3.8. Characteristic changes were apparent in the absorbance bands appearing at 2263, 1728, 1673 and 1643 cm^{-1} [115]. The NCO absorbance intensity at 2263 cm^{-1} , decreased exponentially within the first few minutes of the reaction. This is associated with a concurrent increase in the absorbance at 1728 cm^{-1} , which appears due to the presence of urethane carbonyl. The absorbance at 1632 -1643 cm^{-1} , appearing due to H-bonding between the carbonyl group ($>\text{C}=\text{O}$) and the adjacent N-H functionalities of urea, commonly referred to as “ordered bonding” also increased with time. For the purpose of quantification, the absorbance intensities associated with these characteristic bands were normalized with respect to the absorbance due to benzene appearing at 1600 cm^{-1} [119], and the results are also presented in Figure 3.8. Although the reaction is instantaneous, with solidification occurring in a matter of a few seconds, it was observed that the isocyanate absorbance completely levels off after ~8 h.

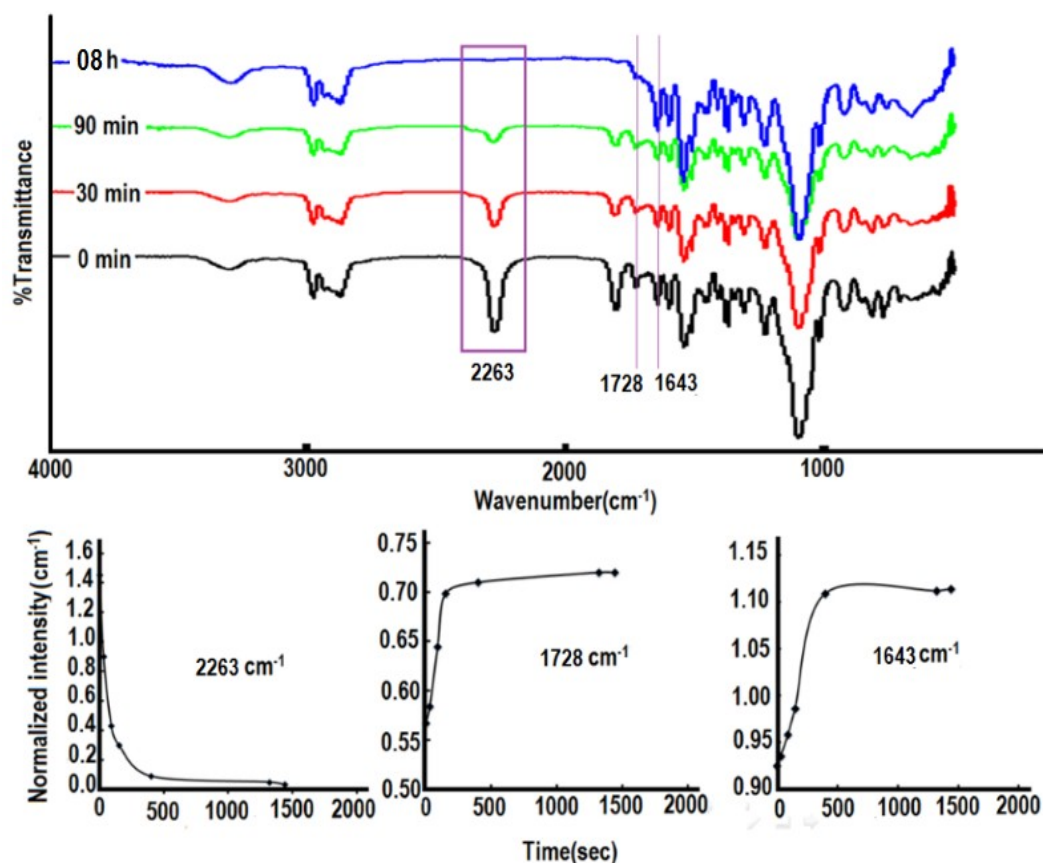


Figure 3.8: Changes in the FTIR spectra due to formation of polyurea

3.3.7 Mechanical properties

In the absence of polypropylene carbonate, spray coating of polyurea led to formation of a fibrous product with low molecular weight. In this case, the ‘tack free’ time is very less (<1 s) and the resulting product is structurally an amine-terminated oligomer containing urea linkages, with low degree of polymerization. It was not possible to determine the mechanical properties of the product obtained.

Upon dilution of the isocyanate with propylene carbonate (10%v/v), the rate of reaction is lowered and the tack free time is substantially extended (~4s), which indicates improved processibility of the formulation. Tack free time and representative mechanical properties (tear strength, tensile strength and elongation at break) are presented in Table 3.7.

Table 3.7: Mechanical properties of polyurea samples

Sample	Tack free time (s)	Tensile strength (kPa)	Elongation at break (%)	Tear strength (kN/mm)
PU1d	4	530± 10	200 ± 15	3.58 ± 0.3
PU2d	4	9730± 1110	168 ± 11	68.79 ± 1.3

The archetypal stress-strain curves are presented in Figure 3.9. The studies reported here belong to the quasi-static regime with strain rate ($\epsilon \sim 10^{-2} \text{s}^{-1}$). It is to be noted that the mechanical response of polyurea is highly strain rate sensitive, and changes from ductile to brittle (at $\epsilon > 10^3 \text{s}^{-1}$). In general, this change due to increase in strain rate is not associated with much energy absorption. However, in the case of polyurea, this very region encompasses a dynamic transition from rubber to glass [55, 121] and is therefore responsible for the unique properties of polyurea.

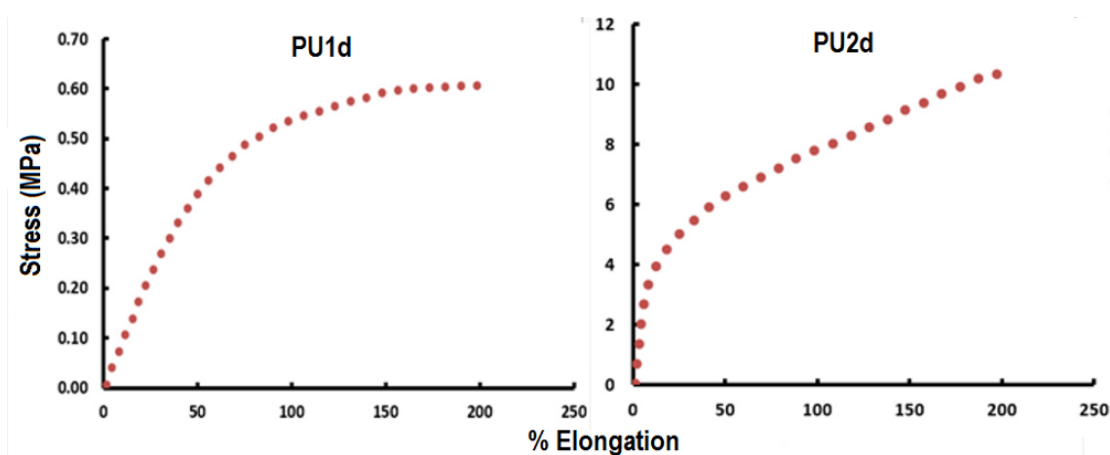


Figure 3.9: Stress-strain curve of polyurea specimens prepared after diluting

3.3.8 Thermal properties

TG-DTG traces of spray coated polyurea samples prepared in the presence of aliphatic and aromatic chain extender are presented in Figure 3.10. Interestingly; the type

of chain extender did not affect the degradation profile appreciably. It is to be noted that dilution of the isocyanate with propylene carbonate did not affect the thermal degradation behavior of the resultant polymer. It is to be noted that the hard-soft segment content and the extent of their segregation plays an important role in defining the thermal stability of polyurea[126]. The initial mass loss observed in the temperature range (250-350°C) is due to the degradation of the hard segments formed from the thermally unstable urea linkages. The subsequent mass loss is associated with the decomposition of the soft segments, which leaves behind a char residue of 6% w/w (at 600°C).

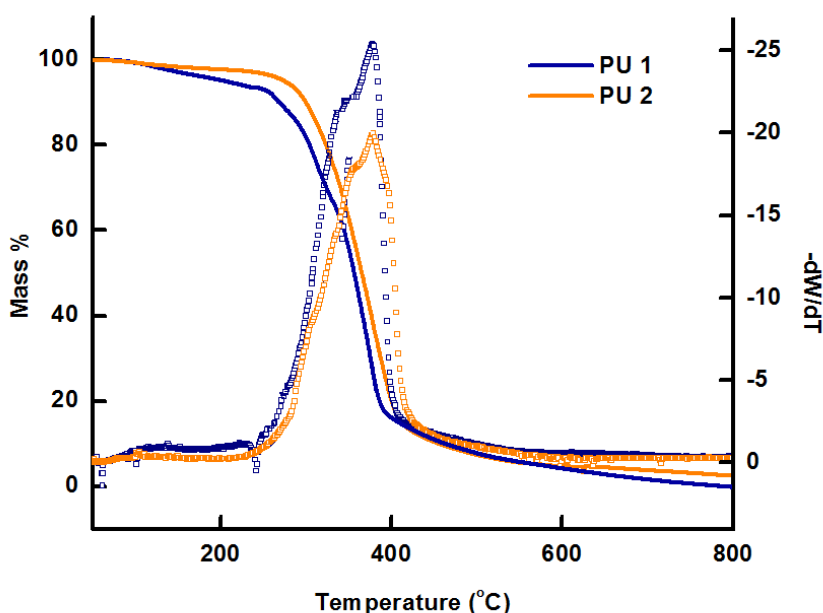


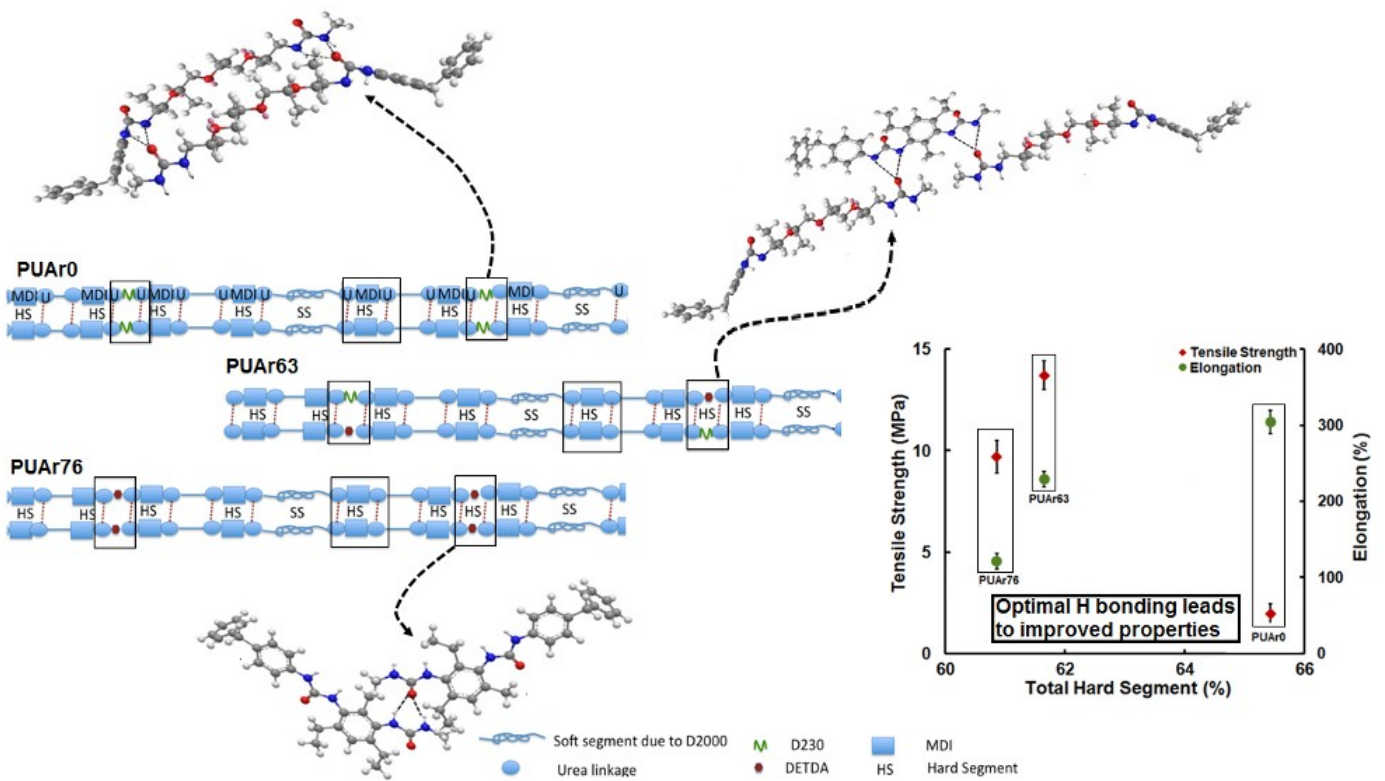
Figure 3.10: TG/DTG traces of polyurea containing aromatic and aliphatic chain extender.

Our studies clearly indicate that for effective spray processing, the viscosity of amine and isocyanate need to match reasonably. For this purpose, blending of the isocyanate with propylene carbonate is mandatory. A comparison of mixing rules was performed which revealed that Chevron equation based on Viscosity Blending Index

predicts the blend viscosity with reasonable accuracy. Spray coating of formulations containing undiluted isocyanate precursors, due to stoichiometric imbalance, led to formation of fibrous amine terminated polyurea with low degree of polymerization and low “tack free” time of <1 s. Diluting the precursor propylene carbonate (10% v/v) led to viscosity matching with the amines and thereby led to formation of smooth-leveled polyurea films with an extended “tack free” time of >3 s. Although the solidification process is extremely rapid in a matter of seconds, but the leveling-off of the isocyanate absorbance took substantially longer periods (~8h).

Chapter 4

Effect of chain-extender on the material properties of polyurea



4.1. Introduction

The micro-structure of polyurea comprises of two distinct domains: “hard” realms formed by hydrogen bonded polar urea linkages ($-\text{NH}-\text{CO}-\text{NH}-$) and “soft” domains comprising of long aliphatic polyether chains [109, 149]. It is this phase-segregated structure, which is responsible for its unusual properties (i.e, enhanced modulus, high extensibility and resiliency) [150, 151]. The properties of polyurea can be tuned by choosing the raw materials judiciously, particularly isocyanates and amines [152]. However, all commercial polyurea formulations contain chain extenders, which can be either aliphatic or aromatic in nature depending upon the targeted final properties. The presence of chain extender in polyurea formulation increases the vicinity of the urea groups, which increases the probability of hydrogen bond formation [153], without altering the total number of urea linkages in the polymer [154]. In view of the increased H-bonds, the mechanical properties of chain-extended polyurea are substantially better than their non-chain extended counterparts.

Bidentate H-bonding within the urea linkages lead to formation of nanometer-sized hard segments, which operate as physical crosslinks between the macromolecules [138, 155]. The N-H group in polyurea serves as proton donor, and the carbonyl ($>\text{C}=\text{O}$) and/or adjacent oxygen atom of ether in the soft segment acts as the acceptor [156]. Improved phase separation in polyurea in-turn strengthens H-bonding in the hard segments and leads to improved physical properties [157].

In general, both aromatic as well as aliphatic chain extenders are commonly included in polyurea formulations, however in view of the commercial nature, there are no guidelines to delineate their optimal amounts which can result in the prime performance of the material. The inclusion of chain extender in the formulation increases

the vicinity of the urea groups, which increases the probability of the urea groups to align and form hydrogen bonds [158], the total number of urea linkages remaining unaltered [154].

Although the effect of chain extension in polyurethanes has been extensively reported [111, 159, 160], little systematic work is available on the effect of chain extension process in polyurea formulations, which inspired us to take up this study. In view of the increasing interest in polyurea in the last few decades, we believe that the underlying physics behind the improvement of properties of polyurea by chain extension process needs to be explored in detail systematically.

In view of the fast kinetics associated with isocyanate-amine reaction, polyurea formation occurs in a matter of seconds. Although polyurea is considered as an “instant-setting” system, but its material properties evolve substantially over time: a phenomenon, which has been studied systematically in this chapter. Surprisingly, despite its fundamental significance, the emergence of time-dependent material properties in polyurea has not been studied till date. It is to be noted that although the curing process has been studied using various analytical techniques, the time frame over which these studies have been performed is rather short [115, 119]. It is to be noted that although the solidification occurs in a matter of seconds, the relaxation of internal stresses mandate much longer periods. In view of the increasing application of this material in specialized fields, it is extremely important to be cognizant about the time frame required for polyurea to reach its optimal properties.

Here, we attempt to understand the factors responsible for the evolution of material properties in the chain extended polyurea with time as well as the optimization of

the ratio the aromatic to aliphatic chain extender content in the polyurea formulations with an aim to appreciate the role of H-bonding towards achieving optimal properties.

4.2 Experimental

4.2.1 Materials

The structure and physical properties of all the reactants, namely Suprasec 2054, Propylene carbonate, Jeffamine D2000, Jeffamine D230 and DETDA are presented in previous chapters (Table 2.1 and 3.1).

4.2.2 Spraying of polyurea

For the purpose of polyurea preparation, duly diluted Suprasec 2054, was used as the source of isocyanate (NCO) [161], and formulated mixture containing requisite amounts of D-230, D-2000 and DETDA was used as the source of amine (NH₂). The amount of the amine used for each formulation was calculated using Eq. 1.1, while maintaining an isocyanate index (i_{NCO}) of 1.1. The hard segment content was determined as per established procedure (Eq. 1.3) [27]. The detailed composition used for preparing different polyurea formulations are presented in Table 4.1. The volume percent of Suprasec 2054 and propylene carbonate was maintained at 90.8 and 9.2 respectively to attain a similar rheological profile for both side ‘A’ and ‘B’ during spray processing conditions (70°C). It is to be noted that the m_{iso} used for the calculation of hard segment refers to the mass of isocyanate prepolymer which also includes the contribution of the long polyether chain. Therefore, this estimated figure of hard segment is much higher than the actual hard segment content in the polymer. The samples have been designated as PU-Ar followed by the contribution (%) of the aromatic chain extender to the total urea content in the polymer.

Table 4.1: Details of polyurea formulations prepared

Sample designation	Amine (part per unit volume)			Total Hard segment (%)	Contribution of aromatic chain extender (%)
	Chain Extender		D2000		
	D 230	DETDA			
PUAr-76	-	21.22	78.78	60.86	76
PUAr-63	5.48	17.52	77.0	61.65	63
PUAr-36	16.41	11.05	72.54	63.72	36
PUAr-10	27.35	2.68	69.97	64.84	10
PUAr-0	31.30	-	68.70	65.43	-

4.2.2.1 Contribution of Amines to total urea linkages

The urea functionalities in polyurea form as a result of the reaction of amine with the isocyanate (stoichiometric ratio 1:1). Since isocyanate is taken slightly in excess (isocyanate index, $i = 1.1$), the number of urea linkages in the polymer can be derived from the number of amines present in the formulation. The individual contribution of a particular amine (D2000) or chain extender (DETDA/ D230) towards the total urea linkages can be estimated from the number of amine groups made available from each amine or chain extender as per the following equation.

$$\text{Individual contribution of chain extender or amine} = \frac{f \times m_a \times 6.023 \times 10^{23}}{M_a} \dots \quad (4.1)$$

Where,

f = functionality of amine/ chain extenders (For all the amines/ chain extender the functionality (number of amine groups per molecule) = 2)

m_a = mass of amine in formulation

M_a = Mol. Mass of amine ($M_{D230} = 230$, $M_{D2000} = 2000$, $M_{DETDA} = 178$)

The individual contributions of amines and the chain extenders to the total urea present in the sample have been tabulated and depicted pictorially in Table 4.2 and Figure 4.1 respectively.

Table 4.2: Individual contribution of long chain amine (D2000), aromatic (DETDA) and aliphatic chain extender (D230) to the total hard segment

Designation	Total HS	Contribution to urea linkages					
		D230	D230 (%)	DETDA	DETDA (%)	D2000	D 2000 (%)
PUAr-76	60.8	-	-	1.34×10^{22}	75.85	4.27×10^{21}	24.14
PUAr-69	61.25	1.22×10^{21}	6.89	1.22×10^{22}	69.21	4.22×10^{21}	23.88
PUAr-63	61.66	2.44×10^{21}	13.79	1.11×10^{22}	62.61	4.17×10^{21}	23.59
PUAr-36	63.73	7.32×10^{21}	40.14	6.38×10^{21}	36.29	3.98×10^{21}	21.56
PUAr-10	64.86	1.22×10^{22}	68.97	1.69×10^{21}	9.57	3.79×10^{21}	21.44
PUAr-0	65.43	1.39×10^2	78.93	-		3.72×10^{21}	21.06

Total urea linkages: 1.76×10^{22}

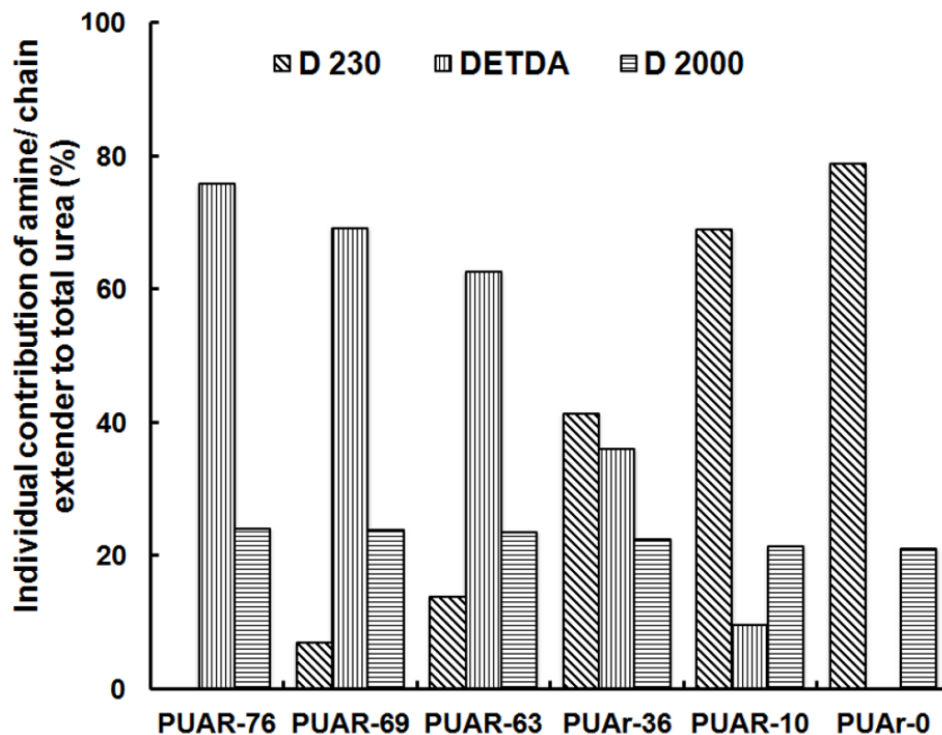


Figure 4.1: Percentage contribution of long chain amine, aliphatic and aromatic chain extender towards the total urea linkage present in the polymer

4.2.3 Characterization

Polyurea films of uniform thickness were prepared by spray coating process discussed in previous chapters. The details of techniques used for characterization of polyurea have also been discussed previously.

4.3 Results and discussions

4.3.1 Rheological behavior of isocyanate and amines

Temperature dependence of reactant viscosities are presented in Figure 4.2. The isocyanate prepolymer had to be suitably diluted with propylene carbonate (10% v/v dilution) to reduce the viscosity to the level of formulated amine [161].

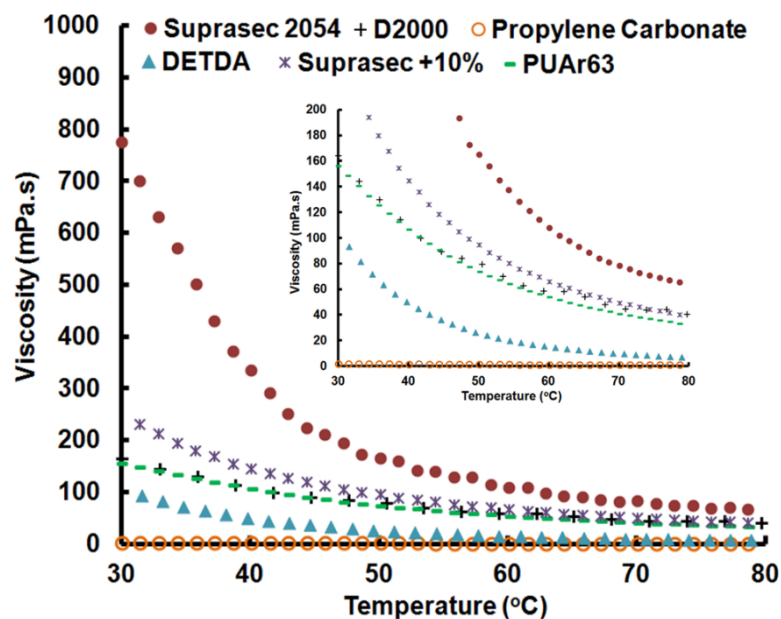


Figure 4.2: Variation of reactant viscosity with temperature

4.3.2 Chemo-rheological response

Many low molecular weight amines react very rapidly with isocyanates and are hence unsuitable for spray processing, as gelation occurs so rapidly that the formulations are practically unsprayable. In fact, one of the major shortcomings associated with formulations containing only DETDA as the chain extender, is the rapid gelation time [162]. The rheological parameters under isothermal conditions (70°C) were monitored with an aim to gain an insight into the kinetics associated with the chain extension process in polyurea formation. The evolution of storage (G') and loss modulus (G'') in representative formulations due to the amine-isocyanate reaction is presented in Figure 4.3. In the initial stages of the reaction, where the reactants are in the liquid state, the loss modulus was substantially higher than the storage modulus. As a result of the amine – isocyanate reaction for the formation of polyurea, both G' and G'' increased rather rapidly, and a crossover gelation region was observed; where the storage modulus increases to the level of loss modulus [161]. This region marks a sudden transition of the viscous liquid to

an elastic solid, where the amount of energy stored by the material becomes equal to the amount of energy dissipated. The time required for the same is referred to as the ‘gelation time’ (t_{gel}). It can be seen that the ‘ t_{gel} ’ of PU-Ar76 (formulation containing only DETDA) is 40s, which increases with increasing amount of aliphatic chain extender (D 230), clearly reflecting upon its ease of processibility. For formulations prepared in the absence of aromatic chain extender (PU-Ar0), the gelation time is significantly higher (~3.5 min), which is undesirable, as it would lead to non-uniform coating thickness. It is interesting to note that, in none of the formulations, the storage and loss modulus level off completely in the time frame of experimentation, although the slope of the curve decreases significantly. This essentially implies that the reaction continues within the polymer, even post-solidification.

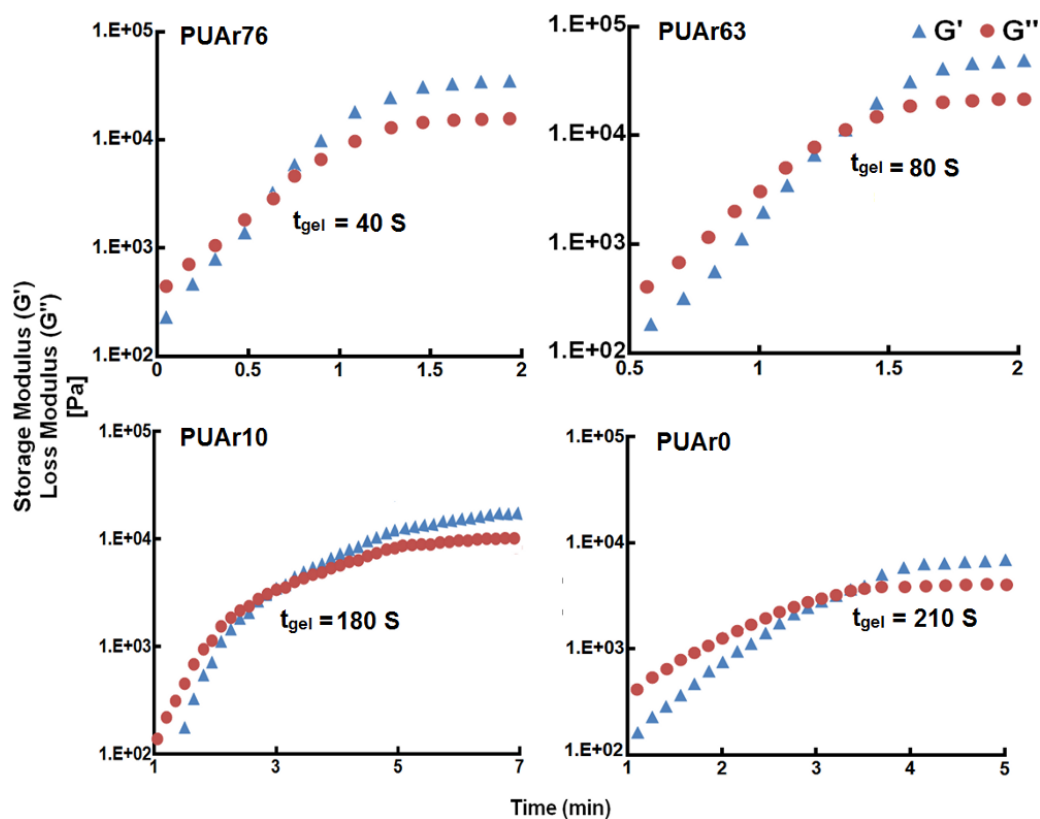


Figure 4.3: Evolution of storage and loss moduli in polyurea formulations (70°C)

4.3.3 Mechanical properties

4.3.3.1 Evolution of mechanical properties

Polyurea films of uniform thickness were prepared using spray coating technique, and in line with the rheological studies, the ‘time to solidification’ was found to depend strongly on the type of chain extender included in the formulation. It can also be seen that the mechanical properties of polyurea are strongly dependent on the nature of isocyanate, amine and the chain extender included in the formulation. The attainment of a sufficiently robust state to resist damage by handling is a critical point during curing, commonly indicated by ‘tack-free’ time. Characteristic parameters, namely ‘gel-time’ and ‘tack free’ time associated with the formulations are presented in Table 4.3. The tack-free time associated with the formulations, reveal that this stage is achieved within 2 min of spraying.

Table 4.3: ‘Gel-time’ and ‘tack free’ time of formulations during spraying

Sample designation	Gel time (s)	Tack free time (s)
PUAr-76	5	30
PUAr-69	6	35
PUAr-63	6	38
PUAr-36	7	41
PUAr-10	9	47
PUAr-0	60	110

As expected, formulations containing aliphatic chain extender (D230) exhibited relatively longer periods for the flow to end. The observed difference in gel time as well

as in tack free time determined during the spray processing and rheological studies can be attributed to the high pressure employed during the processing of the polyurea (2000 ±100 psi).

Although, the solidification process occurs rapidly, the mechanical properties evolve substantially with time. All the formulations exhibited a similar trend of mechanical property evolution, and the development of tensile properties and tear strength of a representative polyurea formulations are presented in Figure 4.4 and Figure 4.5. It is clear that the mechanical properties of polyurea tend to improve with time, and require ~ 15 days to reach a plateau.

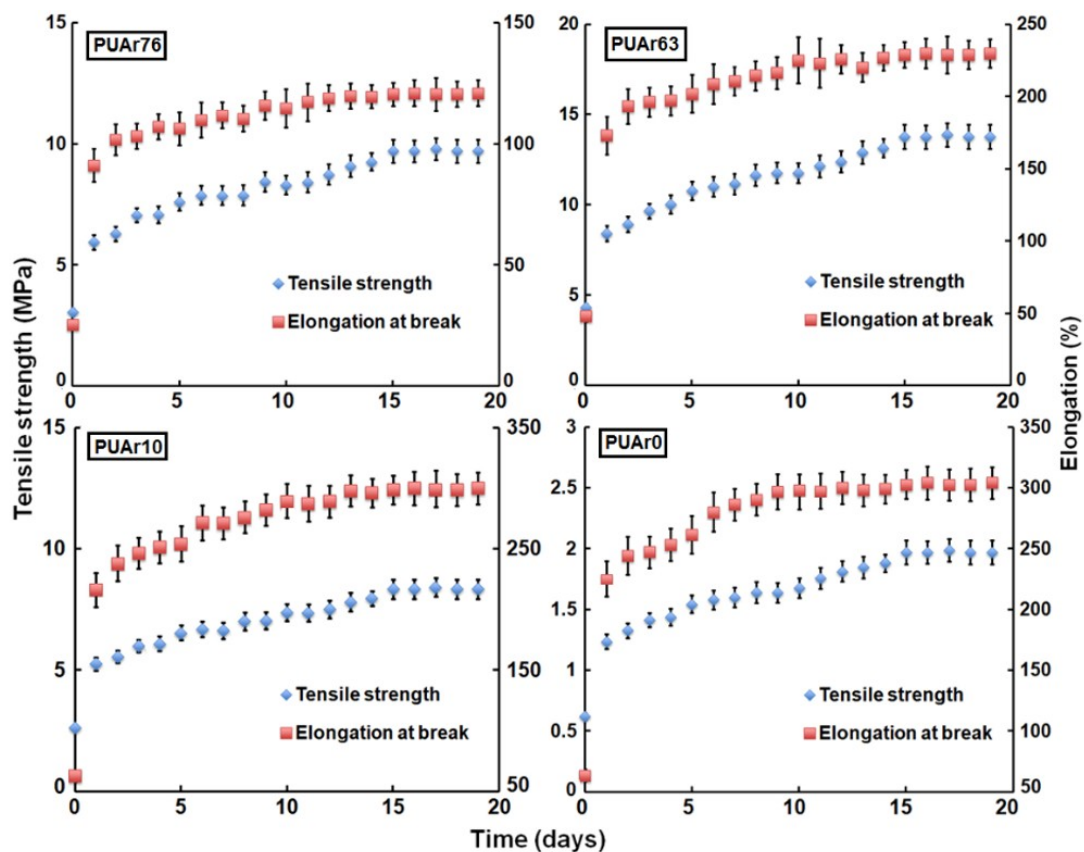


Figure 4.4: Evolution of tensile strength and % elongation of representative polyurea formulations as a function of time

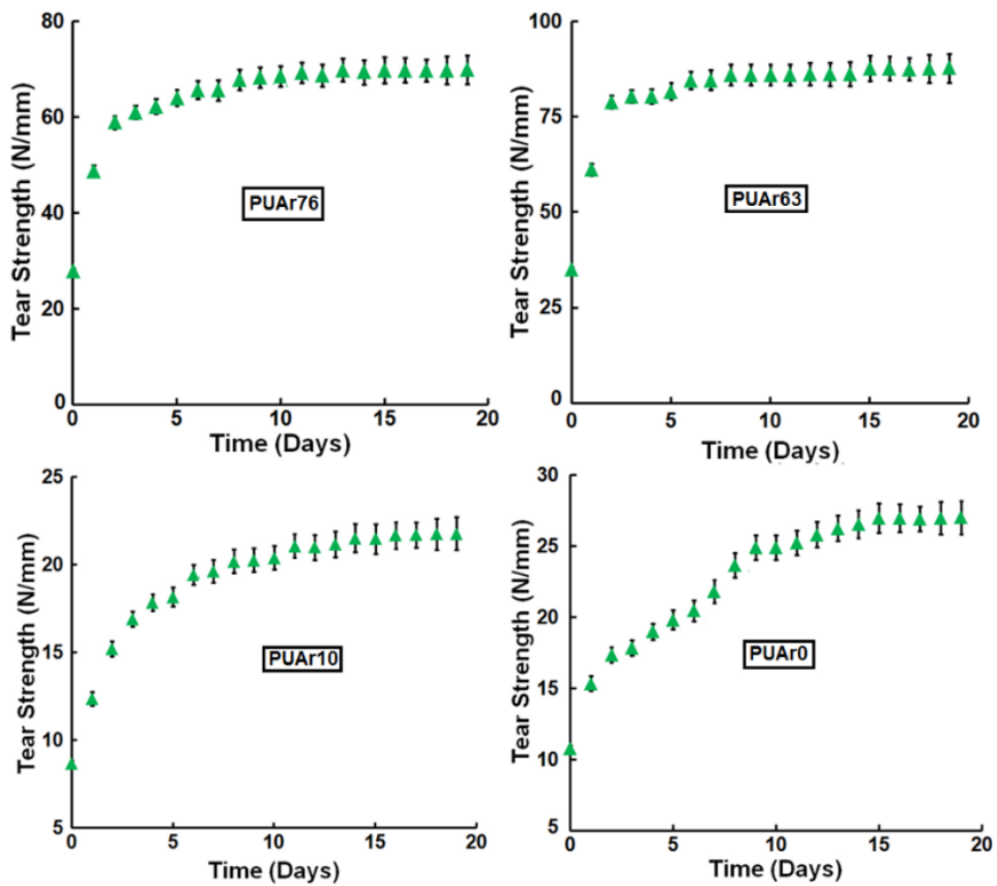


Figure 4.5: Evolution of tear strength of representative polyurea formulations as a function of time

It is to be noted that the solidification process occurs in a matter of seconds, with the urea linkages suddenly ‘freezing’ in space, leading to a precipitous build-up of stresses. Interestingly, the stress buildup in any polymer is a result several competing phenomena [163]. In the present case of polyurea, the most significant contribution comes from the precipitous volume contraction due to fast reactivity of the raw materials. As polyurea cools to ambient conditions, further contraction ensues due to thermal shrinkage. Notably, in comparison to the core, shrinkage in the external surface occurs more rapidly, with the contraction of the core being constrained by the external rigid surface and reduced temperature gradients. This leads to an inhomogeneous stress distribution throughout the

polymer, which is tensile in the core and compressive at the surface [164]. The difference in the coefficient of thermal expansion in the reinforcement and matrix has been reported to result in significant buildup of stress in composite structures [165]. The properties of polyurea are basically a result of its interesting microstructure, which in turn comprises of urea hard segments distributed throughout the polyether soft segment. Since the hard and soft domains in polyurea are expected to exhibit dissimilar thermal expansion coefficients, this is expected to contribute to the development of internal stresses in the polymer. These in-built stresses manifest themselves in the form of relatively inferior mechanical properties, which develop with time due to its eventual relaxation

.However, all the polyurea formulations exhibit a sub-ambient glass transition temperature, therefore segmental motions in polyurea can occur freely under ambient temperatures, especially in the soft segments. These motions eventually lead to a spatial structural arrangement with lowest interatomic force on each atom: a process that continues over extended time periods. This leads to the relaxation of internal stresses, which build-up within the polymer during spray coating. It is to be noted that increasing the temperature of the sample (e.g. annealing) can accelerate this process of stress relaxation, thereby shortening the time frame required for achieving optimal properties [119].

4.3.3.2 Mechanical properties of cured polyurea films (post 15 days)

Characteristic mechanical properties of the fully cured polyurea formulations (post 15 days of spraying) are presented in Figure 4.6 and Figure 4.7.

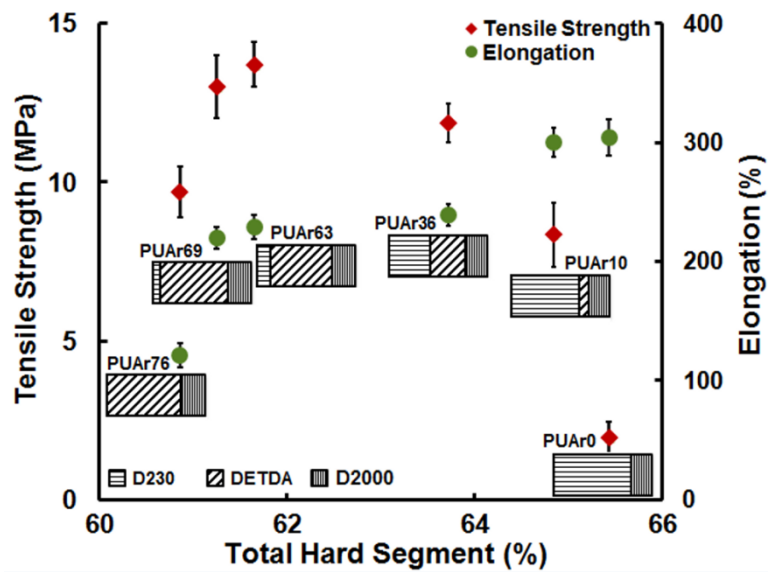


Figure 4.6: Variation in tensile strength and elongation of polyurea (post 15 days) due to chain extension. The relative contribution of aromatic and aliphatic hard segment is also included in the figure

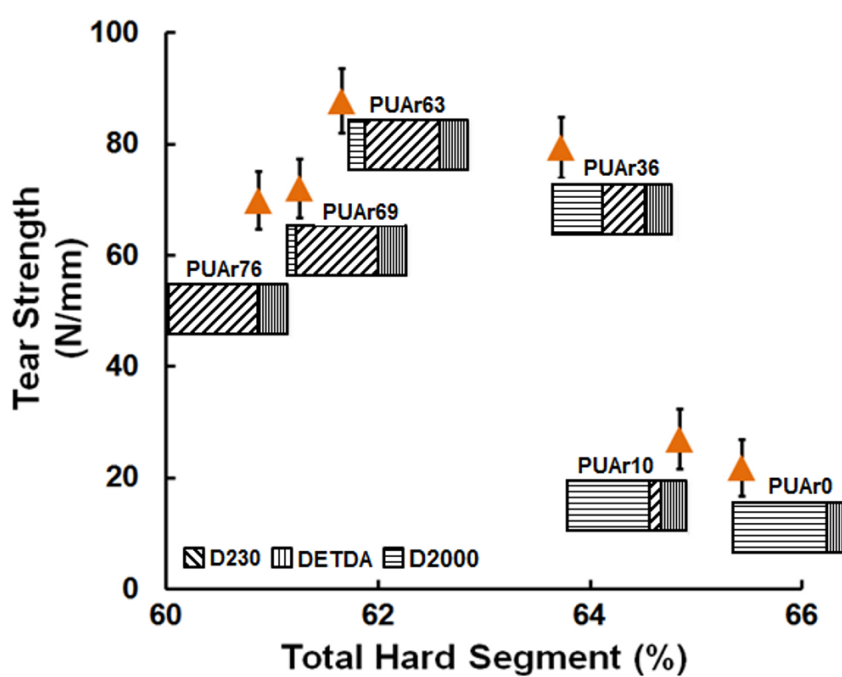


Figure 4.7: Variation in tear strength (post 15 days) due to chain extension. The relative contribution of aromatic and aliphatic hard segment is also included in the figure

Distinguishing properties viz. tensile strength, elongation and tear strength of polyurea formulation are also tabulated in Table 4.4. Table 4.2 can be used as ready reference for the individual contributions of the long chain amine (D2000), aromatic (DETDA) and aliphatic chain extender (D230) in urea linkages.

Table 4.4: Characteristic mechanical properties of polyurea samples (post 15 days)

Sample designation	Tensile Strength (MPa)	Elongation (%)	Tear Strength (N/mm)
PUAr-76	9.7 ± 0.8	121 ± 10	69 ± 5.2
PUAr-69	13.0 ± 1	220 ± 09	72 ± 5.3
PUAr-63	13.7 ± 0.7	229 ± 10	87.8 ± 5.8
PUAr-36	11.8 ± 0.6	239 ± 09	79.4 ± 5.5
PUAr-10	8.3 ± 1	300 ± 12	27.0 ± 5.4
PUAr-0	1.9 ± 0.5	304 ± 15	21.8 ± 5.1

As has been mentioned, the properties of polyurea depend strongly on the extent of hydrogen bonding between the macromolecular chains. In the absence of any chain extender, the urea linkages in polyurea are placed relatively farther from each other. In Figure 4.8 it can be seen that the inclusion of chain extender in the formulation leads to formation of closeby urea linkages, which in-turn favour the formation of hydrogen bonding between them and their further alliance into hard domains.

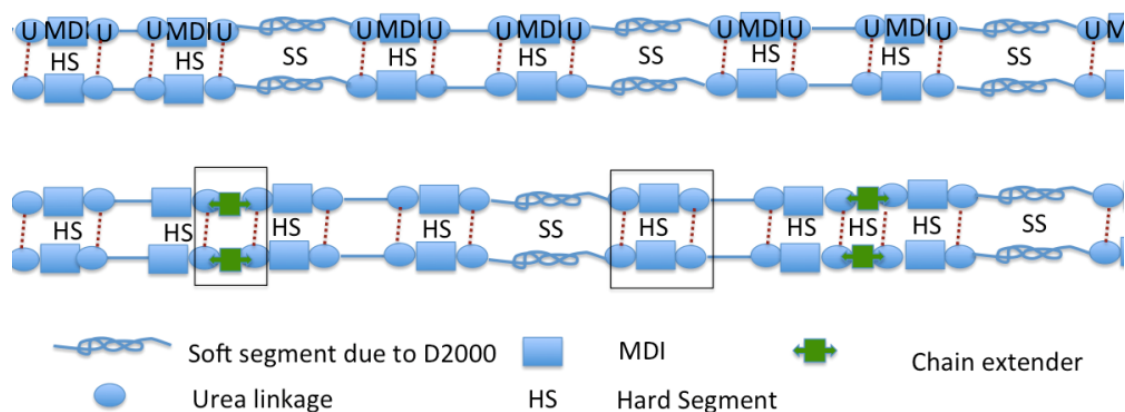


Figure 4.8: Increase in the vicinity of urea linkages through chain extension process

It can be expected that increasing hard segment will lead to higher mechanical properties in terms of its strength. However, our results (Figure 4.6 and Figure 4.7) reveal that the formulations containing only aliphatic chain extender (D230) possess higher hard segment (as determined theoretically) but exhibit relatively lower tensile strength. This can be attributed to several reasons, the most important being the strength of the H-bonds between the molecular chains. As shown in Figure 4.9, the distance between the urea linkages formed due to DETDA is much lower (5.35\AA) as compared to those formed due to D230 (12.6\AA). The increased vicinity of the urea linkages increases the possibility of H-bonding between the groups, although the total number of urea linkages remains the same in all formulations.

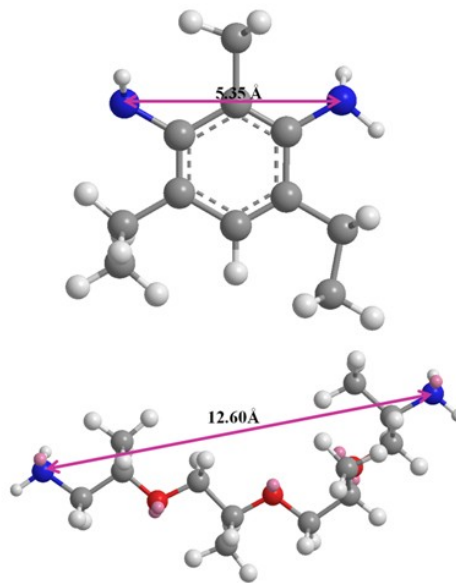


Figure 4.9: Theoretical N-N distance in DETDA and D 230

Another reason for the higher tensile strength in aromatic chain extended formulations is the presence of stiffer aromatic rings in the main chain of polyurea. The pictorial representation of hydrogen bonding sites between the urea linkages formed by aromatic and aliphatic chain extenders is presented in Figure 4.10.

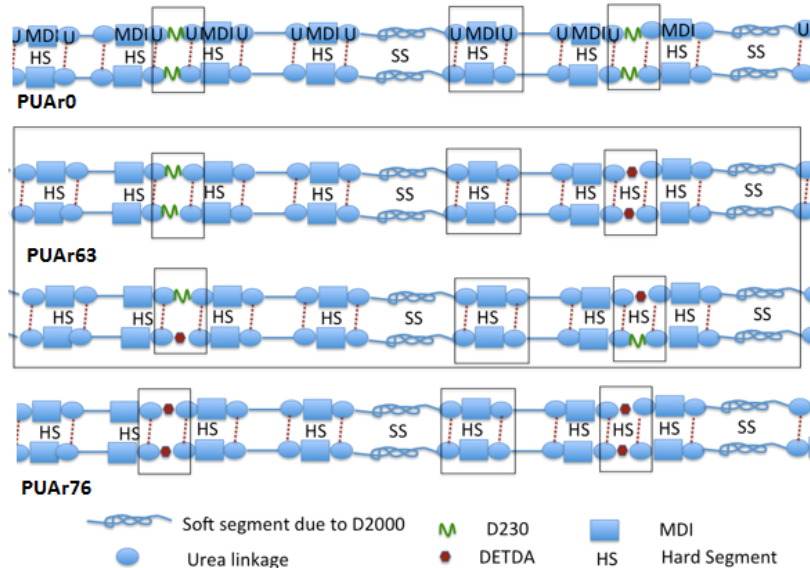


Figure 4.10: Representative Hydrogen bonding sites in polyurea chains formed by aromatic and aliphatic chain extenders

Figure 4.11 depict representative hard-segment models, mainly based on the hydrogen bonding between proton acceptor ($>C=O$) and proton donor ($N-H$).

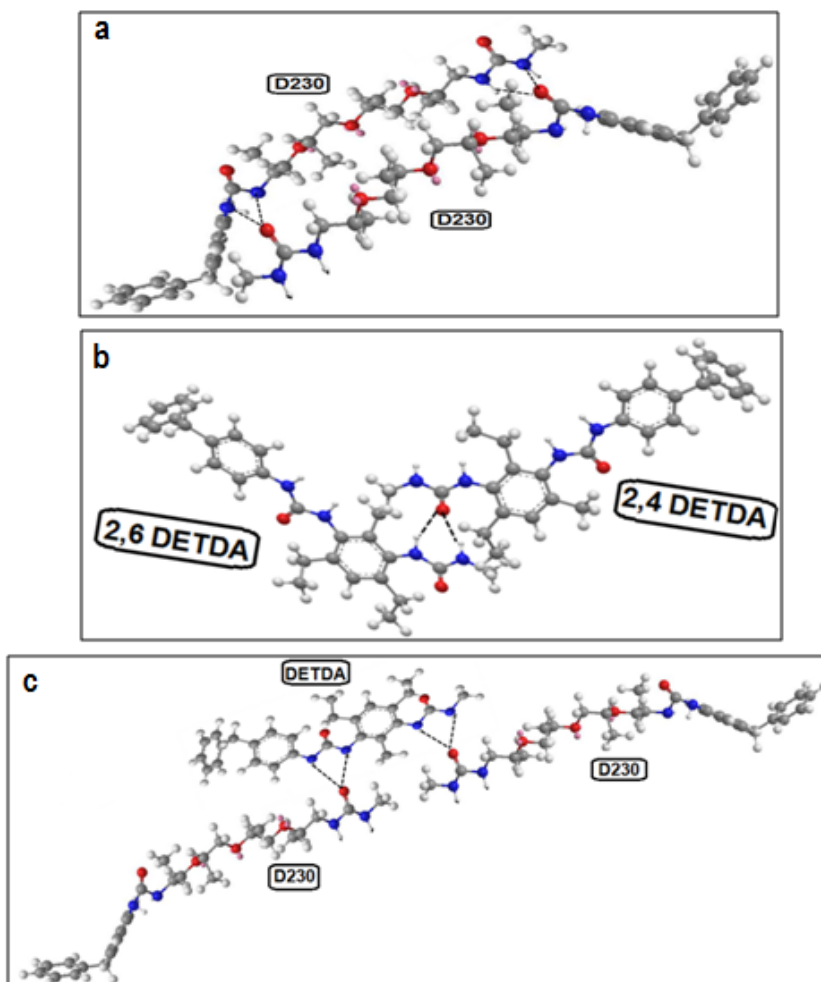


Figure 4.11: Representative hard-segment models, based on the hydrogen bonding between proton acceptor ($>C=O$) and proton donor ($N-H$). a) Between D230 and D230 b) DETDA and DETDA and c) DETDA and D230

Interestingly, formulations containing both aromatic and aliphatic chain extender exhibit better mechanical properties with PU-Ar 63 exhibiting optimal properties. It is envisioned that under the experimental conditions employed for spraying, the formulation with an optimal balance of aromatic and aliphatic chain extender forces the molecules to

align in a manner thereby forming a chain with optimal H-bonding.

Previous theoretical studies have revealed that proper orientation of the planar rings is a pre-requisite for apposite H-bonding in polyureas containing aromatic groups [166]. Since the microphase morphology is strongly dependent on the total hydrogen bonding resulting from various competitive possibilities in the polymer chain, we believe that the presence of both aromatic and aliphatic extenders in optimal amounts helps in aligning the >C=O and N-H groups so as to increase the extent of H-bonding in certain formulations. Proper orientation of the >C=O---N-H leads to a phase separated morphology, which manifests in terms of optimal mechanical properties in PU-Ar 63. Our results indicate that the presence of both aromatic and aliphatic chain extender improves the processing behavior as well as helps in achieving optimal properties.

It is to be noted that in view of the restrictions posed by the spray equipment (1:1 volume ratio), spraying of polyurea is not possible for formulations not containing any chain extender. Therefore, non-chain extended films of polyurea (~3 mm) in the absence of chain extender were prepared by solution casting technique, the composition and properties of which are presented in Table 4.5. It can be seen that films prepared in the absence of chain extender exhibited tensile strength of 0.3MPa and elongation of 1360%.

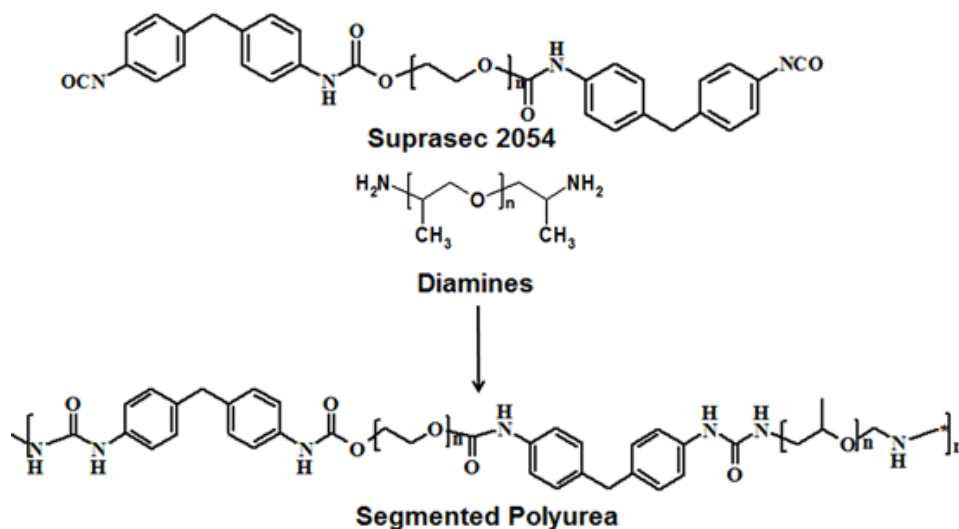
Table 4.5: Details of composition and properties of non-chain extended polyurea

Sample designation	Suprasec 2054 (mL)	Amine D 2000 (mL)	Solvent (Dichloromethane) (mL)	HS %	Tensile strength (MPa)	Elongation (%)
PU2000	32	115	1000	22	0.3 ±0.1	1360 ±34

4.3.4 FTIR spectroscopy

A representative schematic depicting the formation of a representative polyurea macromolecule through the reaction of a diisocyanate with diamine is presented in

Scheme 4.1.



Scheme 4.1: Representative diisocyanate-diamine reaction leading to formation of polyurea

It is clear from the scheme that the reaction is accompanied with several structural changes, which renders this a perfect system to be followed through FTIR spectroscopy [167-170]. The FTIR spectra of all the reactants are presented in the Figure 4.12.

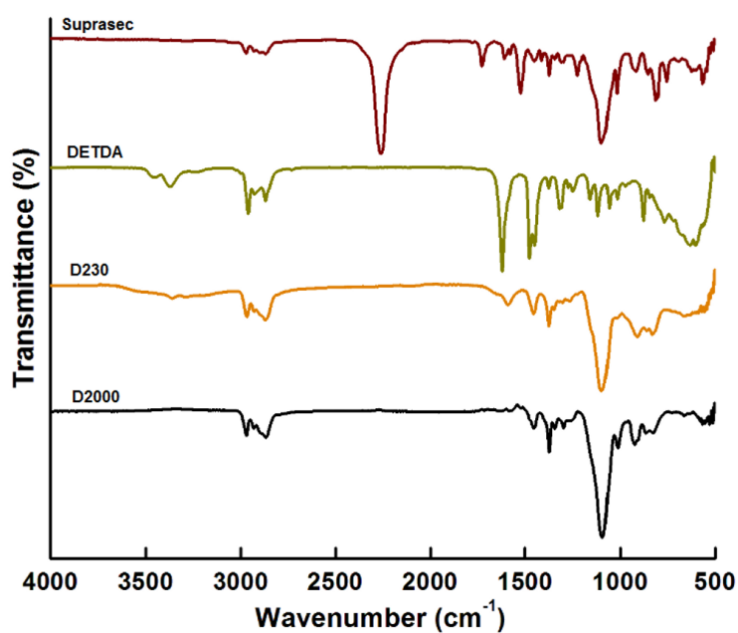


Figure 4.12: FTIR Spectra of individual components of formulations

In the spectra of the primary amines (D230 and D2000), two separate N-H stretching bands are noticeable: a broad peak due to asymmetrical stretching at $\sim 3300\text{--}3400\text{ cm}^{-1}$ and the other due to symmetrical stretching at $\sim 3330\text{--}3250\text{ cm}^{-1}$. Presence of free carbonyl ($>\text{C}=\text{O}$) in the isocyanate prepolymer leads to appearance of a sharp peak in the $1730\text{--}1740\text{ cm}^{-1}$. Characteristic frequencies associated with the $>\text{C}=\text{O}$ and N-H groups have been tabulated in previous chapter (Table 2.2).

4.3.4.1 Structural evolution in polyurea

In view of the structural changes occurring within, this reaction can be consummately followed through FTIR spectroscopy. The formation of polyurea can be characteristically followed by the disappearance of the absorption band at 2263 cm^{-1} ($\nu_{\text{N}=\text{C}=\text{O}}$) [119]. The reaction with amine and isocyanate led to similar changes in the FTIR spectra of all the formulations, and the change in the spectra of a representative formulation (PU-Ar 63) is presented in Figure 4.13. It can be seen that the intensity of NCO absorbance at 2263 cm^{-1} decreased exponentially within the first few minutes of the reaction, however its complete disappearance mandated $\sim 8\text{ h}$. Subsequently, the spectra remained practically unaltered even after 1 month of curing under ambient conditions. It is interesting to note that although the reaction between isocyanate and amine appear to be instantaneous, with solidification occurring in a matter of seconds, structural changes continue within the polymer over much longer periods. Further, due to the existence of polyurea in the rubbery regime at room temperatures, the possibility of polyurea chains restructuring, including H-bond rearrangement is highly probable, however it is not possible to follow these subtle changes through FTIR spectroscopy.

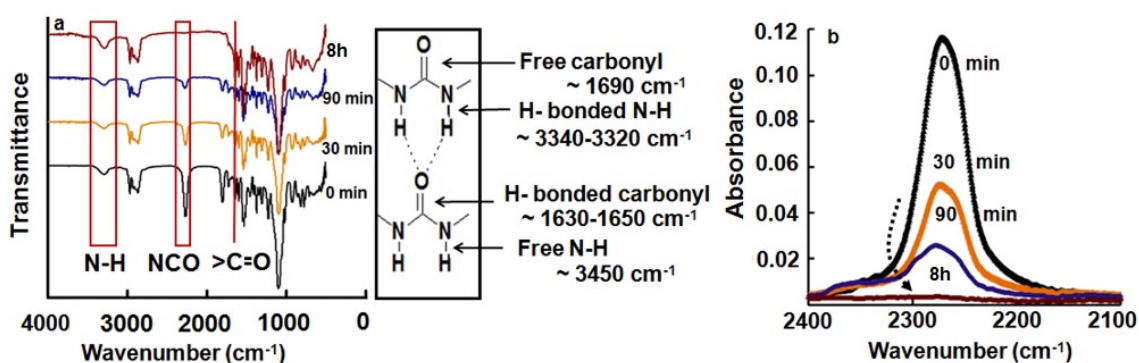


Figure 4.13: a) Change in the FTIR spectra due to reaction of isocyanate with amine b) Decrease in isocyanate absorbance.

4.3.4.2 Structural features of polyurea (post 15 days)

The FTIR spectra of the polyurea formulations sprayed are presented in Figure 4.14. Of particular interest is to observe the spectral features associated with the amine (N-H) and carbonyl (>C=O) regions. The appearance of the absorption band at 1630-1650 cm⁻¹ is attributed to the hydrogen bonded carbonyl (>C=O) with two nearby N-H, which is referred to as “ordered” bonding [115, 119]. A significant red-shift (towards lower frequency) in the position of the >C=O and N-H stretching bands were observed due to inter-molecular or intra-molecular hydrogen bonding [171, 172]. It was observed that the formulations containing aromatic chain extenders exhibited N-H band stretching at much lower frequencies, which are indicative of stronger H bonding in aromatic chain extended polyureas. The shift in the frequency associated with the free groups and the hydrogen-bonded ones present qualitative information regarding the strength of the interactions. It is interesting to note a concomitant decrease in the position of the N-H and >C=O band with increasing amount of aromatic chain extender in the formulation.

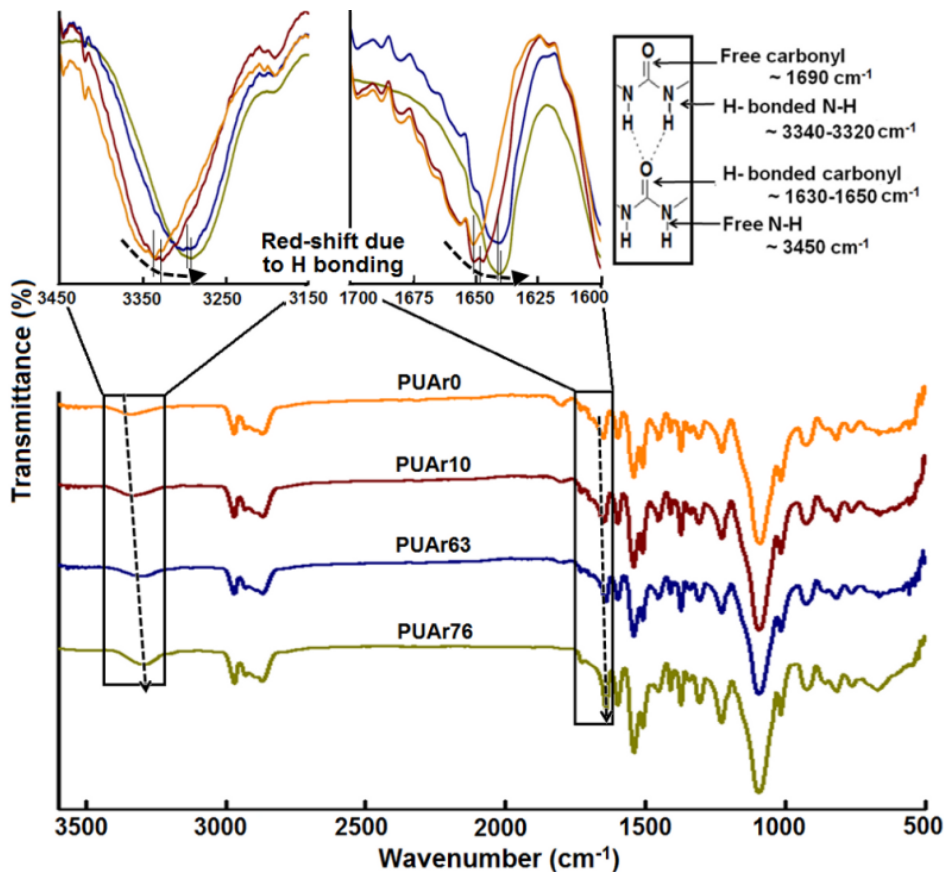


Figure 4.14: FTIR spectra of polyurea formulations

4.3.5 Dynamic mechanical analysis

Dynamic mechanical analysis was performed on the polyurea formulations in dual cantilever mode. The ratio of dynamic stress to dynamic strain yielded complex modulus (E^*), which was resolved to obtain the in-phase component (Storage modulus, $E' = E^* \sin\theta$), and the out-of-phase component (Loss modulus, $E'' = E^* \cos\theta$). The former (E') is indicative of the stiffness of the material, and the latter (E'') is the ability of the material to dissipate mechanical energy. The ratio of loss and storage moduli (referred to as $\tan \delta$) is representative of the ratio of the dissipated and stored mechanical energy in each loading cycle.

4.3.5.1 Evolution of Dynamic mechanical properties

Dynamic mechanical studies on the various polyurea formulations were performed at different stages of curing, and the results in terms of storage and loss modulus is presented in Figure 4.15.

It is interesting to note that the storage modulus increases with time and eventually level off after ~ 15 days of curing. The storage and loss modulus profile characteristically reveal a single relaxation peak in the temperature region studied, which is attributed to the segmental motions linked with the soft segments in the polymer. The glass transition temperature (T_g) was established from the peak of the loss modulus profile [128, 129], which remained unaltered with time and were found to exhibit sub-zero glass transition temperature.

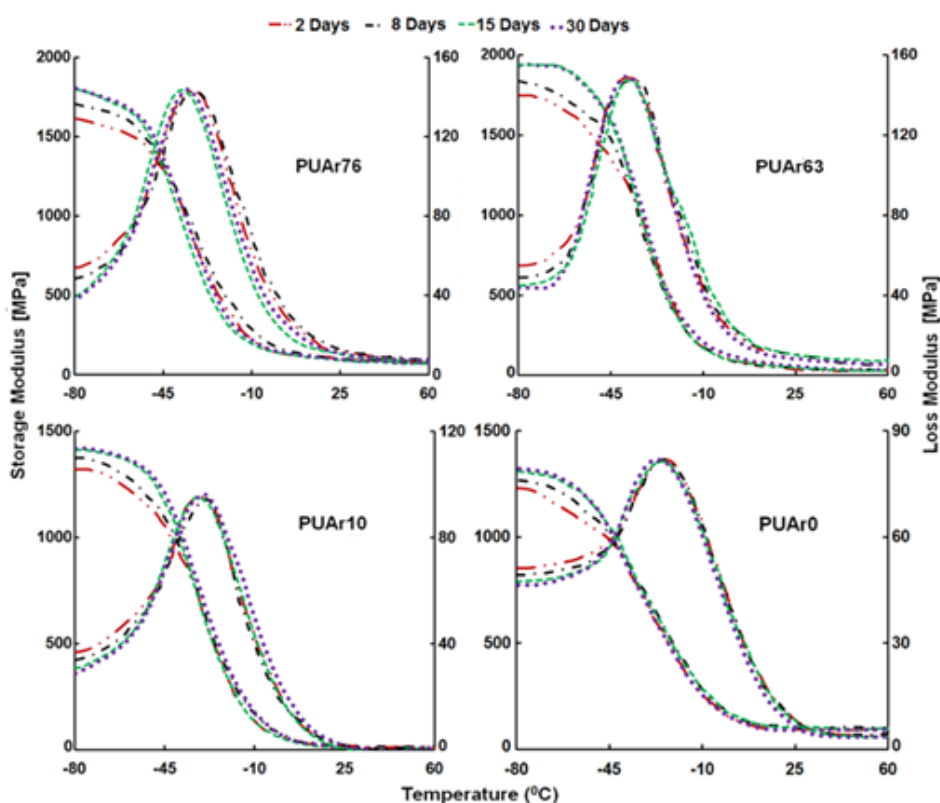


Figure 4.15: Variation of storage and loss modulus of polyurea formulations with temperature

4.3.5.2 Dynamic mechanical properties of polyurea (post 15 days)

The variation of storage and loss modulus of polyurea formulations as a function of temperature and frequency is presented in Figure 4.16. A single relaxation peak can be seen in all the formulations, which is due to the initiation of motions associated with the soft polyether segments in the polymeric chain. Throughout the transition zone of polyurea, its stiffness, as indicated by E' decreases drastically as the material transitions from 'glass' to 'rubber'. As the frequency of the dynamic loading is increased, an organized shift in both the loss and storage modulus trace towards higher temperature is clearly evidenced [118, 128-130].

It is particularly interesting to observe the increase in storage modulus (E') of polyurea sample with increasing aromatic chain extender content, at any particular temperature. This can be attributed to the increase in the number of relatively stiffer sp^2 hybridised aromatic groups in the chain, reflecting in terms of higher storage modulus.

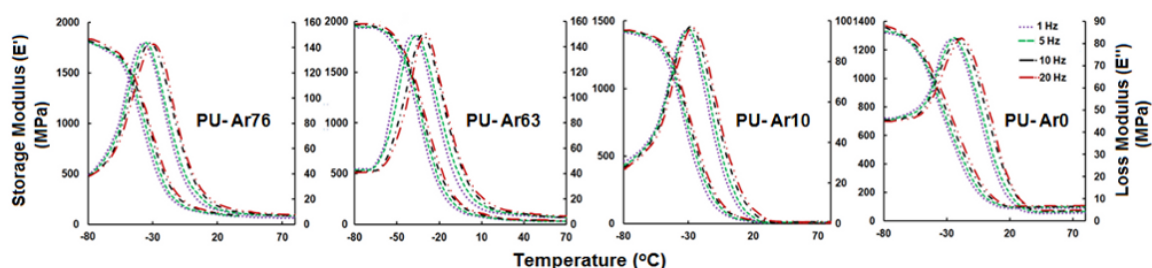


Figure 4.16: Variation of storage and loss modulus with temperature at different frequencies

The glass transition temperature were quantified in terms of the peak of loss modulus trace [118, 128] and the same are pictorially presented in Figure 4.17. Polyurea characteristically exhibits a sub-zero glass transition temperature [128, 129], associated with the soft segmental motions which results in its elastomeric nature under ambient

conditions. A systematic shift of this characteristic parameter (T_g) towards higher temperature is evident with increasing total hard segment content. T_g was evidenced at -40°C (1Hz) for PU-Ar76 (HS = 60.8), which increases to -28°C for PU Ar-0 (HS = 65.4). It is particularly interesting to note the large width associated with the glass transition phenomenon ($\Delta T > 80^\circ\text{C}$): a property rather unique to polyurea [118].

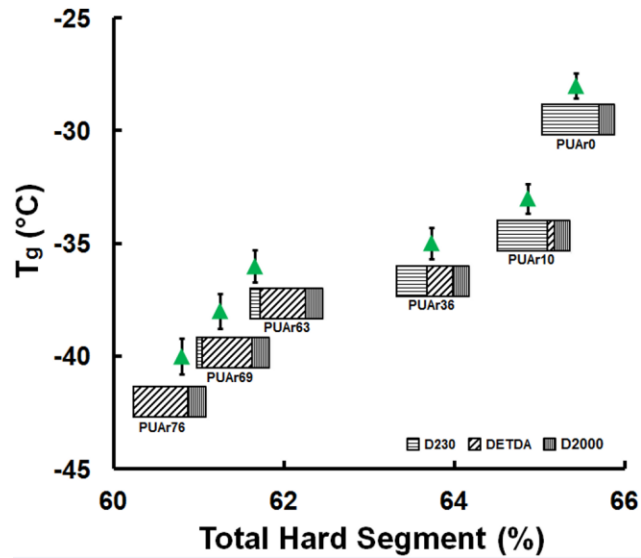


Figure 4.17: Variation of glass transition temperature with increasing hard segment

The energy dissipation potential of the polyurea formulations [129], in terms of the loss factor ($\tan \delta$), is presented in Figure 4.18. Higher $\tan \delta$ suggests relatively higher potential of the material towards energy dissipation as compared to its energy storage. It can be seen from the figure that the ability of the material to dissipate energy is directly proportional to its total hard segment content.

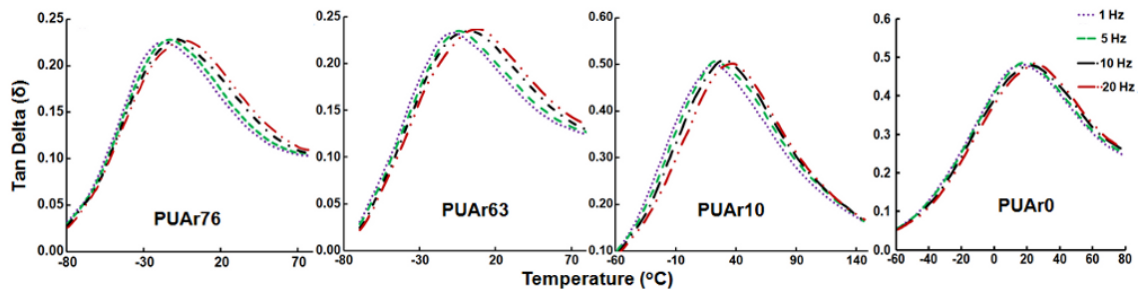


Figure 4.18: Variation of loss factor with hard segment

4.3.6 Thermal properties

4.3.6.1 Thermogravimetry

The thermal properties of polyurea have been reported to be strongly dependent on the hard segment content and the extent of phase segregation in the polymer chain [126]. The TG traces along with the corresponding derivative thermogravimetric (DTG) traces of the polyurea formulations (under N₂ atmosphere) are presented in Figure 4.19.

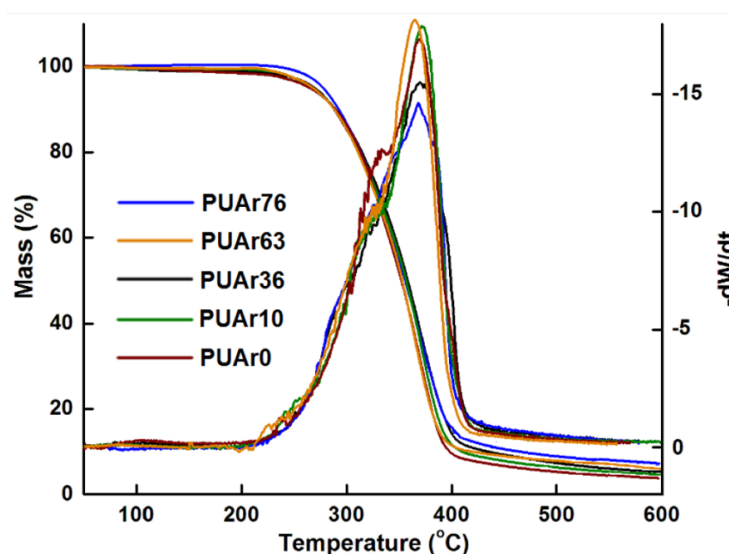


Figure 4.19: TG-DTG traces of polyurea formulations containing aromatic and aliphatic chain extender

It can be seen that all the polyurea samples exhibit a two-step degradation profile, with the peak position of DTG depending on the fraction of hard segment. Initial increase in the temperature of the polyurea sample leads to the disruption of the H-bonds within the hard segments, a process not associated with any gravimetric changes. The first major mass loss (220-350°C) is attributed to the decomposition of hard segments (primarily urea linkages), in view of their relatively low thermal stability. Studies using hyphenated techniques have revealed that this decomposition step leads primarily to the evolution of carbon dioxide. The subsequent mass loss (350-425°C) occurs due to the pyrolytic

decomposition of the polyether chains, leading to evolution of hydrocarbons in larger amounts [126]. The mass loss during the first and second stages of thermal degradation is presented in Table 4.6.

It is to be noted that the mass losses at these steps do not exactly match with the theoretically estimated hard segments, although a direct relationship is clearly evidenced. This discrepancy can be attributed to the fact that for estimation of HS, the mass of isocyanate taken for calculation is the mass of prepolymer, which in turn is formed by the reaction of MDI with a long chain amine/ diol. The complete decomposition leaves behind a char residue of ~ 5-8% w/w (at 600°C).

Table 4.6: Characteristic thermal properties as derived from thermogravimetric analysis

Sample designation	Total hard segment	T _{5%} (°C)	1 st step due to degradation of hard segment		2 nd step due to degradation of soft segment		Char yield (%)
			% Mass loss	T ₁ max	% Mass loss	T ₂ max (°C)	
PUAr-76	60.8	269	30	343	62	370	8
PUAr-63	61.6	276	32	344	61	368	7
PUAr-36	63.7	282	34	348	60	370	6
PUAr-10	64.8	274	35	343	59	369	6
PUAr-0	65.4	289	37	344	58	370	5

The structural changes due to thermal degradation of polyurea were followed using FTIR spectroscopy. For this purpose, the polyurea samples were placed under isothermal conditions for predetermined periods (5 min) at different set-temperatures (50°C, 150°C, 250°C, 350°C and 450°C). The FTIR spectra of the samples recorded at different stages of thermal degradation. All the samples exhibited similar behavior and the

representative spectra for PUAR 63 are presented in Figure 4.20.

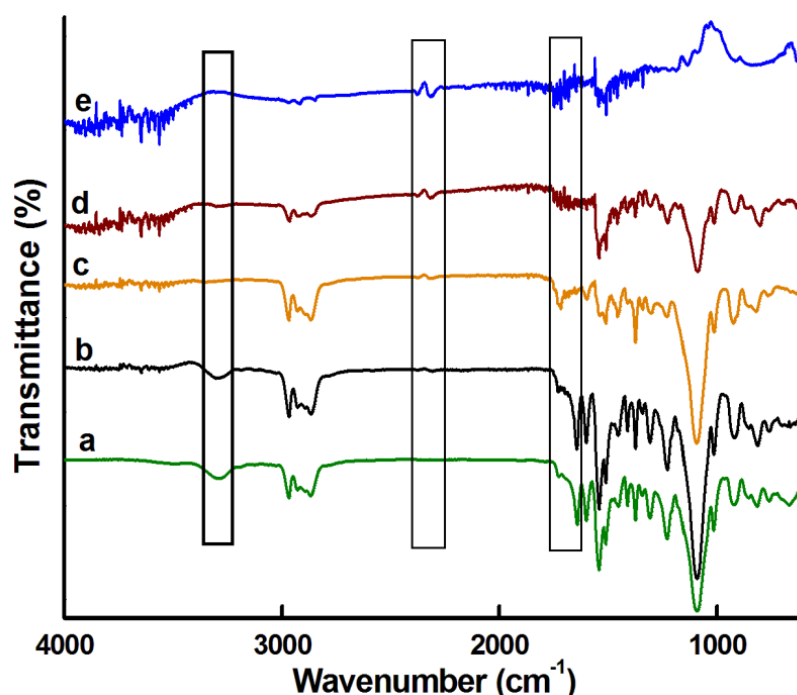


Figure 4.20: Changes in the FTIR spectra of sample as a result of thermal degradation of PUAr63 a) 50°C, b) 150°C, c) 250°C, d) 350°C and e) 450°C)

It can be seen that there are no perceptible change in the FTIR spectra of the sample as the temperature is raised to 150°C. As the temperature is raised further to 250 °C, significant changes can be observed particularly in the region associated with the N-H and C=O. Thermal degradation results in the cleavage of the C-N bond in urea linkages, due to its comparatively lower bond energy (C-N, 293 kJ/mol) as compared to others (C-O, 358 kJ/mol), (C-C, 348 kJ/mol). This leads to evolution of CO₂, which can be seen as a small peak in the region (2320 cm⁻¹). In addition, the peak in the region associated with H bonded N-H stretching shifts to higher frequencies, due to reduced H-bonding. This is also associated with a shift in the position of the C=O bond from 1642 to 1716 cm⁻¹. As the temperature is raised further to 350°C, the absorbance band due to C=O stretching practically disappears. At 450°C, the sample completely chars with the spectra

characteristic of residual carbon. It is interesting to note that at elevated temperatures, the presence of gaseous CO₂ (trapped within the sample) is evident in the form of a peak at 2320 cm⁻¹.

4.3.6.2 Calorimetric studies

DSC scans were performed at definite time periods and the traces obtained for a representative sample (PU-Ar 63) are presented in Figure 4.21. The shift in the baseline of the heat flow curve is indicative of the glass transition phenomenon [173]. In line with DMA results, there is not much change in the T_g values due to curing.

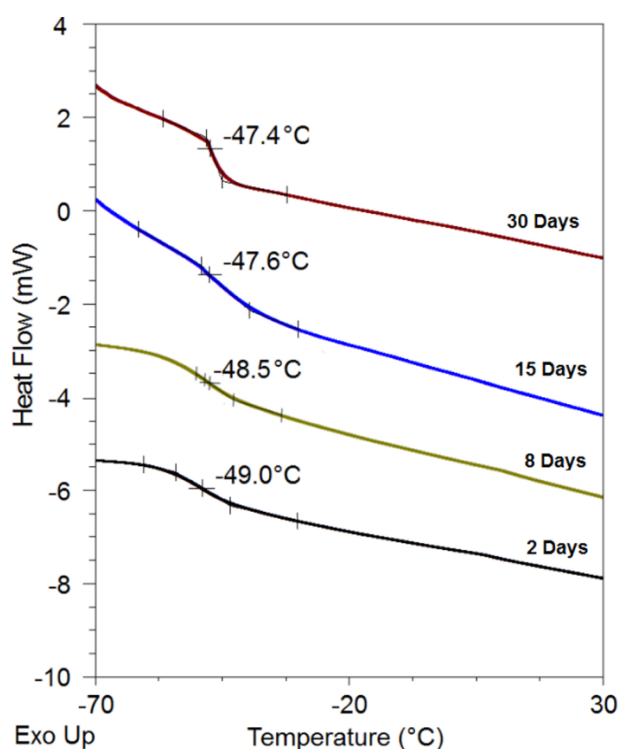


Figure 4.21: DSC traces of polyurea at different periods of curing

The DSC traces of the cured polyurea samples (post 15 days of curing) are presented in Figure 4.22. The shift in the baseline of the heat flow curve is indicative of the glass transition phenomenon [173]. It is to be noted that the T_g determined using DSC is slightly lower than the values obtained from DMA studies. This can be attributed to the difference in the property being measured, i.e. change in specific heat capacity (DSC),

and change in the mechanical properties (DMA). In addition, the difference in the rate of heating also leads to the observed difference in the values.

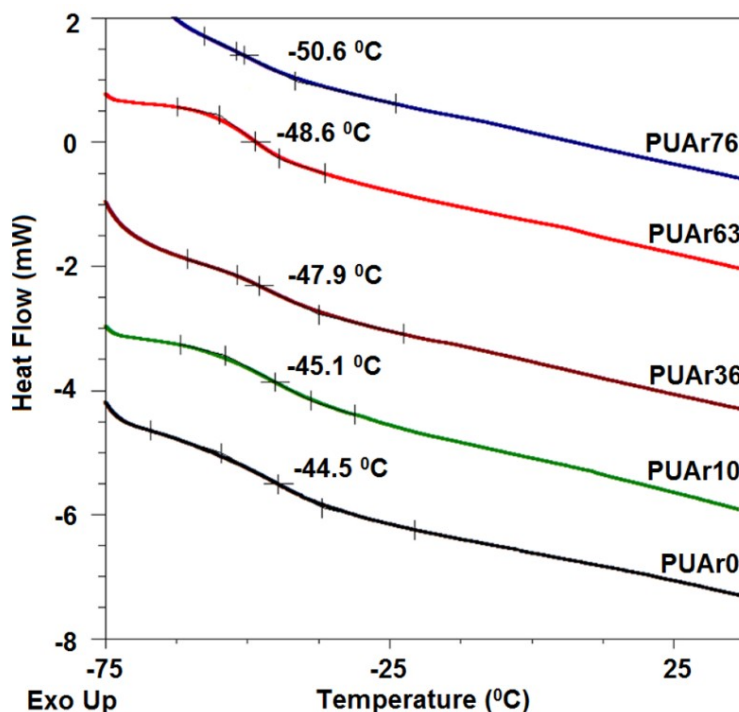
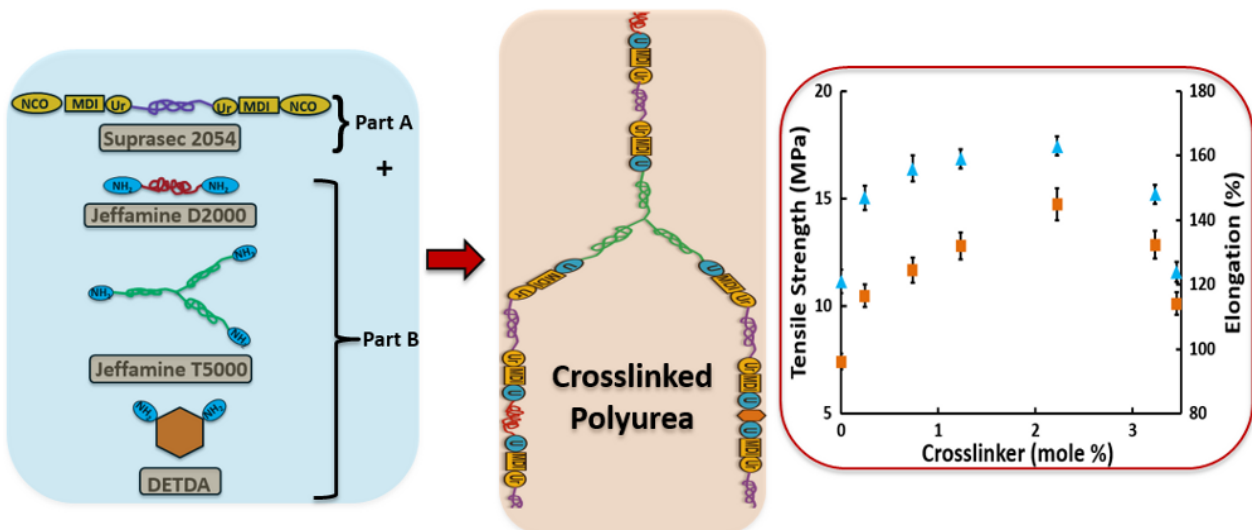


Figure 4.22: DSC traces for polyurea formulations

It appears that since the polymer exists much above its low temperature T_g , therefore segmental motions associated with the soft segments continue within the polymer, which lead to release of inbuilt internal stresses. In addition, there is a distinct possibility of H-bonds rearrangement, which too can lead to disbursement of internal stresses.

Chapter 5

Effect of chemical crosslinker on the material properties of polyurea



5.1 Introduction

Crosslinking and curing are fundamental tools for tuning the structure-property relationship in polymers [174]. The excellent mechanical properties of polyurea are an indirect manifestation of its internal morphology, which is further a result of intermolecular and intra-molecular bidentate H-bonds between the urea linkages [117]. Introduction of chemical crosslinking can further alter the mechanical properties of polyurea by bestowing stiffness, ductility and chemical resistance [175]. The consequences of chemical crosslinking on the material properties has been extensively studied in the relatively more popular class of similar polymer, i.e. polyurethanes [176, 177], however such studies on polyurea are lacking. Most of the commercial formulations contain a long chain crosslinker, but the effect of its introduction on the material properties has not been systematically studied, which inspired us to undertake this study. This chapter deals with the effect of introducing chemical cross-linking on the mechanical, thermal and structural properties of spray-coated polyurea.

The deliberate introduction of chemical crosslinks can alter the material properties of polyurea substantially. In the context of polyurea/polyurethane, common methods of crosslinking include inclusion of a higher-functional amine (functionality > 2) [178] or maintaining a slight excess of isocyanate ($i_{\text{NCO}} > 1$) [179] and combination thereof [177]. The excess isocyanate reacts with the urethane and urea groups to form allophanate and biuret linkages respectively [180, 181].

Studies on the introduction of short chain multifunctional amines like 1,3,5 triaminophenoxylbenzene (TAB)[182, 183], bis(4-aminophenyl) disulphide [184], 0.0 G PAMAM dendrimer [185], for crosslinking purposes has been performed. Short-chain crosslinking affects primarily the tensile properties[177-179, 186-189], swelling behavior

[189-192] and thermal degradation behavior [187, 193, 194]. Interestingly, most of the commercial polyurea formulations include a long chain crosslinker, the effect of introduction of which has not been explicated in the open literature. The present study focuses on the elucidation of the effect of long chain crosslinking on mechanical, thermal as well as the dynamic mechanical properties of polyurea coatings. The swelling behavior was also studied to understand the behavior of crosslinked polyurea in different media.

5.2 Experimental

5.2.1 Materials

Details of all the materials used for preparing polyurea formulations have been listed in previous chapters. The structure and physical properties of all the reactants are presented in Table 3.1.

5.2.2 Spraying of polyurea

The amine resin blend, i.e. Part B of the polyurea formulation comprised of a long chain amine (D-2000), crosslinker (T-5000) and chain extender (DETDA). Isocyanate precursor was diluted with requisite amount of propylene carbonate and used as the isocyanate source, i.e. Part A. The individual contributions of amine, crosslinker and the chain extender to the total urea content in the sample is tabulated and depicted pictorially in Table 5.1 and Figure 5.1 respectively. The contribution of amines, cross linker, and chain extender to the total urea content has been calculated using equation 4.1.

Table 5.1: Individual contribution of isocyanate and chain extenders to the total hard segment

Sample Designation	Total HS*	Contribution to urea linkages					
		T5000	T5000 (%)	DETDA	DETDA (%)	D2000	D2000 (%)
PUX0	60.86	-	-	1.34×10^{22}	75.85	4.27×10^{21}	24.15
PUX2	61.17	1.79×10^{20}	1.02	1.35×10^{22}	76.59	3.96×10^{21}	22.39
PUX7	61.12	5.39×10^{20}	3.05	1.38×10^{22}	78.02	3.34×10^{21}	18.93
PUX12	61.29	8.98×10^{20}	5.08	1.40×10^{22}	79.47	2.73×10^{21}	15.45
PUX22	61.63	1.62×10^{21}	9.15	1.45×10^{22}	82.36	1.50×10^{21}	8.49
PUX32	61.97	2.34×10^{21}	13.21	1.50×10^{22}	85.25	2.72×10^{20}	1.54
PUX35	62.04	2.50×10^{21}	14.11	1.52×10^{22}	85.89	-	-

* Total urea linkages= 1.76×10^{22}

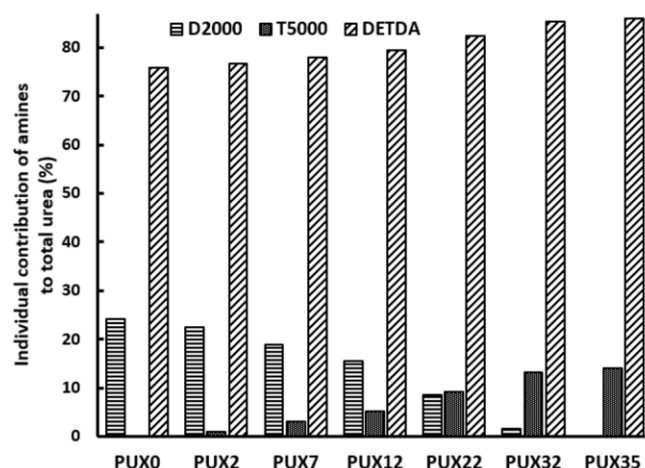


Figure 5.1: Percentage contribution of individual amine towards the total urea linkage present in the polymer

The hard segment content was determined as per established procedure (Equation. 1.3) [27]. The samples have been designated as PUX- followed by the contribution (mole % x10) of the crosslinker in the polymer.

Table 5.2: Formulation details of crosslinked polyurea

Sample designation	Amine (part per unit volume)			Total Hard segment (%)	Contribution of crosslinker (mole %)
	D2000	DETA	T5000 (crosslinker)		
PUX 0	78.78	21.22	-	60.86	0
PUX 2	72.65	21.88	5.47	61.17	0.2
PUX 7	61.75	21.84	16.41	61.12	0.7
PUX 12	50.41	22.44	27.35	61.29	1.2
PUX 22	27.71	23.25	49.24	61.63	2.2
PUX 32	5.03	23.85	71.12	61.97	3.2
PUX 35	-	24.07	75.93	62.06	3.5

Polyurea films of uniform thickness were prepared using a spray coating equipment, the details of which have been discussed in Chapter 3.

5.2.3 Characterization

Thermal (TGA, DSC), structural (FTIR) and mechanical characterization of polyurea samples were performed using technique discussed in previous chapter.

Swelling studies on polyurea samples were performed by placing disc shaped samples (50 mm dia, thickness ~3 mm) in different solvents for extended periods. The extent of swelling was quantified in terms of their swelling ratio.

$$SwellingRatio (\%) = \frac{(M_{swollen} - M_{dry}) \times 100}{M_{dry}} \dots\dots(5.1)$$

where, M_{dry} and $M_{swollen}$ refer to the initially dry specimen and post- equilibrium (7 days) of immersion in solvent.

5.3 Results and discussions

5.3.1 Effect of Crosslinking on mechanical properties

There are primarily two major constraints for preparation of polyurea films through spray coating technique; the most important being the maintenance of a stoichiometric balance of amine and isocyanate. In addition, there exist an operational constraint of maintaining 1:1 v/v ratio of isocyanate and amine. For the latter, the isocyanate prepolymer needs to be diluted with a reactive diluent (10%v/v) to ensure similar viscosities of resin blend and isocyanates [161]. The dependence of viscosity on temperature is presented in Figure 5.2.

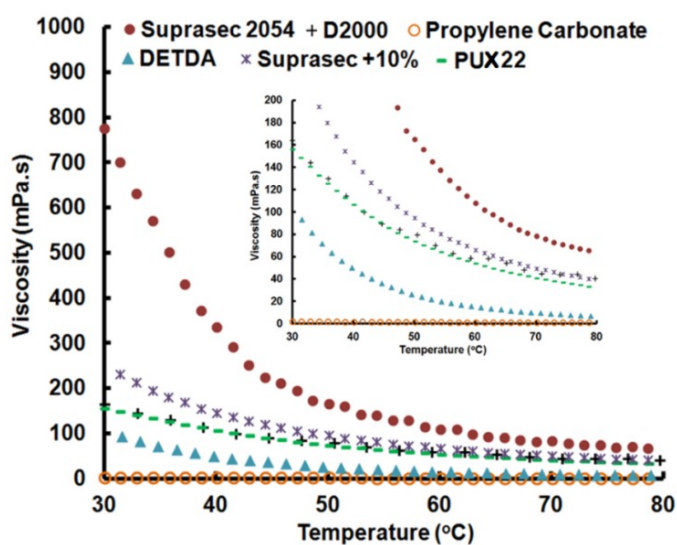


Figure 5.2: Variation of reactant viscosity with temperature

Under these constraints, the maximum amount of crosslinker (T 5000) in the formulation is restricted to 3.5 mole %. (See Appendix A for calculation of upper and lower limit of amines in formulations).

The presence of bidentate H-bonds between the polyurea chains leads to formation of a phase-segregated microstructure, where the hard domains are dispersed throughout the soft domains (comprising of polyether chains). In fact, the interesting mechanical properties of polyurea are a result of its inherent composite microstructure. The mechanical properties of polymers are generally governed by the difficulty of macromolecules to flow past one another, upon application of load. On the other hand, in the case of polyurea, the crystalline hard domains tend to further restrain the chain movement by acting as focal points of physical crosslinking. The introduction of chemical crosslinking is expected to result in further restraint in the chain mobility by forming a relatively rigid, non-flowing bulk in comparison to entanglements. The macromolecular chains thus reach their mobility limit at much smaller deformations, causing the external load to strain the chemical bonds. This is expected to reflect in terms of their mechanical properties and the characteristic properties of the resulting polyurea coatings are presented in Figure 5.3. Characteristic mechanical properties, i.e. tensile strength, elongation and modulus (M100) are also tabulated in Table 5.3. Significant improvement in both tensile strength as well as elongation occurs as a result of crosslinking but reaches a maxima and decreases.

Table 5.3: Characteristic mechanical properties of polyurea coatings

Sample designation	Tensile strength (MPa)	Elongation (%)	Modulus at 100% strain (M100), MPa
PUX0	7.40 ± 0.7	121 ± 3.7	7.0 ± 0.4
PUX2	10.48 ± 0.8	147 ± 3.8	8.7 ± 0.6
PUX7	11.69 ± 0.8	156 ± 4.1	9.2 ± 0.3
PUX12	12.8 ± 0.9	159 ± 3.0	9.7 ± 0.3
PUX22	14.74 ± 1.1	163 ± 3.0	10.7 ± 0.1
PUX32	12.86 ± 0.8	148 ± 3.0	10.9 ± 0.1
PUX35	10.12 ± 0.7	124 ± 3.1	11.1 ± 0.3

Interestingly, the uncrosslinked systems also exhibit tensile strength and elongation of the order of 7.4 ± 0.5 MPa and $121 \pm 10\%$ respectively. It is to be noted that all polyurea films were prepared while maintaining an isocyanate index of 1.1, i.e. 10% excess of isocyanate in the formulation. Thus, there exists a distinct possibility of formation of allophanate and biuret linkages as a result of the reaction of isocyanate with urethane and urea groups respectively [179, 180]. A comparison of the relative reaction rate of reactants with isocyanate reveal that the rate of reaction of isocyanate with primary amines is many-fold higher, which means that the possibility of allophanate and biuret linkages over a time frame of a few days is very less. This essentially implies that even physical crosslinks are capable of bestowing excellent mechanical properties to polyurea.

Introduction of a trifunctional amine based crosslinker (T 5000) is expected to improve the mechanical properties of the polyurea further. The present studies indicate that both strength and elongation improve substantially with increasing crosslinker content upto 2.2 mole % (PU X22) and subsequently deteriorate with increased concentration. This can be attributed to the fact that chemical crosslinking interferes with

the phase separation process [177]. Contrary to previous studies [195], the elongation associated with the formulations was found to increase with increasing cross-linker concentration; which probably was a result of the high molecular weight of the crosslinker.

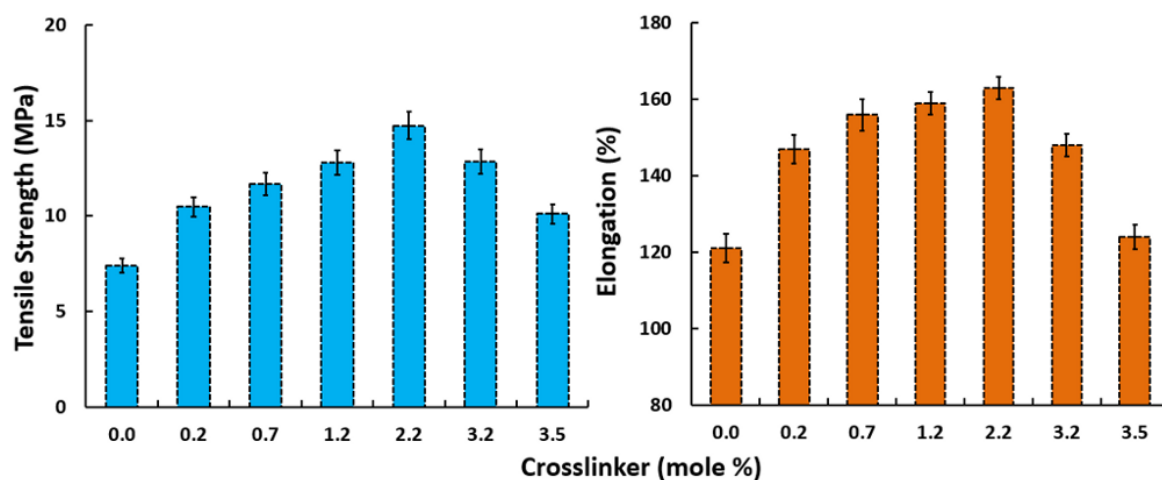


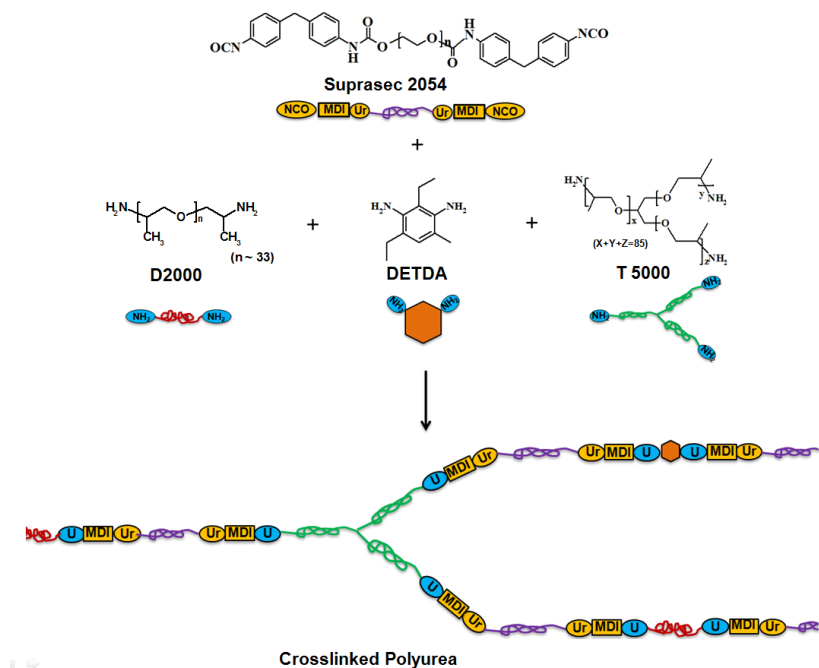
Figure 5.3: Variation in tensile strength and elongation of polyurea due to crosslinking

5.3.2 FTIR spectroscopy

A schematic of the isocyanate–amine reaction (in the presence of a trifunctional amine) is presented in Scheme 5.1 and the structural changes were followed by monitoring the disappearance of absorption band at 2263 cm^{-1} ($\nu_{\text{N}=\text{C}=\text{O}}$) [119] and the shift in the position of the $>\text{C}=\text{O}$ and N-H stretching bands [171, 172]. The FTIR spectra of the isocyanate, amine and that of the reaction product recorded at different intervals of time for a representative formulation (PUX22) are presented in Figure 5.4.

Table 2.2 can be referred for the characteristic frequencies associated with $>\text{C}=\text{O}$ and N-H groups. The sharp peak at $\sim 1730\text{--}1740\text{ cm}^{-1}$ in the FTIR of isocyanate prepolymer is a result of the presence of free carbonyl. In line with previous studies, the complete disappearance of NCO required $\sim 8\text{ h}$. The shifting of the ($>\text{C}=\text{O}$) absorption band from $\sim 1730\text{--}1740$ to $1630\text{--}1650\text{ cm}^{-1}$ is a result of hydrogen bonded carbonyl

(>C=O) with two nearby N-H, which is referred to as “ordered” bonding [115, 119, 196].



Scheme 5.1: Schematic of formation of crosslinked polyurea

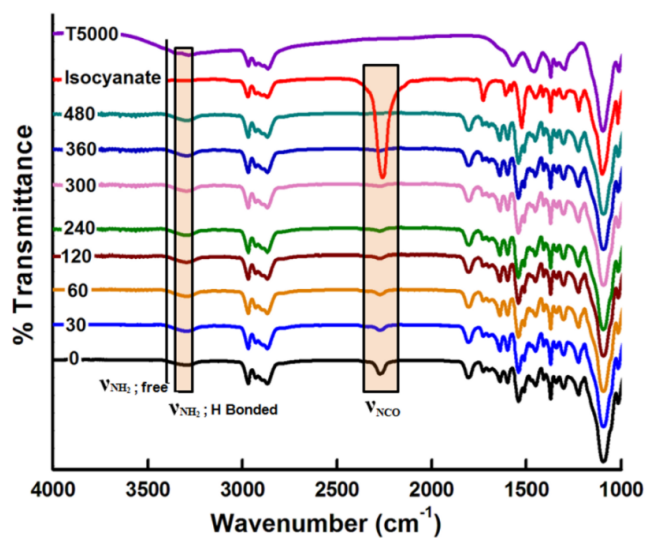


Figure 5.4: Change in the FTIR spectra of PUX22 as a function of time (in minutes)

Varying the amount of crosslinker in the formulation did not lead to any change in the FT-IR spectra, which are presented in Figure 5.5.

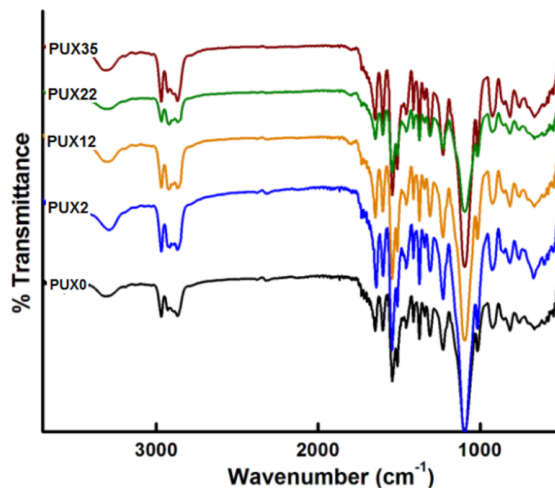


Figure 5.5: FTIR spectra of polyurea formulations

5.3.3 Dynamic mechanical analysis

The dynamic response of the polyurea formulations in terms of the variation of E' and E'' with temperature at constant frequency of 1Hz is presented in Figure 5.6.

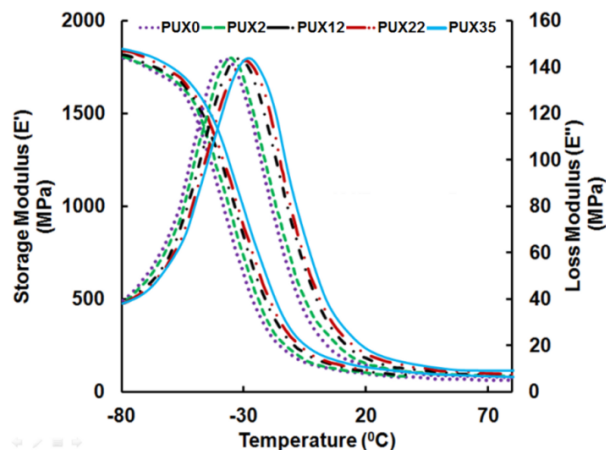


Figure 5.6: Variation of storage and loss modulus with temperature

At sub- T_g temperatures ($T < T_g$), all the formulations exhibited storage modulus of the same order (1800 ± 5 MPa). With increase in temperature, the storage modulus decreased substantially due to initiation of segmental motions of the mobile long chains at temperatures approached the glass transition region. For the purpose of quantification of T_g , the temperature associated with the loss moduli maxima was employed. A slight shift towards higher temperature was observed as the amount of crosslinker in the formulation

was increased. This can be attributed to the replacement of the mobile long chain diamines with trifunctional amines, which present relatively larger restriction on the segmental motions. All the formulations characteristically exhibited a sub-zero glass transition temperature [128, 129], which results in the elastomeric behavior of polyurea under ambient conditions.

. The storage moduli eventually reach a plateau, beyond which no further decrease in storage modulus is evidenced. The storage moduli (at 150°C) were used to estimate the crosslink density of the polymer. Assuming the rubber elasticity theory, the equilibrium shear modulus G is given by [197].

$$G = G^{\circ}_N T_e + (v-h\mu)RT \dots\dots\dots (5.2)$$

Where, the first and second term refer to the contribution of ‘physical entanglements’ and ‘chemical crosslinks’ towards the shear modulus of the polymer. In the first term ($G^{\circ}_N T_e$), the plateau modulus due to physical entanglements is represented by G°_N , and ‘ T_e ’ refers to the proportion of elastically active entanglements.

The second term $[(v-h\mu)RT]$, refers to the contribution of chemical crosslinks to the shear modulus. Here, the concentration of elastically active chains (crosslink density) is referred to as v . The value of the empirical parameter ‘ h ’ varies between 0 and 1, μ being the concentration of elastically active junctions, R being the gas constant, and T being the absolute temperature. In a perfect network with functionality f , the concentration of elastically active junctions (μ) is equal to $2v/f$. The elastic moduli of elastomeric materials can be predicted using ‘affine’ [198], ‘phantom’ [199] or ‘junction affine’ [200, 201] network models. For a ‘phantom’ network, movement of the junctions around its mean position is permitted and h has a value of 1. On the other hand, in an affine network, these fluctuations are completely suppressed and h has a value of 0. The

network can exhibit intermediate properties, where h can have any value in between. For a trifunctional crosslinker ($\mu = 2\nu/3$), the shear modulus (G) is represented as

$$G = \frac{\nu RT}{3} \dots \dots \dots (5.3)$$

Further, the Young's modulus E can be related to the equilibrium shear modulus G as [202].

$$E = 2G(1+n) \dots \dots \dots (5.4)$$

Where n is Poisson's ratio (~ 0.5 , for elastomers). The value of E' can roughly be approximated to E in the rubbery plateau region. The approximate crosslink density can be determined by rearranging the above equations to yield $\nu = \frac{E'}{RT}$ (for phantom network, $h=1$) and $\nu = \frac{E'}{3RT}$ (for affine network, $h=0$). For calculation purposes, the incremental value of moduli is assumed to be the contribution of chemical crosslinks to the moduli.

The crosslink density obtained experimentally was also compared with the theoretical model of 'Scanlan', the details of which are presented in Appendix B. The crosslink densities as calculated according to affine and phantom network models along with the predictions of the theoretical 'Scanlan' model are presented in Figure 5.7.

Interestingly, for all crosslinked polyurea samples, the crosslink densities obtained experimentally using DMA data is substantially higher than those predicted on the basis of 'Scanlan' model, with the theoretical values closer to the 'affine' network model. Our results are in line with molecular dynamic simulations, which reveal that the chain length deformation is non-affine for short chain networks, and becomes closer to affine for networks of long, entangled chains [203]. However, the significant difference between the experiment and theoretical values can be attributed to several factors, the most important being the contribution of physical crosslinking (Bidentate H-bond

between the urea linkages) to the moduli. Another factor involves determination of the crosslink density as $\frac{E'}{3RT}$ (affine) and $\frac{E'}{RT}$ (phantom), which is only an approximation. Moreover, the Poisson's ratio of all the samples has been approximated to be 0.5, which can vary. In addition, the possibility of existence of dangling units in the network, due to unreacted crosslinker cannot be ruled out completely, which in turn can lead to non-ideal behaviour. It is to be noted that the Scanlan model is basically meant for ideal networks with an iso:amine stoichiometric ratio of 1:1, while all the crosslinked samples have been prepared using a stoichiometric ratio of 1.1:1.

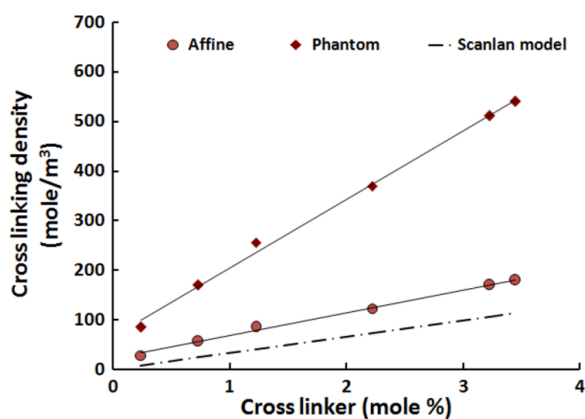


Figure 5.7: Comparison of experimentally determined (affine and phantom) and theoretically predicted (Scanlan) crosslink density as a function of crosslinker concentration

5.3.4 Swelling studies

Varying the extent of chemical crosslinking in polyurea is expected to have a pronounced effect on the degree of swelling in suitable solvent. In view of the extensive H-bonding, polyurea exhibits excellent chemical resistance and is practically insoluble in any solvent. Swelling studies were performed in various solvents (polar/non-polar) and the swelling ratio of all the formulations, defined as the amount of solvent uptake by the sample to its initial dry mass, are presented in Table 5.4.

Table 5.4: Variation in swelling ratio with extent of crosslinking

Sample Designation	Swelling ratio (%)		
	Ethanol	Toluene	DMF
PUX0	79 ± 2.0	152 ± 8.6	890 ± 50
PUX2	74 ± 1.9	107 ± 9.1	190 ± 10
PUX12	68 ± 2.1	89 ± 5.1	166 ± 8
PUX22	31 ± 1.12	56.7 ± 2.3	80 ± 3.2
PUX32	28 ± 1.2	50.3 ± 1.2	73 ± 4.1
PUX35	25 ± 0.9	40 ± 2.2	68 ± 1.9

The swelling studies were performed till a stage of constant volume is reached beyond which no further swelling was observed. At this stage the diluting forces become equivalent to the elastic response of the network chains[189].The samples exhibited negligible solvent uptake (<1%) in aqueous solutions (NaCl,10%(w/v), NaOH, 60%(w/v), CH₃COOH, 5% (w/v) and H₂SO₄, 30%(w/v)), but underwent extensive swelling in organic solvents like DMF. Images of a representative formulation showing the samples both before and after swelling are presented in Figure 5.8.

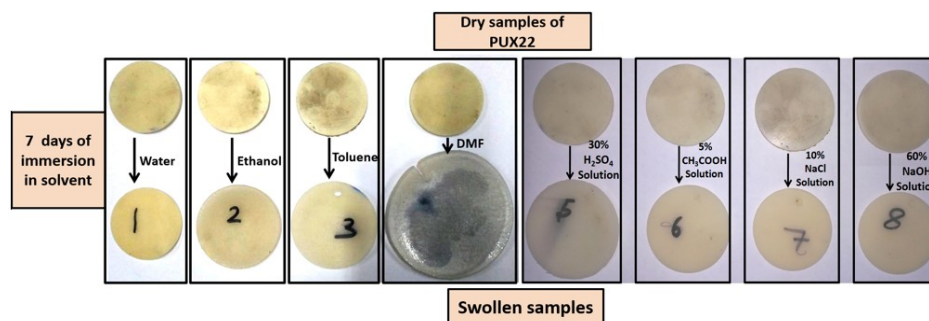


Figure 5.8: Representative formulation (PUX22) showing samples before and after swelling

As expected, the ability of the sample towards swelling reduces appreciably with the increase in the crosslinker concentration. The reduction in the capability towards swelling can be attributed to the decrease in the elastic response of the network chains which, in turn can be understood as the result of the decrease in the distance between two crosslinks due to increased crosslinking.

5.3.5 Thermal properties

5.3.5.1 Calorimetric studies

The DSC traces associated with the cured polyurea films are presented in Figure 5.9. DSC studies reveal that as the concentration of trifunctional component increases, the T_g quantified in terms of the temperature associated with the shift in the baseline [173], slightly shifts to higher temperatures which can be attributed to the restricted molecular motion of the polymer chains.

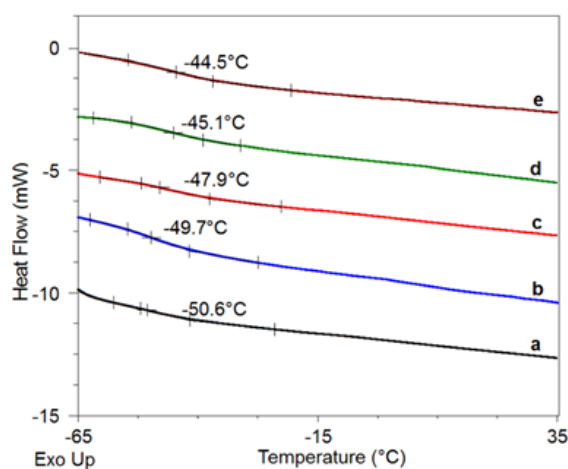


Figure 5.9: DSC traces for polyurea formulations a) PUX0 b) PUX2 c) PUX12 d) PUX22 e) PUX35

5.3.5.2 Thermogravimetry

The thermal properties of polyurea has been reported to be strongly dependent on the hard segment content and the extent of phase segregation in the polymer chain [126]. The TG traces along with the corresponding derivative thermogravimetric (DTG) traces of the polyurea formulations (under N_2 atmosphere) are presented in Figure 5.10.

It can be seen that the peak position of DTG trace depends on the hard segment percentage. It has been reported that the first major mass loss (220-350°C) is attributed to the decomposition of hard segments (primarily urea linkages), in view of the relatively low dissociation energy of C-N (300 kJ/mol) as compared to C-O and C-C (350kJ/mol).

Studies using hyphenated techniques have revealed that the first decomposition step leads primarily to the evolution of carbon dioxide. The subsequent mass loss (350-425°C) occurs due to the pyrolytic decomposition of the polyether chains, leading to evolution of hydrocarbons in larger amounts [126].

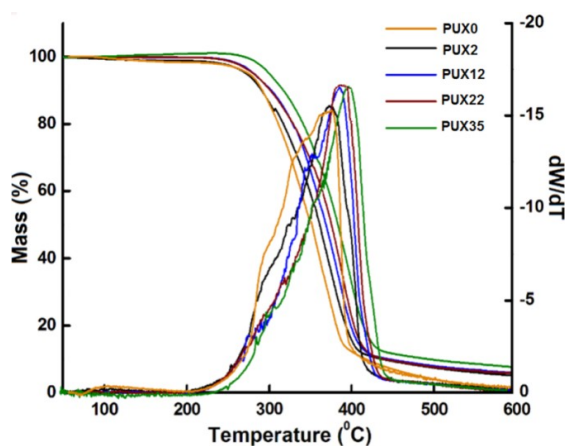


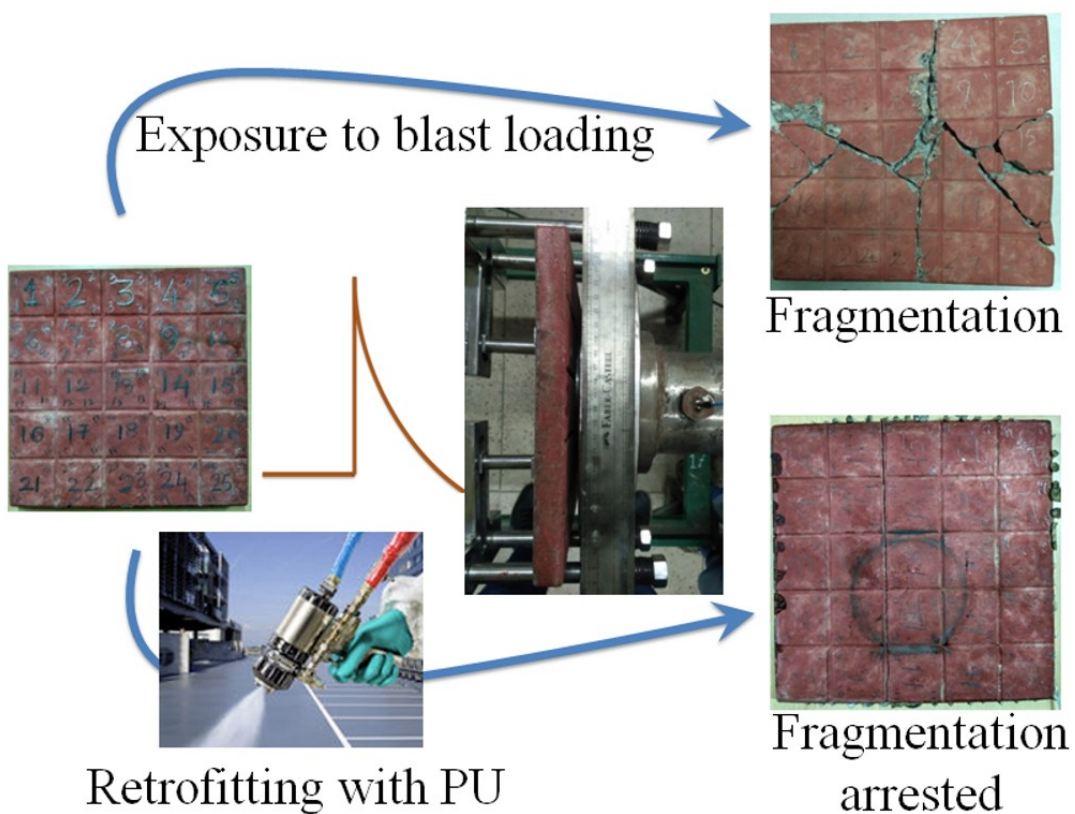
Figure 5.10: TG-DTG traces of the crosslinked polyurea formulations

Interestingly, it was observed that the mass loss during the first stage occurs in the same temperature range for all the samples in view of similar hard segment contents. A slight shift in the temperature associated with the second stage of thermal degradation is observed, which is in turn proportional to the extent of crosslinking. It is to be noted that the mass losses at these steps do not exactly match with the theoretically estimated hard segments, although a direct relationship is clearly evidenced. This discrepancy can be attributed to the fact that for estimation of HS, the mass of isocyanate taken for calculation is the mass of prepolymer, which in turn is formed by the reaction of MDI with a long chain amine/ diol. The complete decomposition leaves behind a char residue of ~ 5-8% w/w (at 600°C).

Our studies on crosslinked polyurea reveal that the mechanical properties can be significantly increased by introducing chemical crosslinker (long chain trifunctional amine) in the resin blend (Side B) formulation.

Chapter 6

Improving the blast survivability of concrete by coating with polyurea



6.1 Introduction

In this chapter, the efficacy of the polyurea towards improving the performance of the underlying concrete substrate under blast loadings through controlled shock tube experimentations has been demonstrated. The underlying mechanism responsible for the improvement has also been discussed. Spray coating yields a continuous membrane devoid of seams and joints, which improves the abrasion, corrosion and chemical resistance of structures. In view of the zero Volatile Organic Content (VOC) content of polyurea, the Environmental Protection Agency (EPA) has also approved their use as a coating over concrete.

In addition to enhance the structural performance of concrete [204-206], coating with polyurea has been reported to lead to improvement in the blast survivability as well. In this context, preliminary studies were performed by the Air Force Research Laboratory, where polyurea coating was used towards strengthening of masonry and light weight steel structures[207]. Coating polyurea on the interior face of walls was found to be more beneficial, in comparison to the blast facing side and both side application was found to be economically prohibitive[208]. Polyurea reinforced masonry structures, upon being subjected to transient dynamic loads, were found to undergo large deflections thereby endowing the much-needed ductility during flexural failure of the masonry walls [2]. Polyurea coatings have also been reported to improve the survivability of substrates like steel plates [85, 86, 209] and fiber-reinforced face-sheets [25, 40-43]. Here, in this work, polyurea formulation was sprayed over a representative concrete tile, the thickness of which was varied. A formulation with an optimal ratio of aromatic to aliphatic chain extender was chosen for coating purposes. Of particular interest was to establish the effect of increasing coating thickness towards improving its blast survivability.

Another aim of the present work is to establish the underlying contributory mechanism behind the role of polyurea towards improving the blast resistance of the composite. Several mechanisms have been reported [33, 43, 60, 117, 121], including a dynamic “Rubber-glass transition” where a vitrification process reportedly transpires in the polyurea coating upon being subjected to blast loads [55, 121]. However, we hypothesize that the occurrence of such a dynamic transition is unlikely, as exceptionally high frequencies would be required for its incidence: conditions not achievable under blast loadings. Such conditions can be simulated by systematic dynamic mechanical studies over a wide range of frequencies. In the present study, time–temperature superposition (TTS) is used to establish the mechanical properties of polyurea using the dynamic mechanical analysis data, since direct measurement over such a broad frequency range is not possible. Of particular interest is to identify the frequency associated with the dynamic loading process, which can initiate the dynamic ‘glass transition’ process in polyurea coating.

6.2 Experimental

6.2.1 Materials

Concrete tiles (25 cm × 25 cm × 2 cm) conforming to IS 8112-1989 (M35 Grade, 28 day compressive strength 35 MPa) were used as the underlying substrate for polyurea spray coating. The details of the concrete are as follows

- Grade designation: M 35
- Type of cement: OPC 53 Grade conforming IS 12269
 - Specific gravity: 3.15
- Type of aggregate: Crushed Angular Aggregates
- Maximum nominal size of aggregate: 20mm

- Specific gravity
 - Coarse aggregate (20mm): 2.67 kg/m³
 - Fine aggregate: 2.65kg/m³
 - Ground-granulated blast-furnace slag (GGBS): 2.84 kg/m³(JSW)
- Water absorption:
 - Coarse aggregate: 0.5 %
 - Fine aggregate: 2.5 %
- Minimum cement content: 340 kg/m (IS 456:2000)
- Maximum water-cement ratio: 0.45 (IS 456:2000)
- Workability: 100-120 mm slump
- Chemical admixture type: Super Plasticizer ECMAS HP 890 (conforming to IS 9103)

The description of the components used for polyurea preparation has been discussed in previous chapters. (Table 2.1 and 3.1) can be used as a ready reference for the structure and the properties of the reactants used for preparation of polyurea coating. Formulation PU Ar 63 (See Table 4.1) was chosen for coating purposes. Additionally, to improve the adhesion of the coating with the concrete tile, Coatosil MP 200 (Momentive) was included in the formulation.

6.2.2 Coating on concrete tiles

Coating performance is strongly influenced by its ability to adhere properly to the substrate material, which in turn is dependent on the surface preparation. Proper surface preparation allowed creation of suitable profile for strong mechanical bond to exist between polyurea and the underlying concrete substrate. Concrete tiles (25 cm × 25 cm × 2 cm) were cleaned to remove excessive cement slurry, laitance, loose and crumbly

particles, joints and oily substances. The substrate was primed with epoxy following which the polyurea formulation was sprayed using a spray-coating machine (E 10 HP equipped with a fusion air-purge spray gun AW2222, Graco). In all the runs, block and hose heaters were maintained at a constant temperature of 75°C and the spraying operation was performed at 2000 ± 100 psi.

6.2.3 Characterization

The adhesive strength of the Polyurea (with concrete) was measured according to ASTM D4541 using an adhesion tester (Elcometer 510T) with a 20 mm diameter dolly. An epoxy-based adhesive (Araldite) was used to fix the dolly to the polyurea coating. The techniques used for characterization of polyurea have been discussed in previous chapters.

6.2.4 Shock loading system

A shock tube facility was employed to subject the coated concrete tiles to dynamic loadings. A schematic is presented as Figure 6.1, and the actual photograph of the shock tube used is presented in Figure 6.2.

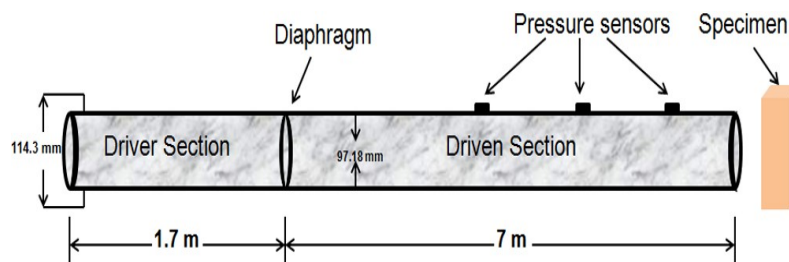


Figure 6.1: Shock tube layout

The shock tube consists of a long rigid cylinder, divided into a high-pressure driver section and a low pressure driven section, separated by a Mylar diaphragm; which is made to rupture at pre-determined pressure differences. The rapid release of gas results in the creation of a shock wave, which travels down the tube to impart blast dynamic loadings on the specimen. The shock tube facility has an overall length of 8.7 m, which is divided into a 1.7 m driver section and a 7 m driven section.



Figure 6.2: Shock tube facility

Pressurized air is used as the driver gas, the driven gas being ambient air. Pressure sensor (113B21, PCB make), placed at a distance of 11.3 cm from the sample was used to capture the pressure profile during the testing. Strain gauge (HBM: K-LY4-1-11-120-3-2) was affixed on the blast-opposing face of the concrete tile to measure the deflection in the sample.

6.2.4.1 Concrete tile geometry and boundary conditions

Concrete tiles (25 cm × 25 cm × 2 cm) were coated with polyurea of varying thickness (1-6 mm) and subjected to controlled blast loadings as shown in Figure 6.3.

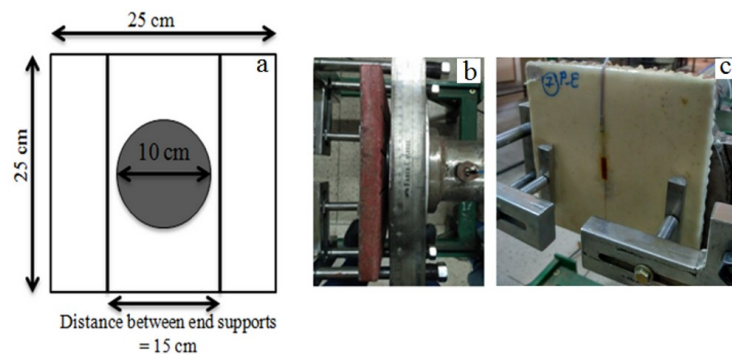


Figure 6.3: a) Sketch of the specimen depicting the loading and boundary areas. (b)

Actual specimen placement c) Front view

All tiles were simply supported over a span of 10 cm along any two edges, with the remaining edges free and a circular region of 10 cm diameter was effectively subjected to blast loading.

6.3 Results and Discussions

The mechanical response of polyurea coated concrete tiles subjected to controlled blast loadings was studied to establish the effect of increasing thickness on the blast survivability and to gain an insight into the underlying mechanism responsible for the improved blast resistance.

6.3.1 Mechanical properties of polyurea

In chapter 4, the focus was given to study, systematically the emergence of material properties in the chain extended polyurea with time as well as the optimization of the ratio the aromatic to aliphatic chain extender content in the polyurea formulations with an aim to achieve the optimal properties.

It is clear that an optimal ratio of aromatic: aliphatic chain extender directs the growing polyurea macromolecule in such a way so as to result in optimal H-bonding. Polyurea formulation with 61 % hard segment (aromatic contribution to urea linkages =63%) exhibited best properties (Tensile strength 13.7 ± 0.7 MPa, elongation $229 \pm 10\%$, Tear strength 87.78 ± 5.8 N/mm). Hence, the formulation was sprayed over concrete tiles, which in turn were subjected to adhesion tests followed by shock tube experiments. It is to be noted that for any coating to perform its role as an effective protective layer, a high level of adhesion is essential. The adhesion strength could not be determined experimentally, due to the cohesive failure of the epoxy adhesive between polyurea film and the pull-off adhesive test dolly at ~ 13 MPa. The concrete-polyurea debonding was not observed under the experimental conditions employed for adhesion testing.

6.3.2 Blast performance of polyurea coated concrete tiles

The blast response of polyurea-coated tiles was evaluated by subjecting them to controlled blast loadings on a shock tube followed by macroscopic visual examinations and strain measurements. The pressure profile obtained at the sensors located at 11.3 cm from the sample is recorded. A representative blast loading profile is presented in Figure 6.4.

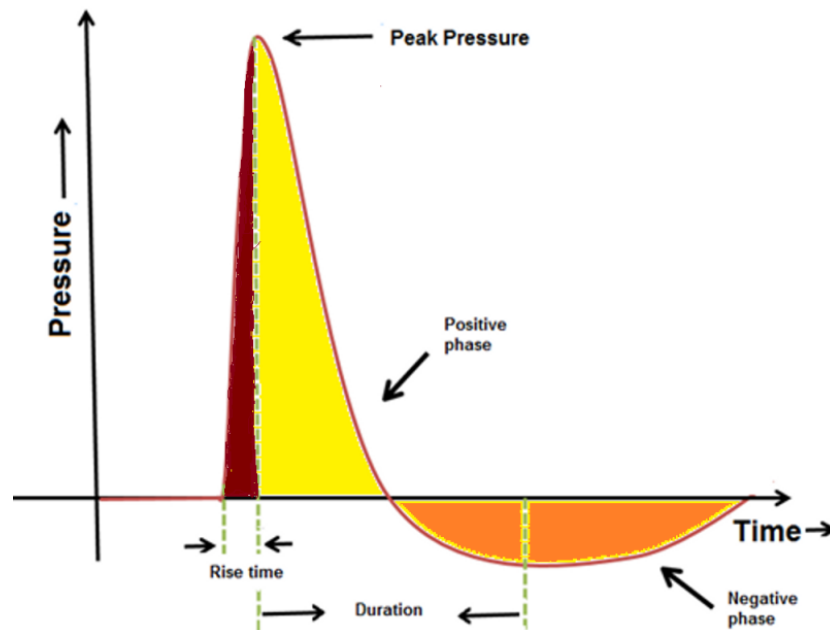





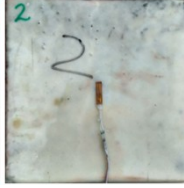
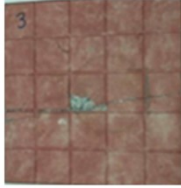





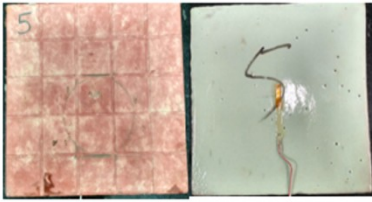
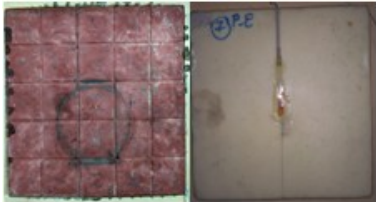
Figure 6.4: Representative pressure time profile during shock tube experiments. The time duration (“rise time”) considered for estimation of blast loading frequency is also labeled for reference

$$\text{Frequency associated with blast loading (Hz)} = v_{blast} = \frac{1}{t_{rise (s)}} \dots \dots \dots (6.1)$$

A set of control experiments on uncoated tiles were also performed for direct evaluation of polyurea retrofitting effectiveness. In the present context, “effectiveness” is defined as the ability of polyurea to prevent failure and to arrest the fragments formed from being propelled, if any. Table 6.1 summarizes the values for reflected overpressure, impulse, strain along with the summary of observations, and post-blast visuals.

Table 6.1: Response of polyurea coated concrete tiles.

PU thickness (mm)	Peak pressure / impulse	Observations	Visual inspection (post blast)	
			Blast face	Opposite face
Control (Nil)	50 psi/ 404 psi.ms	Extensive fragmentation was evidenced, with the fragments being propelled at high velocities (expected to cause harm to occupants on the other side).		
1	70 psi/ 406 psi.ms	Strain: 165 $\mu\epsilon$ Cracks formed on the tile. Slight tearing of polyurea, but the polyurea membrane proved effective in holding the tile together. Concrete-polyurea debonding was not evidenced.		
2	72 psi/ 435 psi.ms	Strain: Nil A single line crack formed on the tile. Polyurea tearing was not observed and the membrane was effective in holding the tile together. Tearing of the polyurea membrane was not evidenced.		
3	74 psi/ 601 psi.ms	Same as above.		
4	74 psi/ 610 psi.ms	Same as above		

5	82 psi/ 724 psi.ms	Strain: Nil The coated tile was intact with no visible cracks even on the blast facing side. Concrete-polyurea debonding was not observed. Tearing of the polyurea membrane was not evidenced.	
6	86 psi/ 798 psi.ms	Strain: 234 $\mu\epsilon$ The coated tile was intact with no visible cracks even on the blast facing side. Concrete-polyurea debonding was not observed. Tearing of the polyurea membrane was not evidenced.	

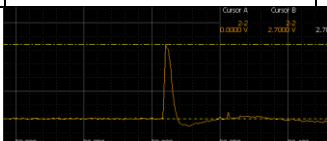

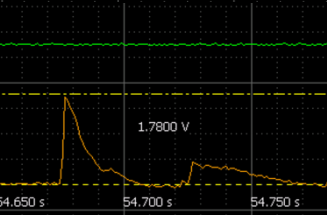

Neat concrete tiles were found to fail at a reflected shock pressure of ~ 50 psi, and the fragments formed were propelled at high velocities. It is to be noted that most casualties sustained by inhabitants during external explosions are not caused by heat/overpressure. Instead, it is the disintegration and fragmentation of walls followed by propulsion of non-secured objects, which lead to blunt trauma and penetration injuries. Retrofitting with polyurea coating can significantly reduce such damages, however the coating thickness may vary depending on the type of structure.

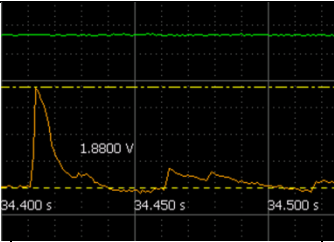
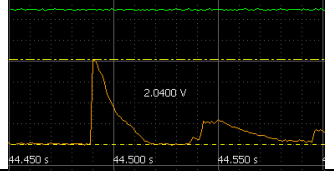
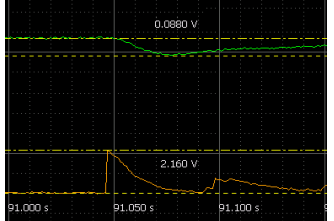

Coating the concrete tile with polyurea led to arrest of fragments and the extent of mitigation was found to be proportional to the coating thickness. Coating of tile with polyurea (thickness ~ 1 mm) was found to be effective in holding back the fragments formed, when subjected to higher blast loads. The retrofitted tile (6 mm thickness) finally underwent fragmentation at ~ 90 psi, with concrete-polyurea debonding and failure of strain gauge. Earlier studies on polyurea coated walls (~ 6 mm thickness) were found to resist peak pressures greater than ~ 60 psi for one-way action walls, compared to a capacity of ~ 5 psi for unreinforced masonry walls [2].

6.3.3 Mechanism behind improved blast resistance

The pressure-time profile associated with the shock tube experiments are presented in Table 6.2. Frequencies, associated with the blast loading experiments were estimated as the inverse of rise-time (t_{rise}) in pressure-time profile. Under the experimental conditions, t_{rise} was found to vary between 2 to 2.5ms, i.e. blast frequency (v_{blast}) of ~400-500 Hz. In fact, in most of the shock tube tests, the rise-time is of the same order [25, 131]. To gain an insight into the underlying mechanism behind the improved blast survivability of coated tiles, the mechanical response of the completely cured polyurea (PU-Ar 63) under dynamic loading conditions was studied in detail.

Table 6.2: Pressure time profile and operating conditions associated with blast loading (shock tube test)

Coating thickness (mm)	ΔP (Driver pressure-driven pressure)	Pressure profile Oscilloscope data*	v_{blast} (Hz)
Nil	2.5		5×10^2
1	5		4.5×10^2
2	5		4.8×10^2
3	5		4.7×10^2

4	5		4.9×10^2
5	5		4.1×10^2
6	10		4.6×10^2
6	15		4.2×10^2

*Pressure sensor placed at a distance of 11.3 cm from the specimen

The variation of storage and loss modulus of PU Ar 63, obtained from DMA studies, at various frequencies as a function of temperature is presented in Figure 6.5. The loss factor ($\tan \delta$) is also presented. A single relaxation peak is clearly evident in the profile, which is attributed to the segmental motions linked with the soft segments in the polymer. A sub-zero T_g (peak of the loss modulus) [128, 129] was evidenced at -36°C (@1Hz), which leads to an elastomeric response of polyurea under ambient conditions. It is interesting to observe the large width associated with the glass transition region ($\Delta T \sim 80^\circ\text{C}$), which is a property rather unique to polyurea [118]. As the frequency of the dynamic loading is increased, both the loss and storage modulus trace shift towards higher temperature [118, 128-130].

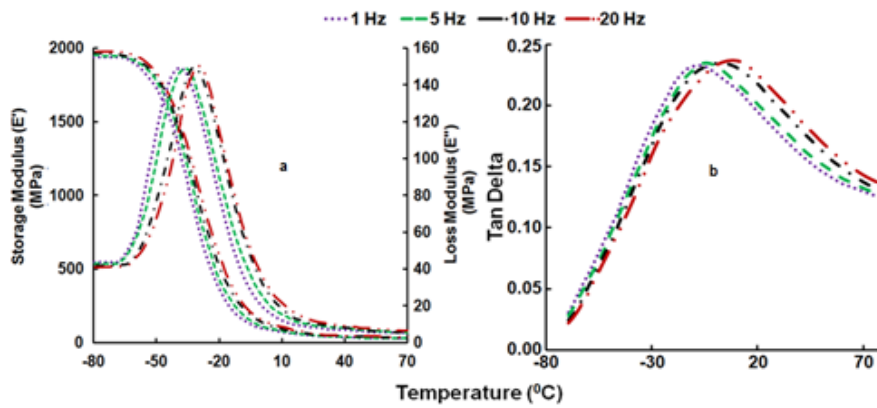


Figure 6.5: Variation of (a) Storage and loss modulus (b) Tan delta with temperature at different frequencies

The master curves hence obtained in terms of loss modulus variation at different reference temperatures (245 K to 298 K) are presented in Figure 6.6. It is evident from the figure that a significant shift in the loss modulus peak (encompassing dynamic glass transition phenomenon) occurs upon increasing temperature. This can be attributed to the fact that segmental motions at higher temperatures mandate relatively higher frequencies to get arrested [121]. In fact, this ‘vitrification’ process has been considered to be one of the most contributory mechanism behind the ability of polyurea to withstand blast loadings [60, 121].

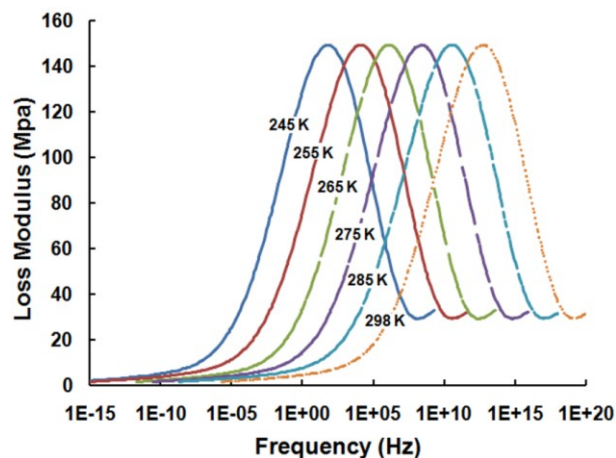


Figure 6.6: Master curves representing the variation in loss modulus in PU-Ar 63

Interestingly, our present studies indicate that under ambient temperatures, the dynamic glass transition process necessitate far high frequencies ($\sim 10^{13}$ Hz) than those accomplishable under shock tube conditions. Therefore, instead of undergoing a vitrification process, the polyurea retains its elastomeric nature and flexes to act as a “catcher system” for the fragments formed due to the fracture of the underlying concrete.

Polyurea helps in the dissipation and absorption of shock wave kinetic energy by undergoing irreversible densification, which in turn results from the hard domain ordering and crystallization. These micro structural changes and H-bond restructuring reportedly dissipate and absorb significant amount of shock-wave kinetic energy [33]. Theoretical studies have also brought out the providence of “shock wave capture and neutralization” mechanism in polyurea[33, 43, 109, 132]. Shock waves usually travel as a single wave in homogeneous materials. However, due to the heterogeneous microstructure of polyurea, a two-wave structure is obtained—a leading shock front followed by a time variable complex pattern. It is this impedance mismatch over the length scales and nonlinearities arising from material inelasticity, which leads to a dual shock-wave pattern. The secondary trailing shock-wave (release wave), catches up and attenuates the leading shockwave, thereby leading to shock attenuation [210].

It is to be noted that the blast facing side of the concrete tile is exposed to compressive loadings, while the opposite face is subjected to tensile forces. Plain Cement Concrete (PCC) exhibits high compressive strengths (σ_c) with the tensile strength (σ_t) being only a small fraction ($\sigma_t = 10\% \sigma_c$) [211]. As the shock wave propagates, the structure is weakened and the stresses localize at the weak sections. Concrete is an essentially heterogeneous material consisting of aggregates and cement bonded together,

with lots of inherent weak sites capable of acting as initiating sites for subsequent failure.

The primary modes of failure in the retrofitted tile are presented in Figure 6.7.

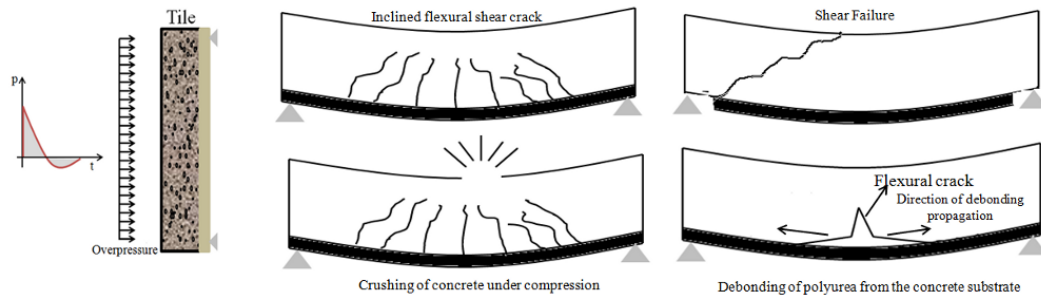


Figure 6.7: Failure mechanisms in retrofitted plain cement concrete

Due to high local tensile stresses, “inclined flexural shear cracks” propagate within the structure, resulting in shear failure. The flexural failure is accompanied with the crushing of concrete, which occurs primarily on the side facing the blast load. As the fragmented tile flexes which is shown in Figure 6.8, polyurea is subjected to tensile forces, which leads to tearing of the coating. This was observed only when the coating thickness was less (~ 1 mm).

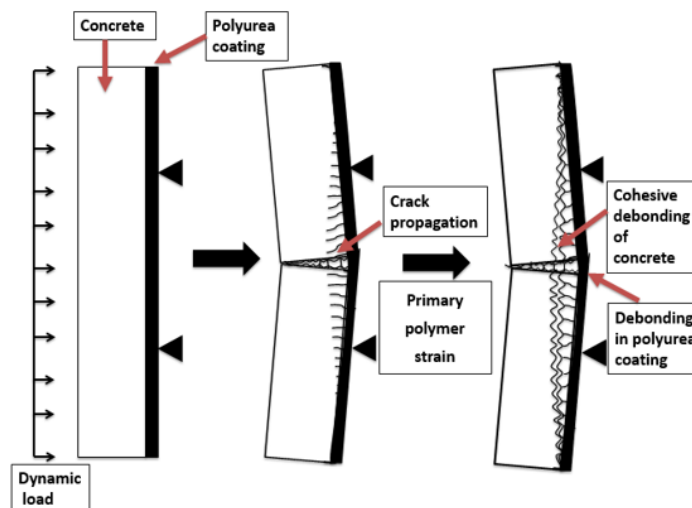


Figure 6.8: Progressive failure in polyurea coated concrete

The overall efficiency of the polyurea-coated concrete system is limited by the adhesive strength between the polyurea and the concrete surface. For all practical

purposes, the cohesive strength of concrete is much lower in comparison to the adhesive strength between polyurea and the substrate [212]. Inclined microcracks are initiated in the superficial layer of concrete in view of its lower tensile strength as compared to the adhesive Figure 6.8. These, however, cannot propagate more than few millimeters within the concrete specimen as the stresses decrease very rapidly with depth along polyurea-concrete interface. Concrete-polyurea debonding was evidenced at higher loadings, when the coated tile (6mm PU coating thickness) was subjected to 90 psi overpressure, with ~3 mm of substrate adhering to the polyurea membrane. A visual of the debonded polyurea is depicted pictorially as Figure 6.9.

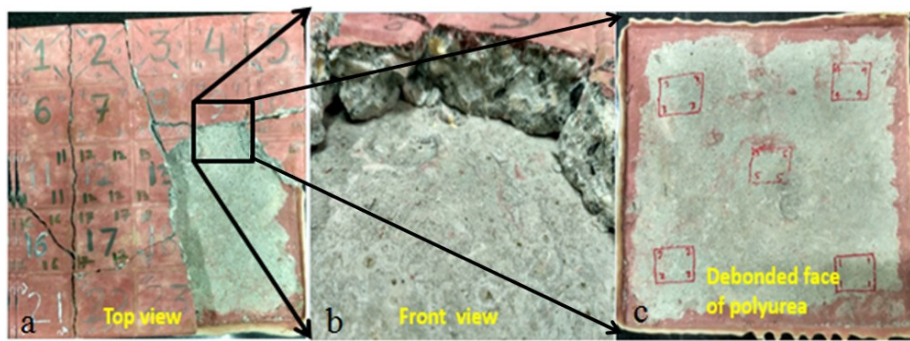


Figure 6.9: Visual examination a) View of the blast facing side (fragment removed to reveal the adhering layer of concrete) b) enlarged view c) debonded polyurea To understand the nature of the interface, FTIR studies were performed, and the spectra of concrete, polyurea and debonded surface of polyurea is presented in Figure 6.10. The detailed assignment of the spectral bands is presented in Table 6.3.

Table 6.3: Assignment of bands in the spectra (before and after debonding)

Assignment	Wavenumber (cm ⁻¹)	Cement	Polyurea coating	Debonded polyurea
C=O; CaCO ₃	1413, 873 & 712	✓	-	✓
Si-O; Silica	797, 777	✓	-	✓
N-H; Urea	3335	-	✓	✓
C=O; Urea (ordered)	1644	-	✓	✓

Polyurea exhibits characteristic absorption peaks at 1644 cm^{-1} due to urea carbonyl (ordered) [119] and absorption at 3335 cm^{-1} due to the NH vibration. In the spectra of concrete, characteristic absorption bands were observed at 797 and 777 cm^{-1} due to Si-O vibrations. Additional peaks at 1413 and 873 cm^{-1} were observed, which could be attributed to the presence of calcium carbonate C=O further confirming the presence of the adhered cementitious layer onto the polyurea coating [213].

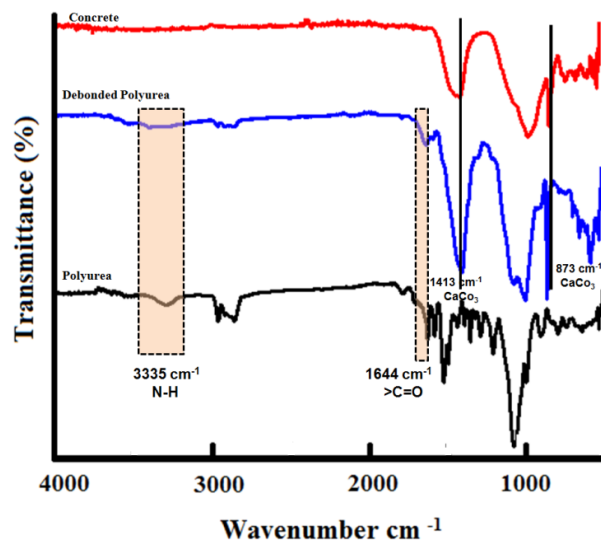


Figure 6.10: FTIR spectra of polyurea, concrete and debonded polyurea

Our studies clearly highlight the potential of polyurea coating towards improving the ability of concrete to withstand blast loads. The effect of increasing thickness of polyurea coating was also demonstrated. Neat concrete tiles undergo fragmentation at 50 psi blast loads, while polyurea coated tiles could withstand ~ 87 psi dynamic loads. Our studies further revealed that the polyurea films remain in the rubbery regime under blast loading conditions, due to which it acts as a catcher system for the fragments generated under blast loading conditions.

Chapter 7

Summary & Conclusions

The potential of polyurea in the context of blast mitigation and ballistic protection has been well demonstrated by numerous investigations. It is clear that these interesting properties of polyurea are direct consequence of its composite microstructure, where hard domains (resulting from hydrogen bonding within urea linkages) are dispersed throughout a largely homogenous soft domain. The properties of polyurea can be tuned for a particular application through judicious choice of the reactants. Here, we have attempted to study the effect of various factors viz. soft segment length, type and concentration of chain extender and crosslinker on the material properties of polyurea. The importance of viscosity matching of the co-reactants, i.e. amine and isocyanate for effective polyurea spray processing has also been studied. The factors responsible for the evolution of material properties in the chain extended polyurea with time were also discussed in detail. The effectiveness of polyurea as a blast resistant coating was demonstrated using concrete tile as an underlying substrate.

7.1 Effect of increasing soft segment length on polyurea mechanical properties

- The soft segment chain length was found to play a pronounced role in defining the characteristic material properties of polyurea.
- The tensile strength was found to vary inversely with the soft segment length, while the elongation was found to be directly proportional.
- The low temperature T_g associated with the segmental motions associated with the polyether soft segments was found to increase significantly with its chain length (-43°C for PU 2000 to -10°C for PU 230), while the high temperature T_g remained practically constant at 140-144°C.
- Detailed dynamic mechanical studies indicated that the arresting of segmental motions associated with longer 'soft segments' mandate relatively higher

frequencies. As a consequence, the dynamic glass transition process necessitates much high frequency for polyurea with longer soft segment length ($\sim 10^{15}$ Hz for PU 2000), while the same is much lower for polyurea with lower chain length ($\sim 10^5$ Hz for PU 230).

7.2 Spray coating of polyurea: Importance of viscosity matching of co-reactants

- Spray coating of formulations containing undiluted isocyanate precursors, due to stoichiometric imbalance, led to formation of fibrous amine terminated polyurea with low degree of polymerization and low “tack free” time of <1 s.
- The isocyanate prepolymer needs to be diluted with a reactive diluent, namely propylene carbonate for effective spraying. To estimate the amount of propylene carbonate required for isocyanate dilution, the applicability of several mixing rules was explored, and Chevron equation based on Viscosity Blending Index was found to predict the blend viscosity with reasonable accuracy.
- Diluting the precursor with a VOC exempt propylene carbonate (10% v/v) led to viscosity matching with the amines and thereby led to formation of smooth-levelled polyurea films with an extended “tack free” time of >3 s.
- Spectroscopic studies revealed that although the solidification process is extremely rapid in a matter of seconds, but the levelling-off of the isocyanate absorbance takes substantially longer periods (~ 8 h).
- Polyurea films prepared using aromatic chain extenders exhibited better mechanical properties, both in terms of tensile strength, elongation as well as tear strength in comparison to their aliphatic counterparts.

7.3 Effect of introducing chain extender on polyurea mechanical properties

- Studies on a series of polyurea formulation with varying amount and type of chain extender revealed that although the reaction transpire in a matter of seconds, but the mechanical properties tend to evolve substantially over a period of time.
- Aromatic chain extenders were significantly more reactive than their aliphatic counterparts, which lead to significantly short 'gel-time' as quantified by rheometry.
- The levelling-off of the absorbance band due to -NCO stretching mandated $\sim 8\text{h}$, as indicated by FTIR studies. Interestingly, the mechanical properties improved significantly over a period of time and reach a plateau over ~ 15 days, irrespective of the type of chain extender included in the formulation.
- Chain extender forces the formation of urea linkages close to each other, which in turn favors the formation of H-bonds in the hard segments.
- Although both aromatic and aliphatic chain extenders are routinely used as chain extenders, it appears that an optimal ratio of the two forces the growing macromolecule to orient in a way so as to result in optimal H-bonding which in turn reflected in improved mechanical properties, which in turn was qualitatively established by the red-shift associated with N-H and $>\text{C}=\text{O}$ bands in the polymer.
- Dynamic Mechanical Analysis reveal that the storage modulus is proportional to the extent of hydrogen bonding between the urea linkages in the polymer, which in-turn can be adjusted by the amount of aromatic and aliphatic chain extender. All polyurea formulations were found to exhibit sub-zero glass transition temperature (T_g) with the breadth of this region being exceptionally large

(~80°C), which shifted methodically towards higher temperature as the total hard segment content increased. However, the T_g remained unaltered with time.

- Under ambient conditions, all polyurea formulations exist much above its lower glass transition temperature, which permit segmental motions within the soft segments of the polymer, thereby leading to release of inbuilt internal stresses. These motions eventually lead to a spatial structural arrangement with lowest interatomic force on each atom: a process that continues over extended periods leading to optimal properties. The temperatures associated with the thermal decomposition of polyurea does not vary significantly with the type of extender employed, but the mass losses associated with each step is proportional to the hard and soft segment present in the polymer.

7.4 Effect of introducing chemical crosslinking on polyurea mechanical properties

- The mechanical properties of polyurea could be tailored by introducing a trifunctional chemical crosslinker in the amine co-reactant side of the formulation. Although physical crosslinks are formed spontaneously in polyurea, additional chemical crosslinking was found to improve the mechanical properties and chemical resistance of polyurea appreciably.
- Although the introduction of crosslinking should lead to an increase in the tensile strength and modulus, it was observed that beyond an optimal ratio, the mechanical strength decreases. A theoretical model (Scanlan) was used to predict the crosslinking density, assuming complete conversion of the reactant stoichiometrically.
- Dynamic Mechanical Analysis was used to quantify the crosslinking density in the sample, which was found to vary from 28 to 180 mol/m³ for affine network, and 85

to 540 mol/m^3 for phantom network. Significant differences were observed between the theoretical and experimental crosslink densities with the ‘affine’ network model being closer to theoretical predictions.

- The temperatures associated with the thermal decomposition of polyurea does not vary significantly with the amount of crosslinker employed, but the mass losses associated with each step is proportional to the hard and soft segment present in the polymer.
- Polyurea exhibit excellent chemical resistance in aqueous media. The introduction of chemical crosslinking improved the chemical resistance substantially, with a proportional decrease in the extent of swelling with increasing crosslinker content.

7.5 Blast loading on concrete substrate: Effect of polyurea coating

- Coating the concrete tile with polyurea led to arrest of fragments and the extent of mitigation was found to be proportional to the coating thickness. Coating of tile with polyurea (thickness $\sim 1 \text{ mm}$) was found to be effective in holding back the fragments formed, when subjected to higher blast loads. The retrofitted tile (6 mm thickness) finally underwent fragmentation at $\sim 90 \text{ psi}$, with concrete-polyurea debonding and failure of strain gauge.
- Detailed dynamic mechanical studies clearly indicated that a minimum of 10^{13} Hz was required for the polyurea to undergo glass transition under ambient temperatures. Interestingly, the frequency associated with the blast loading conditions ($\sim 10^2 \text{ Hz}$) was found to be insufficient to permit the vitrification of polyurea vide the much-cited “dynamic glass transition” phenomenon. Instead, shock-wave-induced hard domain ordering and crystallization, rearrangements in the H-bonds and shock wave capture and neutralization appear to be the primary

modes of energy dissipation in polyurea during blast loading conditions.

- The flexible nature of polyurea permitted it to flex, thereby preventing the fractured concrete tiles from turning into secondary fragment hazards.

Appendices

Appendix: A

Calculation for determining the upper and lower limit of different amines in polyurea formulation:

Characteristic properties of isocyanate and amines used in formulation are presented in Table below.

Table: Characteristic properties of isocyanate and amine

Isocyanate (Part A)	Density (ρ) (g/cm^3)	N_{eq}
Suprasec 2054	1.09	3.5714

Amine (Part B)	Density (ρ) (g/cm^3)	N_{eq}
T 5000	0.995	0.6
D2000	0.985	1
DETDA	1.022	11.24

There are primarily two constraints associated with the spraying of polyurea using E10 HP spray coater.

(A) Volume of amine = Volume of isocyanate

$$V_{\text{amine}} = V_{\text{iso}} \dots\dots\dots(\text{A})$$

$$(\text{B}) \text{Mass}_{\text{iso}} \times N_{\text{iso}} = (\text{Mass}_{\text{amine}} \times N_{\text{amine}}) \times i_{Nco} \dots\dots\dots(\text{B})$$

Where, ($i_{Nco} = 1.1$)

Effective spraying of polyurea mandates dilution of the isocyanate prepolymer with Propylene Carbonate (10%).

For a representative formulation, 10 g of formulated isocyanate reacts with 10 g of formulated amine

10 g of diluted isocyanate contains 9 g Suprasec 2054 (8.3 ml) and 1 g of propylene carbonate (0.84 ml).

So the total volume in part A

$$V_{iso} = V_{suprasec} + V_{propyl\ ene\ carbonate}$$

$$V_{iso} = 8.3\ ml + 0.84\ ml$$

$$= 9.14\ ml$$

In view of the first constraint equation (A)

$$V_{iso} = V_{amine} = 9.14\ ml$$

$$V_{amines} = \frac{x}{0.995} + \frac{y}{0.985} + \frac{z}{1.022} = 9.14\ ml$$

$$V_{amin\ es} = 1.005\ x + 1.015\ y + 0.978\ z = 9.14\ ml \quad \dots\dots\dots(1)$$

where,

x= mass of T5000 taken in formulation

y = mass of D2000 taken in formulation

z = mass of DETDA taken in formulation

Taking into the account of second constraint (equation B)

$$Mass_{iso} \times N_{iso} = 32.31$$

$$\therefore (Mass_{amine} \times N_{amine}) \times i_{Nco} = 32.31$$

As, $i_{Nco} = 1.1$

Then,

$$(Mass_{amine} \times N_{amine}) = 29.37$$

Hence we can write the above equation as;

$$(Mass_{T5000} \times N_{T5000}) + (Mass_{D2000} \times N_{D2000}) + (Mass_{DETDA} \times N_{DETDA}) = 29.37 \dots \dots \dots (2)$$

By solving these two equation (1) and (2)

So the range for DETDA is as

$$1.6993 \text{ g} \leq Z \leq 1.9817 \text{ g}$$

or

$$1.6627 \text{ ml} \leq Z \leq 1.939 \text{ ml}$$

the range for T5000 are as

$$0.0025 \text{ g} \leq X \leq 7.4415 \text{ g}$$

or

$$0.00251 \text{ ml} \leq X \leq 7.4788 \text{ ml}$$

and range for D2000 are as

$$0 \text{ g} \leq Y \leq 7.0953 \text{ g}$$

or

$$0 \text{ ml} \leq Y \leq 7.203 \text{ ml}$$

So by summarizing the data we have,

Amines	Minimum amount (ml)	Maximum amount (ml)
T5000	0.00251	7.47
D2000	0	7.203
DETDA	1.6627	1.939

Appendix: B

Theoretical prediction of crosslinking density by Scanlan method

The theoretical crosslink density for step growth polymer, e.g. polyurethane/ polyurea can be determined using Scanlan method. For this method, the network is considered to be ideal network with a stoichiometric ratio of 1 and full conversion of reactants.

The crosslink density ν was determined from

$$\nu = \sum_{f=3}^{\infty} \frac{f}{2} C_f \dots\dots\dots 1$$

Where f is the functionality of the reactants and the C_f is the concentration of reactant with functionality f , expressed as moles per volume of fully cured polymer. The functionality f is 3 or greater because species with functionalities of 2 or smaller do not form junction points in the network. In the present scenario, the triamine was the only reactant with a functionality of 3 or greater. Therefore, equation 1 is simplified to

$$\nu = \frac{3\rho n_{A_3}}{2(M_{B_1} n_{B_1} + M_{B_2} n_{B_2} + M_{A_1} n_{A_1} + M_{A_2} n_{A_2} + M_{A_3} n_{A_3})} \dots\dots\dots 2$$

where n_{A_1} , n_{A_2} and n_{A_3} are the number of moles of A_1 (D2000), A_2 (chain extender) and A_3 (crosslinker) respectively, whereas, n_{B_1} is number of moles of B_1 (isocyanate prepolymer) and n_{B_2} is number of moles of B_2 (isocyanate MDI).

Detailed calculations reveal that the commercial isocyanate (Suprasec 2054) with a 15% NCO is prepared by reacting 49.2 phr diol of M.Wt = 2000 and 50.8 phr MDI. Assuming complete

reaction (Stoichiometric ratio of 1:2) out of 50.8 phr MDI, 12.3 phr reacted with 49.2 phr of diol and the rest (~36 phr) of unreacted MDI is present in the commercial isocyanate (Suprasec 2054). ρ is the density of fully cured polymer for each particular mole % of crosslinker. The respective molecular weight of the components is given below.

$$M_{A_1} = 2000 \text{ g/mole}$$

$$M_{A_2} = 178 \text{ g/mole}$$

$$M_{A_3} = 5000 \text{ g/mole}$$

$$M_{B_1} = 2500 \text{ g/mole}$$

$$M_{B_2} = 250 \text{ g/mole}$$

Equation 2 can be solved for obtaining crosslinking density of each sample. The number of moles of each constituent and density are presented in Table.

Sample designation	Number of moles of D2000 (n_{A_1})	Number of moles of chain extender (n_{A_2})	Number of moles of crosslinker (n_{A_3})	Number of moles of isocyanate (prepolymer) (n_{B_1})	Number of moles of isocyanate (MDI) (n_{B_2})	Density (ρ)
PUX0	3.55E-03	1.11E-02	0.00E+00	2.21E-03	1.39E-02	0.98
PUX2	3.27E-03	1.15E-02	9.95E-05	2.21E-03	1.39E-02	0.981
PUX7	2.78E-03	1.15E-02	2.99E-04	2.21E-03	1.39E-02	0.983
PUX12	2.27E-03	1.17E-02	4.98E-04	2.21E-03	1.39E-02	0.985
PUX22	1.25E-03	1.21E-02	8.96E-04	2.21E-03	1.39E-02	0.987
PUX32	2.26E-04	1.25E-02	1.29E-03	2.21E-03	1.39E-02	0.988
PUX35	0.00E+00	1.26E-02	1.38E-03	2.21E-03	1.39E-02	0.99

References

References

1. Knox, K.J.H., M.I Lewis, T.T. Porter, J.R., *Polymer material for structural retrofit*. Polymer Materials for Structural Retrofit. **Florida** (2000): p. 2000.
2. Davidson, J., et al., *Explosive Testing of Polymer Retrofit Masonry Walls*. Journal of Performance of Constructed Facilities, 2004. **18**(2): p. 100-106.
3. Brode, H.L., *Numerical Solutions of Spherical Blast Waves*. Journal of Applied Physics, 1955. **26**(6): p. 766-775.
4. Moradi, L.G., et al., *Resistance of Concrete Masonry Walls with Membrane Catcher Systems Subjected to Blast Loading*. International Journal of Protective Structures, 2011. **2**(1): p. 83-102.
5. John J. Myers, A.B., and Khaled A. El-Domiatty, *Blast Resistance of FRP Retrofitted Un-Reinforced Masonry (URM) Walls with and without Arching Action*. The Masonry Society, 2004: p. 9-26.
6. Chundawat, T.S., et al., *Blast mitigation using FRP retrofitting and coating techniques*. Polymer Composites, 2016. DOI: **10.1002/pc.24116**.
7. Malvar, L., J. Crawford, and K. Morrill, *Use of Composites to Resist Blast*. Journal of Composites for Construction, 2007. **11**(6): p. 601-610.
8. Morrill, K., et al., *Blast Resistant Design and Retrofit of Reinforced Concrete Columns and Walls*, in *Structures 2004*. 2004. p. 1-8.
9. Buchan, P.A. and J.F. Chen, *Blast resistance of FRP composites and polymer strengthened concrete and masonry structures – A state-of-the-art review*. Composites Part B: Engineering, 2007. **38**(5–6): p. 509-522.

10. Mosalam, K.M., Mosalam, A., *Nonlinear Transient Analysis of Reinforced Concrete Slabs Subjected to Blast Loading and Retrofitted with CFRP Composites*. Composites Part B: Engineering, 2001. **32**(8): p. 623-636.
11. Ghani Razaqpur, A., A. Tolba, and E. Contestabile, *Blast loading response of reinforced concrete panels reinforced with externally bonded GFRP laminates*. Composites Part B: Engineering, 2007. **38**(5–6): p. 535-546.
12. Alae, F., Karihaloo, B., *Retrofitting of Reinforced Concrete Beams with CARDIFRC*. Journal of Composites for Construction, 2003. **7**(3): p. 174-186.
13. Toutanji, H. and P. Balaguru, *Durability Characteristics of Concrete Columns Wrapped with FRP Tow Sheets*. Journal of Materials in Civil Engineering, 1998. **10**(1): p. 52-57.
14. Mirmiran, A. and M. Shahawy, *Behavior of Concrete Columns Confined by Fiber Composites*. Journal of structural engineering, 1997. **123**(5): p. 583-590.
15. Van Den Einde, L., L. Zhao, and F. Seible, *Use of FRP composites in civil structural applications*. Construction and Building Materials, 2003. **17**(6–7): p. 389-403.
16. Seica, M.V. and J.A. Packer, *FRP materials for the rehabilitation of tubular steel structures, for underwater applications*. Composite Structures, 2007. **80**(3): p. 440-450.
17. Pichandi, S., et al., *Fibrous and composite materials for blast protection of structural elements-A state-of-the-art review*. Journal of Reinforced Plastics and Composites, 2013. **32**(19): p. 1477-1500.

18. Roy, P.K., et al., *Effect of SBA-15 on the energy absorption characteristics of epoxy resin for blast mitigation applications*. Iranian Polymer Journal, 2013. **22**(9): p. 709-719.
19. Wu, C., et al., *Blast testing of ultra-high performance fibre and FRP-retrofitted concrete slabs*. Engineering Structures, 2009. **31**(9): p. 2060-2069.
20. Muszynski, L.C. and M.R. Purcell, *Composite Reinforcement to Strengthen Existing Concrete Structures against Air Blast*. Journal of Composites for Construction, 2003. **7**(2): p. 93-97.
21. Pham, T.M., Hao, Hong., *Review of Concrete Structures Strengthened with FRP Against Impact Loading*. Structures, 2016. **7**: p. 59-70.
22. Raman, S.N., et al., *Elastomeric Polymers for Retrofitting of Reinforced Concrete Structures against the Explosive Effects of Blast*. Advances in Materials Science and Engineering, 2012. **2012**: p. 8.
23. Raman, S.N., T. Ngo, and P. Mendis, *A Review on the Use of Polymeric Coatings for Retrofitting of Structural Elements against Blast Effects*. Electronic Journal of Structural Engineering, 2011. **11**: p. 69-80.
24. Hutchinson, T., K. Nicolaisen, and K. Morrill, *Blast Retrofit Strategies For Masonry Walls: Exploratory Experimental Study*, in *Structures*. 2004, American Society of Civil Engineers. p. 1-8.
25. Tekalur, S.A., A. Shukla, and K. Shivakumar, *Blast resistance of polyurea based layered composite materials*. Composite Structures, 2008. **84**(3): p. 271-281.
26. Chen, C., et al., *Effectiveness of advanced coating systems for mitigating blast effects on steel components*. Structures Under Shock or Impact, 2008: p. 14-16.

27. Sreenivasan, K., *Estimation of Hard Segment Content in Polyurethane from Solvent Absorption*. Polymer Journal, 1990. **22**: p. 620.
28. Primeaux, D.J., *100% Solids Aliphatic Spray Polyurea Elastomer Systems*. Journal of Elastomers and Plastics, 1992. **24**(4): p. 323-336.
29. Pathak, J.A., et al., *Structure Evolution in a Polyurea Segmented Block Copolymer Because of Mechanical Deformation*. Macromolecules, 2008. **41**(20): p. 7543-7548.
30. Reinecker, M., et al., *Two glass transitions of polyurea networks: effect of the segmental molecular weight*. Soft Matter, 2014. **10**(31): p. 5729-5738.
31. Grujicic, M., et al., *Coarse-grained Molecular-level Analysis of Polyurea Properties and Shock-mitigation Potential*. Journal of Materials Engineering and Performance, 2013. **22**(7): p. 1964-1981.
32. Castagna, A.M., et al., *The Role of Soft Segment Molecular Weight on Microphase Separation and Dynamics of Bulk Polymerized Polyureas*. Macromolecules, 2012. **45**(20): p. 8438-8444.
33. Grujicic, M., et al., *Concept-Level Analysis and Design of Polyurea for Enhanced Blast-Mitigation Performance*. Journal of Materials Engineering and Performance, 2012. **21**(10): p. 2024-2037.
34. Grujicic, M., et al., *Meso-scale Computational Investigation of Shock-Wave Attenuation by Trailing Release Wave in Different Grades of Polyurea*. Journal of Materials Engineering and Performance, 2014. **23**(1): p. 49-64.
35. Saotome, K. and H. Komoto, *Polyurethanes and polyureas having long methylene chain units*. Journal of Polymer Science Part A-1: Polymer Chemistry, 1967. **5**(1): p. 119-126.

36. Primeaux, D.J. *Polyurea vs Polyurethane & Polyurethane/Polyurea: What's the Difference?* in "Polyurea Coatings: That Was Then, This is Now" 2004 PDA Annual Conference,. 2004. Tampa, Florida.
37. Billmeyer, F.W., ed. *Textbook of Polymer Science*. 1984, Interscience Publishers, John Wiley & Sons: New York.
38. Das, S., et al., *Structure–property relationships and melt rheology of segmented, non-chain extended polyureas: Effect of soft segment molecular weight*. *Polymer*, 2007. **48**(1): p. 290-301.
39. Das, S., et al., *Probing the urea hard domain connectivity in segmented, non-chain extended polyureas using hydrogen-bond screening agents*. *Polymer*, 2008. **49**(1): p. 174-179.
40. Grujicic, A., et al., *Potential Improvements in Shock-Mitigation Efficacy of a Polyurea-Augmented Advanced Combat Helmet*. *Journal of Materials Engineering and Performance*, 2012. **21**(8): p. 1562-1579.
41. Grujicic, M., et al., *Fluid/Structure Interaction Computational Investigation of Blast-Wave Mitigation Efficacy of the Advanced Combat Helmet*. *Journal of Materials Engineering and Performance*, 2011. **20**(6): p. 877-893.
42. Grujicic, M., et al., *Blast-wave impact-mitigation capability of polyurea when used as helmet suspension-pad material*. *Materials & Design*, 2010. **31**(9): p. 4050-4065.
43. Grujicic, M., et al., *Molecular-level computational investigation of shock-wave mitigation capability of polyurea*. *Journal of Materials Science*, 2012. **47**(23): p. 8197-8215.

44. Sarva, S.S., et al., *Stress–strain behavior of a polyurea and a polyurethane from low to high strain rates*. *Polymer*, 2007. **48**(8): p. 2208-2213.
45. S.N. Raman, T.N., J. Lu, P. Mendis, *Experimental investigation on the tensile behavior of polyurea at high strain rates*. *Materials and Design*, 2013. **50**: p. 124-129.
46. Plazek, D.J., et al., *Viscoelastic properties of polymers. 4. Thermorheological complexity of the softening dispersion in polyisobutylene*. *Macromolecules*, 1995. **28**(19): p. 6432-6436.
47. Roland, C.M., et al., *Temperature Dependence of Segmental and Terminal Relaxation in Atactic Polypropylene Melts*. *Macromolecules*, 2001. **34**(18): p. 6159-6160.
48. Santangelo, P.G. and C.M. Roland, *Temperature Dependence of Mechanical and Dielectric Relaxation in cis-1,4-Polyisoprene*. *Macromolecules*, 1998. **31**(11): p. 3715-3719.
49. Lindholm, U.S. and L.M. Yeakley, *High strain-rate testing: Tension and compression*. *Experimental Mechanics*, 1968. **8**(1): p. 1-9.
50. Shim, J. and D. Mohr, *Using split Hopkinson pressure bars to perform large strain compression tests on polyurea at low, intermediate and high strain rates*. *International Journal of Impact Engineering*, 2009. **36**(9): p. 1116-1127.
51. Johnson, T.P.M., S.S. Sarva, and S. Socrate, *Comparison of Low Impedance Split-Hopkinson Pressure Bar Techniques in the Characterization of Polyurea*. *Experimental Mechanics*, 2010. **50**(7): p. 931-940.
52. Roland, C.M., et al., *High strain rate mechanical behavior of polyurea*. *Polymer - Plastics Technology and Engineering*, 2007. **48**(2): p. 574-578.

53. Zhao, J., Knauss, W.G., Ravichandaran, G., *Applicability of time temperature superposition principle in modelling dynamic response of polyurea*. Mech. Time Depend. Mater., 2007. **11**: p. 289-308.
54. Li, J. and G.J. Weng, *Strain-Rate Sensitivity, Relaxation Behavior, and Complex Moduli of a Class of Isotropic Viscoelastic Composites*. Journal of Engineering Materials and Technology, 1994. **116**(4): p. 495-504.
55. Fragiadakis, D., et al., *Segmental dynamics of polyurea: Effect of stoichiometry*. Polymer, 2010. **51**(1): p. 178-184.
56. Roland, C.M. and R. Casalini, *Effect of hydrostatic pressure on the viscoelastic response of polyurea*. Polymer, 2007. **48**(19): p. 5747-5752.
57. Bogoslovov, R.B., Roland, C. M., Gamache, R. M., *Impact-induced glass transition in elastomeric coatings*. Applied Physics Letters, 2007. **90**(22): p. 221910.
58. Moshe, E., et al., *An increase of the spall strength in aluminum, copper, and Metglas at strain rates larger than 10^7 s⁻¹*. Journal of Applied Physics, 1998. **83**(8): p. 4004-4011.
59. Jajam, K.C. and N.R. Sottos, *Energy Absorption Behavior of Polyurea Under Laser-Induced Dynamic Mixed-Mode Loading*. Journal of Dynamic Behavior of Materials, 2016. **2**(3): p. 379-390.
60. Roland, C.M., D. Fragiadakis, and R.M. Gamache, *Elastomer-steel laminate armor*. Composite Structures, 2010. **92**(5): p. 1059-1064.
61. Sarva, S.S. and A.J. Hsieh, *The effect of microstructure on the rate-dependent stress-strain behavior of poly(urethane urea) elastomers*. Polymer, 2009. **50**(13): p. 3007-3015.

62. Abouzahr, S., G.L. Wilkes, and Z. Ophir, *Structure-property behaviour of segmented polyether-MDI-butanediol based urethanes: effect of composition ratio*. Polymer, 1982. **23**(7): p. 1077-1086.
63. Yi, J., et al., *Large deformation rate-dependent stress-strain behavior of polyurea and polyurethanes*. Polymer, 2006. **47**(1): p. 319-329.
64. Wang, C.B. and S.L. Cooper, *Morphology and properties of segmented polyether polyurethaneureas*. Macromolecules, 1983. **16**(5): p. 775-786.
65. Martin, D.J., et al., *The influence of composition ratio on the morphology of biomedical polyurethanes*. Journal of Applied Polymer Science, 1999. **71**(6): p. 937-952.
66. Martin, D.J., et al., *The effect of average soft segment length on morphology and properties of a series of polyurethane elastomers. I. Characterization of the series*. Journal of Applied Polymer Science, 1996. **62**(9): p. 1377-1386.
67. O'Sickey, M.J., B.D. Lawrey, and G.L. Wilkes, *Structure-property relationships of poly(urethane urea)s with ultra-low monol content poly(propylene glycol) soft segments. I. Influence of soft segment molecular weight and hard segment content*. Journal of Applied Polymer Science, 2002. **84**(2): p. 229-243.
68. Kaushiva, B.D. and G.L. Wilkes, *Influence of diethanolamine (DEOA) on structure-property behavior of molded flexible polyurethane foams*. Journal of Applied Polymer Science, 2000. **77**(1): p. 202-216.
69. Christenson, E.M., et al., *Relationship between nanoscale deformation processes and elastic behavior of polyurethane elastomers*. Polymer, 2005. **46**(25): p. 11744-11754.

70. Sheth, J.P., et al., *Influence of system variables on the morphological and dynamic mechanical behavior of polydimethylsiloxane based segmented polyurethane and polyurea copolymers: a comparative perspective*. *Polymer*, 2004. **45**(20): p. 6919-6932.
71. Korley, L.T.J., et al., *Effect of the degree of soft and hard segment ordering on the morphology and mechanical behavior of semicrystalline segmented polyurethanes*. *Polymer*, 2006. **47**(9): p. 3073-3082.
72. Qi, H.J. and M.C. Boyce, *Stress-strain behavior of thermoplastic polyurethanes*. *Mechanics of Materials*, 2005. **37**(8): p. 817-839.
73. Sup Lee, H., S. Ra Yoo, and S. Won Seo, *Domain and segmental deformation behavior of thermoplastic elastomers using synchrotron SAXS and FTIR methods*. *Journal of Polymer Science Part B: Polymer Physics*, 1999. **37**(22): p. 3233-3245.
74. Yeh, F., et al., *In-Situ Studies of Structure Development during Deformation of a Segmented Poly(urethane-urea) Elastomer*. *Macromolecules*, 2003. **36**(6): p. 1940-1954.
75. Amirkhizi, A.V., et al., *An experimentally-based viscoelastic constitutive model for polyurea, including pressure and temperature effects*. *Philosophical Magazine*, 2006. **86**(36): p. 5847-5866.
76. Grujicic, M., et al., *Experimental Characterization and Material-Model Development for Microphase-Segregated Polyurea: An Overview*. *Journal of Materials Engineering and Performance*, 2012. **21**(1): p. 2-16.
77. Bai, Y., et al., *A Hyper-Viscoelastic Constitutive Model for Polyurea under Uniaxial Compressive Loading*. *Polymers*, 2016. **8**(4): p. 133.

78. Li, C. and J. Lua, *A hyper-viscoelastic constitutive model for polyurea*. Materials Letters, 2009. **63**(11): p. 877-880.
79. Moradi, L.G., J.S. Davidson, and R.J. Dinan, *Response of Bonded Membrane Retrofit Concrete Masonry Walls to Dynamic Pressure*. Journal of Performance of Constructed Facilities, 2009. **23**(2): p. 72-80.
80. Moradi, L.G., J.S. Davidson, and R.J. Dinan, *Resistance of Membrane Retrofit Concrete Masonry Walls to Lateral Pressure*. Journal of Performance of Constructed Facilities, 2008. **22**(3): p. 131-142.
81. Davidson, J., et al., *Failure Mechanisms of Polymer-Reinforced Concrete Masonry Walls Subjected to Blast*. Journal of structural engineering, 2005. **131**(8): p. 1194-1205.
82. Hoo Fatt, M.S., Ouyang X., Dinan R.J., *Blast Response of Walls Retrofitted with Elastomer Coatings, Structures under Shock and Impact*. Structures under Shock and Impact VIII, 2004. **73**(2004): p. 129-138.
83. Baylot, J., et al., *Blast Response of Lightly Attached Concrete Masonry Unit Walls*. Journal of structural engineering, 2005. **131**(8): p. 1186-1193.
84. Hrynyk, T. and J. Myers, *Out-of-Plane Behavior of URM Arching Walls with Modern Blast Retrofits: Experimental Results and Analytical Model*. Journal of structural engineering, 2008. **134**(10): p. 1589-1597.
85. Ackland, K., C. Anderson, and T.D. Ngo, *Deformation of polyurea-coated steel plates under localised blast loading*. International Journal of Impact Engineering, 2013. **51**(0): p. 13-22.

86. Ackland, K., Anderson, C. & St John, N., *Polymeric Coatings for Enhanced Protection of Structures from the Explosive Effects of Blast*. RNSA Security Technology, 2007. **Melbourne, Australia**: p. 90-96.
87. Amini, M.R. and S. Nemat-Nasser, *Micromechanisms of ductile fracturing of DH-36 steel plates under impulsive loads and influence of polyurea reinforcing*. International Journal of Fracture, 2010. **162**(1-2): p. 205-217.
88. Amini, M.R., J. Isaacs, and S. Nemat-Nasser, *Investigation of effect of polyurea on response of steel plates to impulsive loads in direct pressure-pulse experiments*. Mechanics of Materials, 2010. **42**(6): p. 628-639.
89. Xue, L., W. Mock Jr, and T. Belytschko, *Penetration of DH-36 steel plates with and without polyurea coating*. Mechanics of Materials, 2010. **42**(11): p. 981-1003.
90. El Sayed, T., et al., *Computational assessment of ballistic impact on a high strength structural steel/polyurea composite plate*. Computational Mechanics, 2009. **43**(4): p. 525-534.
91. Xue, Z. and J.W. Hutchinson, *Neck retardation and enhanced energy absorption in metal–elastomer bilayers*. Mechanics of Materials, 2007. **39**(5): p. 473-487.
92. Amini, M.R., Isaacs, J.B. & Nemat-Nasser, S., *Effect of Polyurea on the Dynamic Response of Steel Plates*. Experimental and Applied Mechanics, 2006. **St. Louis, MO, US**.
93. Amini, M.R., J.B. Isaacs, and S. Nemat-Nasser, *Experimental investigation of response of monolithic and bilayer plates to impulsive loads*. International Journal of Impact Engineering, 2010. **37**(1): p. 82-89.

94. Amini, M.R., A.V. Amirkhizi, and S. Nemat-Nasser, *Numerical modeling of response of monolithic and bilayer plates to impulsive loads*. International Journal of Impact Engineering, 2010. **37**(1): p. 90-102.
95. Chen, C.C., Alpman, E., Linzell, D.G., & Long, L.N. *Effectiveness of Advanced Coating Systems for Mitigating Blast Effects on Steel Components*. in *Structures under Shock and Impact X*. 2008. Algarve, Portugal.
96. Librescu, L. and A. Nosier, *Response of laminated composite flat panels to sonic boom and explosive blast loadings*. AIAA Journal, 1990. **28**(2): p. 345-352.
97. Lam, K.a.C., L., *Analysis of Clamped Laminated Plates Subjected to Conventional Blast*. Compos. Struct, 1994. **29**(3): p. 311-321.
98. Tekalur, S.A., K. Shivakumar, and A. Shukla, *Mechanical behavior and damage evolution in E-glass vinyl ester and carbon composites subjected to static and blast loads*. Composites Part B: Engineering, 2008. **39**(1): p. 57-65.
99. Gardner, N., et al., *Blast Mitigation in a Sandwich Composite Using Graded Core and Polyurea Interlayer*. Experimental Mechanics, 2012. **52**(2): p. 119-133.
100. Bahei-El-Din, Y.A. and G.J. Dvorak, *Behavior of Sandwich Plates Reinforced with Polyurethane/Polyurea Interlayers under Blast Loads*. Journal of Sandwich Structures and Materials, 2007. **9**(3): p. 261-281.
101. Bahei-El-Din, Y.A. and G.J. Dvorak, *Wave Propagation and Dispersion in Sandwich Plates Subjected to Blast Loads*. Mechanics of Advanced Materials and Structures, 2007. **14**(6): p. 465-475.
102. Bahei-El-Din, Y.A., G.J. Dvorak, and O.J. Fredricksen, *A blast-tolerant sandwich plate design with a polyurea interlayer*. International Journal of Solids and Structures, 2006. **43**(25–26): p. 7644-7658.

103. Pinto, M., Shukla, Arun., *Mitigation of pressure pulses from implosion of hollow composite cylinders*. Journal of Composite Materials, 2015.
104. M. Grujicic, A.A., B. Pandurangan, A. Grujicic, A.A. Littlestone, and R.S. Barsoum, *Computational Investigation of Shock-Mitigation Efficacy of Polyurea When Used in a Combat Helmet: A Core Sample Analysis*. Multidiscipl. Model. Mater. Struct., 2012. **8**(3): p. 297-331.
105. Grujicic, M., et al., *Computational investigation of impact energy absorption capability of polyurea coatings via deformation-induced glass transition*. Materials Science and Engineering: A, 2010. **527**(29–30): p. 7741-7751.
106. Grujicic, M., et al., *Multi-length scale modeling and analysis of microstructure evolution and mechanical properties in polyurea*. Journal of Materials Science, 2011. **46**(6): p. 1767-1779.
107. Grujicic, M., T. He, and B. Pandurangan, *Development and parameterization of an equilibrium material model for segmented polyurea*. Multidiscipline Modeling in Materials and Structures, 2011. **7**(2): p. 96-114.
108. M. Grujicic, B.P., T. He, J. Hunt, J. Tarter, and G. Dillon, *Development and Parameterization of a Time-Invariant (Equilibrium) Material Model for Segmented Elastomeric Polyureas*. J. Mater. Des. Appl., 2011. **225**(3): p. 182-194.
109. Grujicic, M., et al., *Molecular-level simulations of shock generation and propagation in polyurea*. Materials Science and Engineering: A, 2011. **528**(10–11): p. 3799-3808.
110. Grujicic, M. and B. Pandurangan, *Mesoscale analysis of segmental dynamics in microphase-segregated polyurea*. Journal of Materials Science, 2012. **47**(8): p. 3876-3889.

111. Sheth, J.P., et al., *Role of chain symmetry and hydrogen bonding in segmented copolymers with monodisperse hard segments*. *Polymer*, 2005. **46**(18): p. 7317-7322.
112. Luo, Wang, and Ying, *Hydrogen-Bonding Properties of Segmented Polyether Poly(urethane urea) Copolymer*. *Macromolecules*, 1997. **30**(15): p. 4405-4409.
113. Cho, H., R.G. Rinaldi, and M.C. Boyce, *Constitutive modeling of the rate-dependent resilient and dissipative large deformation behavior of a segmented copolymer polyurea*. *Soft Matter*, 2013. **9**(27): p. 6319-6330.
114. Grujicic, M., J. Snipes, and S. Ramaswami, *Meso-scale computational investigation of polyurea microstructure and its role in shockwave attenuation/dispersion*. *AIMS Materials Science*, 2015. **2**(3): p. 163-188.
115. Wang, S.-K. and C.S.P. Sung, *Fluorescence and IR Characterization of Cure in Polyurea, Polyurethane, and Polyurethane-Urea*. *Macromolecules*, 2002. **35**(3): p. 883-888.
116. Chen, Z.S., W.P. Yang, and C.W. Macosko, *Polyurea Synthesis and Properties as a Function of Hard-Segment Content*. *Rubber Chemistry and Technology*, 1988. **61**(1): p. 86-99.
117. Iqbal, N., et al., *Polyurea coatings for enhanced blast-mitigation: a review*. *RSC Advances*, 2016. **6**(111): p. 109706-109717.
118. Qiao, J., et al., *Dynamic mechanical and ultrasonic properties of polyurea*. *Mechanics of Materials*, 2011. **43**(10): p. 598-607.
119. Zhou, Q., et al., *Investigation of the curing process of spray polyurea elastomer by FTIR, DSC, and DMA*. *Journal of Applied Polymer Science*, 2012. **125**(5): p. 3695-3701.

120. Willkomm, W.R., et al., *Properties and phase separation of reaction injection molded and solution polymerized polyureas as a function of hard block content*. Polymer Engineering & Science, 1988. **28**(14): p. 888-900.
121. Bogoslovov, R.B., C.M. Roland, and R.M. Gamache, *Impact-induced glass transition in elastomeric coatings*. Applied Physics Letters, 2007. **90**(22): p. 221910.
122. Roland, C.M., et al., *High strain rate mechanical behavior of polyurea*. Polymer, 2007. **48**(2): p. 574-578.
123. Sarva, S., et al., *The effect of thin membrane restraint on the ballistic performance of armor grade ceramic tiles*. International Journal of Impact Engineering, 2007. **34**(2): p. 277-302.
124. Iqbal, N., D. Kumar, and P. Roy, *Understanding the role of isocyanate dilution toward spraying of polyurea*. Journal of Applied Polymer Science, 2017. **DOI: 10.1002/APP.45869**.
125. Mica, G., et al., *Molecular- and domain-level microstructure-dependent material model for nano-segregated polyurea*. Multidiscipline Modeling in Materials and Structures, 2013. **9**(4): p. 548-578.
126. Awad, W.H. and C.A. Wilkie, *Investigation of the thermal degradation of polyurea: The effect of ammonium polyphosphate and expandable graphite*. Polymer, 2010. **51**(11): p. 2277-2285.
127. Tsagaropoulos, G. and A. Eisenberg, *Dynamic Mechanical Study of the Factors Affecting the Two Glass Transition Behavior of Filled Polymers. Similarities and Differences with Random Ionomers*. Macromolecules, 1995. **28**(18): p. 6067-6077.

128. Jia, Z., et al., *Experimentally-based relaxation modulus of polyurea and its composites*. *Mechanics of Time-Dependent Materials*, 2016. **20**(2): p. 155-174.
129. Huang, W., et al., *Characterization and Damping Property of a Modified Polyurea Material*. *DEStech Transactions on Materials Science and Engineering*, 2017(ictim).
130. Ghezzi, F., et al. *On the damping properties of a polyurea elastomer*. in *Advanced Materials Research*. 2014: Trans Tech Publ.
131. LeBlanc, J., N. Gardner, and A. Shukla, *Effect of polyurea coatings on the response of curved E-Glass/Vinyl ester composite panels to underwater explosive loading*. *Composites Part B: Engineering*, 2013. **44**: p. 565-574.
132. Ning, L., W. De-Ning, and Y. Sheng-Kang, *Hydrogen-bonding properties of segmented polyether poly (urethane urea) copolymer*. *Macromolecules*, 1997. **30**(15): p. 4405-4409.
133. Primeaux, D.J., *Spray polyurea elastomers containing organic carbonates to improve processing characteristics*. (Huntsman Corporation) US Patent, 1995. **US5442034 A**(US 08/252,031): p. Aug 15,1995.
134. Carothers, W.H., *Studies on polymerisation and ring formation I. An introduction to the general theory of condensation polymers* *Journal of the American Chemical Society*, 1929. **51**(8): p. 2548-2559.
135. Cai, J., et al., *Generalized Modeling of Spontaneous Imbibition Based on Hagen–Poiseuille Flow in Tortuous Capillaries with Variably Shaped Apertures*. *Langmuir*, 2014. **30**(18): p. 5142-5151.

136. Sharma, P., et al., *Sustainable Bis-benzoxazines from Cardanol and PET-Derived Terephthalamides*. ACS Sustainable Chemistry & Engineering, 2016. **4**(3): p. 1085-1093.
137. Sharma, P., D. Kumar, and P.K. Roy, *Poly(benzoxazine-co-urea): A Solventless Approach Towards The Introduction of Alternating Urea Linkages In Polybenzoxazine*. ChemistrySelect, 2017. **2**(19): p. 5372-5377.
138. Jiang, X., et al., *Polyurea Structure Characterization by HR-MAS NMR Spectroscopy*. Industrial & Engineering Chemistry Research, 2017. **56**(11): p. 2993-2998.
139. Primeaux, D.J., *Spray polyurea elastomers*. (Huntsman Co) European Patent 1996. **EP0748827A1**(EP19950109286): p. 18 Dec, 1996
140. Nodelman, N.H., *Polyurea-cyclic carbonate RIM systems having improved flow properties*. (Mobay Corporation) US Patent, 1991. **US5028635 A**(US 07/546,078): p. 2 Jul,1991.
141. Primeaux, D.J., *Polyurea elastomer systems with improved adhesion to substrates*. (Huntsman Co) US Patent, 1998. **US5759695 A**(US 08/869,385): p. 2 Jun
142. Clements, J.H., *Reactive Applications of Cyclic Alkylene Carbonates*. Industrial & Engineering Chemistry Research, 2003. **42**(4): p. 663-674.
143. Rahmes, M.H. and W.L. Nelson, *Viscosity Blending Relationships of Heavy Petroleum Oils*. Analytical Chemistry, 1948. **20**(10): p. 912-915.
144. Kanaveli, I.-P., M. Atzemi, and E. Lois, *Predicting the viscosity of diesel/biodiesel blends*. Fuel, 2017. **199**: p. 248-263.
145. Bingham, E.C., *The Viscosity of Binary Mixtures*. The Journal of Physical Chemistry, 1913. **18**(2): p. 157-165.

146. Kendall, J. and K.P. Monroe, *The viscosity of liquids. II. The viscosity-composition curve for ideal liquid mixtures*. Journal of the American Chemical Society, 1917. **39**(9): p. 1787-1802.
147. Centeno, G., et al., *Testing various mixing rules for calculation of viscosity of petroleum blends*. Fuel, 2011. **90**(12): p. 3561-3570.
148. Fernández, B., et al., *Rheokinetic variations during curing of a tetrafunctional epoxy resin modified with two thermoplastics*. European Polymer Journal, 2001. **37**(9): p. 1863-1869.
149. Choi, T., et al., *Microstructure and Segmental Dynamics of Polyurea under Uniaxial Deformation*. Macromolecules, 2012. **45**(8): p. 3581-3589.
150. Chen, C.-P., et al., *Polyurethane elastomers through multi-hydrogen-bonded association of dendritic structures*. Polymer, 2005. **46**(25): p. 11849-11857.
151. Mattia, J. and P. Painter, *A Comparison of Hydrogen Bonding and Order in a Polyurethane and Poly (urethane– urea) and Their Blends with Poly (ethylene glycol)*. Macromolecules, 2007. **40**(5): p. 1546-1554.
152. Iqbal, N., et al., *Tuning the properties of segmented polyurea by regulating soft-segment length*. Journal of Applied Polymer Science, 2018. **10.1002/app.46284**.
153. Negim.E.S.M, K.J.M., Faizova.E., and a.M.S. Shilibekov. S., *The Effect of Diamine Extender on the Properties of Polyurethane Dispersions*. Middle-East Journal of Scientific Research, 2013. **16**(7): p. 890-895.
154. Toader, G., et al., *Novel polyurea polymers with enhanced mechanical properties*. Journal of Applied Polymer Science, 2016. **133**(38).
155. Johnson, J.C., N.D. Wanasekara, and L.T.J. Korley, *Influence of secondary structure and hydrogen-bonding arrangement on the mechanical properties of*

- peptidic-polyurea hybrids*. Journal of Materials Chemistry B, 2014. **2**(17): p. 2554-2561.
156. Chattopadhyay, D.K. and K.V.S.N. Raju, *Structural engineering of polyurethane coatings for high performance applications*. Progress in polymer science, 2007. **32**(3): p. 352-418.
157. Yilgör, E., et al., *Comparison of hydrogen bonding in polydimethylsiloxane and polyether based urethane and urea copolymers*. Polymer, 2000. **41**(3): p. 849-857.
158. E.S.M. Negim, J.M.K., E. Faizova, and S.S.a.S. Mussylmanbek, *The Effect of Diamine Extender on the Properties of Polyurethane Dispersions*. Middle-East Journal of Scientific Research, 2013. **16**(7): p. 890-895.
159. Skarja, G.A. and K.A. Woodhouse, *Structure-property relationships of degradable polyurethane elastomers containing an amino acid-based chain extender*. Journal of Applied Polymer Science, 2000. **75**(12): p. 1522-1534.
160. Das, S., et al., *Effect of Symmetry and H- bond Strength of Hard Segments on the Structure- Property Relationships of Segmented, Nonchain Extended Polyurethanes and Polyureas*. Journal of Macromolecular Science, Part B: Physics, 2007. **46**(5): p. 853-875.
161. Iqbal, N., D. Kumar, and P.K. Roy, *Understanding the role of isocyanate dilution toward spraying of polyurea*. Journal of Applied Polymer Science, 2018. **135**(9).
162. Dudley, J.P., R.A. Grigsby, and D.M. Rice, *Sprayable polyurea elastomer made from reaction of isocyanate compound with amine terminated polyether and di(methylthio)toluene diamine and diethyltoluene diamine chain extenders*, in *Google Patents*, US, Editor. 1992, Texaco Chemical Company.

163. White, J.R., *Origins and measurements of internal stress in plastics*. Polymer Testing, 1984. **4**(2): p. 165-191.
164. Zoetelief, W.F., L.F.A. Douven, and A.J.I. Housz, *Residual thermal stresses in injection molded products*. Polymer Engineering & Science, 1996. **36**(14): p. 1886-1896.
165. Chowdhury, N., et al., *Residual Stresses Introduced to Composite Structures due to the Cure Regime: Effect of Environment Temperature and Moisture*. Journal of Composites, 2016. **2016**: p. 13.
166. Isare, B., et al., *Conformational Control of Hydrogen-Bonded Aromatic Bis-Ureas*. Langmuir, 2012. **28**(19): p. 7535-7541.
167. Teo, L.-S., C.-Y. Chen, and J.-F. Kuo, *Fourier transform infrared spectroscopy study on effects of temperature on hydrogen bonding in amine-containing polyurethanes and poly (urethane– urea) s*. Macromolecules, 1997. **30**(6): p. 1793-1799.
168. Coleman, M.M., et al., *Hydrogen bonding in polymer blends. 1. FTIR studies of urethane-ether blends*. Macromolecules, 1988. **21**(1): p. 59-65.
169. Jena, K.K. and K.S.N. Raju, *Synthesis and characterization of hyperbranched polyurethane hybrids using tetraethoxysilane (TEOS) as cross-linker*. Industrial & Engineering Chemistry Research, 2008. **47**(23): p. 9214-9224.
170. Garrett, J., J. Lin, and J. Runt, *Influence of preparation conditions on microdomain formation in poly (urethane urea) block copolymers*. Macromolecules, 2002. **35**(1): p. 161-168.

171. Marcos-Fernandez, A., et al., *Hydrogen Bonding in Copoly (ether– urea) s and Its Relationship with the Physical Properties*. *Macromolecules*, 1997. **30**(12): p. 3584-3592.
172. Bergsman, D.S., et al., *Effect of Backbone Chemistry on the Structure of Polyurea Films Deposited by Molecular Layer Deposition*. *Chemistry of Materials*, 2017. **29**(3): p. 1192-1203.
173. Collins, E.A., J. Bareš, and F.W. Billmeyer, *Experiments in Polymer Science*. 1973: Wiley.
174. Kinstle, J.F. and L.E. Sepulveda, *Synthesis and Characterisation of Linear and Crosslinked AB-Type Polyurethanes LABANA, SANTOKH S*, in *Chemistry & Properties of Crosslinked Polymers*, S.S. LABANA, Editor. 1977, Academic Press. p. 21-47.
175. Patel, A.N., M.M. Patel, and A. Dighe, *Influence of compositional variables on the morphological and dynamic mechanical behavior of fatty acid based self-crosslinking poly (urethane urea) anionomers*. *Progress in Organic Coatings*, 2012. **74**(3): p. 443-452.
176. Dadbin, S. and M. Frounchi, *Effects of polyurethane soft segment and crosslink density on the morphology and mechanical properties of polyurethane/poly(allyl diglycol carbonate) simultaneous interpenetrating polymer networks*. *Journal of Applied Polymer Science*, 2003. **89**(6): p. 1583-1595.
177. Chiou, B.-S. and P.E. Schoen, *Effects of crosslinking on thermal and mechanical properties of polyurethanes*. *Journal of Applied Polymer Science*, 2002. **83**(1): p. 212-223.

178. Petrović, Z.S., et al., *The effect of crosslinking on properties of polyurethane elastomers*. Journal of Applied Polymer Science, 1991. **42**(2): p. 391-398.
179. Kontou, E., et al., *Physical and chemical cross-linking effects in polyurethane elastomers*. Colloid and Polymer Science, 1990. **268**(7): p. 636-644.
180. Okuto, H., *Studies on the structure of polyurethane elastomers. II. High resolution NMR spectroscopic determination of allophanate and biuret linkages in the cured polyurethane elastomer: Degradation by amine*. Macromolecular Chemistry and Physics, 1966. **98**(1): p. 148-163.
181. Petrović, Z.S. and J. Ferguson, *Polyurethane elastomers*. Progress in Polymer Science, 1991. **16**(5): p. 695-836.
182. Shinko, A., S.C. Jana, and M.A. Meador, *Crosslinked polyurea aerogels with controlled porosity*. RSC Advances, 2015. **5**(127): p. 105329-105338.
183. Shinko, A., S.C. Jana, and M.A. Meador, *Crosslinked polyurea-co-polyurethane aerogels with hierarchical structures and low stiffness*. Journal of Non-Crystalline Solids, 2018. **487**: p. 19-27.
184. Martin, R., et al., *The processability of a poly(urea-urethane) elastomer reversibly crosslinked with aromatic disulfide bridges*. Journal of Materials Chemistry A, 2014. **2**(16): p. 5710-5715.
185. Tatiya, P.D., P.P. Mahulikar, and V.V. Gite, *Designing of polyamidoamine-based polyurea microcapsules containing tung oil for anticorrosive coating applications*. Journal of Coatings Technology and Research, 2016. **13**(4): p. 715-726.
186. Jung, H., et al., *Properties of crosslinked polyurethanes synthesized from 4, 4'- diphenylmethane diisocyanate and polyester polyol*. Journal of Applied Polymer Science, 2000. **78**(3): p. 624-630.

187. Desai, S., et al., *Effect of polyols and diisocyanates on thermo-mechanical and morphological properties of polyurethanes*. European Polymer Journal, 2000. **36**(4): p. 711-725.
188. Smith, T.L. and A.B. Magnusson, *Diisocyanate-linked polymers. III. Relationships between the composition and ultimate tensile properties of some polyurethane elastomers*. Journal of Applied Polymer Science, 1961. **5**(14): p. 218-232.
189. Ahmad, N., et al., *The influence of cross-linking/chain extension structures on mechanical properties of HTPB-based polyurethane elastomers*. Arabian Journal for Science and Engineering, 2014. **39**(1): p. 43-51.
190. Smith, T.L. and A.B. Magnusson, *Diisocyanate-linked polymers. II. Mechanical and swelling properties of some polyurethane elastomers*. Journal of Polymer Science Part A: Polymer Chemistry, 1960. **42**(140): p. 391-416.
191. Consaga, J.P. and D.M. French, *Properties of hydroxyl-terminated polybutadiene-urethane systems*. Journal of Applied Polymer Science, 1971. **15**(12): p. 2941-2956.
192. Špírková, M., et al., *Polybutadiene-based polyurethanes with controlled properties: preparation and characterization*. Journal of Applied Polymer Science, 2000. **77**(2): p. 381-389.
193. Kothandaraman, H., K. Venkatarao, and B.C. Thanoo, *Preparation, properties, and crosslinking studies on polyurethane elastomers*. Polymer Journal, 1989. **21**(10): p. 829.

194. Paulmer, R., et al., *Effect of crosslinking agents on the structure and properties of polyurethane millable elastomer composites*. Journal of Applied Polymer Science, 1991. **43**(10): p. 1953-1959.
195. Thomas, O., et al., *Effect of cross- link density on the morphology, thermal and mechanical properties of flexible molded polyurea/urethane foams and films*. Journal of Polymer Science Part B: Polymer Physics, 1994. **32**(13): p. 2155-2169.
196. Iqbal, N., et al., *Aromatic versus Aliphatic: Hydrogen Bonding Pattern in Chain- Extended High- Performance Polyurea*. ChemistrySelect, 2018. **3**(7): p. 1976-1982.
197. Queslel, J. and J. Mark, *Molecular interpretation of the moduli of elastomeric polymer networks of known structure*, in *Analysis/Networks/Peptides*. 1984, Springer. p. 135-176.
198. Flory, P.J., *Principles of polymer chemistry*. 1953: Cornell University Press.
199. James, H.M. and E. Guth, *Statistical thermodynamics of rubber elasticity*. The Journal of Chemical Physics, 1953. **21**(6): p. 1039-1049.
200. Flory, P., *Theory of elasticity of polymer networks. The effect of local constraints on junctions*. The Journal of Chemical Physics, 1977. **66**(12): p. 5720-5729.
201. Flory, P.J., *Molecular theory of rubber elasticity*. Polymer, 1979. **20**(11): p. 1317-1320.
202. Han, C.D., *Mechanical properties of solid polymers, 2nd ed., I. M. Ward, Wiley, New York, 1983, 475 pp. Price: \$54.95*. Journal of Polymer Science: Polymer Letters Edition, 1985. **23**(2): p. 119-119.

203. Davidson, J. and N. Goulbourne, *Nonaffine chain and primitive path deformation in crosslinked polymers*. Modelling and Simulation in Materials Science and Engineering, 2016. **24**(6): p. 065002.
204. Toutanji, H.A., et al., *Applying a polyurea coating to high-performance organic cementitious materials*. Construction and Building Materials, 2013. **38**: p. 1170-1179.
205. Ping, L., Xin Mao Li, and W.B. Huang, *Effect of Dry-Wet Circulation and Temperature Change on Properties of Polyurea Coatings*. Advanced Materials Research, 2011. **150-151**: p. 1203-1208.
206. Parniani, S. and H. Toutanji, *Monotonic and fatigue performance of RC beams strengthened with a polyurea coating system*. Construction and Building Materials, 2015. **101**: p. 22-29.
207. K. J. Knox, et al., *Polymer materials for structural retrofit, Florida*. 2000.
208. Davidson, J.S., et al., *Failure mechanisms of polymer-reinforced concrete masonry walls subjected to blast*. Journal of Structural Engineering, 2005. **131**(8): p. 1194-1205.
209. Cai, L., et al., *Protection of steel railcar tank containing liquid chlorine from high speed impact by using polyhedral oligomeric silsesquioxane-enhanced polyurea*. International Journal of Impact Engineering, 2015. **75**(Supplement C): p. 1-10.
210. M. Grujicic, et al., *Meso-scale Computational Investigation of Shock-Wave Attenuation by Trailing Release Wave in Different Grades of Polyurea*. Journal of Material Engineering and Performance, 2014. **23**: p. 49.
211. Al-Amoudi, O., et al., *Shrinkage of plain and silica fume cement concrete under hot weather*. Cement and Concrete Composites, 2007. **29**(9): p. 690-699.

212. Mazzotti, C., et al., *Bond Between EBR FRP and Concrete*, in *Design Procedures for the Use of Composites in Strengthening of Reinforced Concrete Structures: State-of-the-Art Report of the RILEM Technical Committee 234-DUC*, C. Pellegrino and J. Sena-Cruz, Editors. 2016, Springer Netherlands: Dordrecht. p. 39-96.
213. Hognies, M., P. Willieme, and O. Gabet, *Influence of the surface properties of concrete on the adhesion of coating: characterization of the interface by peel test and FT-IR spectroscopy*. *progress in organic coatings*, 2011. **72**(3): p. 360-379.

LIST OF PUBLICATIONS

1. **N. Iqbal**, M. Tripathi, S. Parthasarathy, D. Kumar , P. K. Roy**Polyurea coatings for enhanced blast-mitigation: A Review** *RSC Adv.*, DOI: 10.1039/C6RA23866A, 2016,6, 109706-109717
2. **N. Iqbal**, D. Kumar , P. K. Roy**Understanding the role of isocyanate dilution toward spraying of polyurea.** *Journal of Applied Polymer Science (2017)* DOI: 10.1002/app.45869,135 (9), 45869
3. **N. Iqbal**, M. Tripathi, S. Parthasarathy, D. Kumar , P. K. Roy**Tuning the properties of segmented polyurea by regulating soft-segment length.**, *Journal of Applied Polymer Science (2018)* DOI: 10.1002/app.46284 135(21), 46284
4. **N. Iqbal**, M. Tripathi, S. Parthasarathy, D. Kumar , P. K. Roy**Aromatic versus Aliphatic: Hydrogen Bonding Pattern in Chain-Extended High-Performance Polyurea**, *Chemistry Select (2018)*, 3, 1976– 1982 DOI: 10.1002/slct.201703176. 3 (7), 1976-1982
5. **N. Iqbal**, P.K. Sharma, D. Kumar and P. K. Roy**Protective polyurea coatings for enhanced blast survivability of concrete.** *Construction and building material (2018)* 175, 682-690 DOI:10.1016/j.conbuildmat.2018.04.204 175, 682-690
6. **N. Iqbal**, D. Kumar , P. K. Roy**Emergence of time-dependent structural and mechanical properties in chain extended polyureas.** *Journal of Applied Polymer Science* 10.1002/app.20180773.
7. **N. Iqbal**, M. Tripathi, S. Parthasarathy, D. Kumar , P. K. Roy**Polyurea spray coatings: Tailoring material properties through chemical crosslinking.** *Progress in organic coatings (Revision submitted)*

LIST OF CONFERENCE PROCEEDINGS

1. N. Iqbal, Mitra Arnab, Kumar Devendra, Roy Prasun Kumar Effect Of Increasing Soft Segments On Properties Of Polyurea for blast mitigating applications, *Macro 2017 Thiruvananthapuram, India.*

2.N. Iqbal, D. Kumar, Prasun Roy (2015) Toughening of Vinyl Ester with core-shell poly(siloxane)-Vinyl Ester microspheres, *Macro 2015 Kolkata India.*

BIO-DATA

Nahid Iqbal

D-1, 7/1, Street no. 14/A, Wazirabad extension Delhi-110085

Email ID: inahid2504@gmail.com

PERSONAL DETAILS

Male, Married

Date of Birth: 25 April, 1987

Languages Known: Hindi, English & Urdu

EDUCATION

M.Tech (Polymer Technology), 2013

Department of Applied Chemistry and
Polymer Technology

Delhi Technological University, Delhi

HONOURS

DTU-TRF qualified

GATE qualified